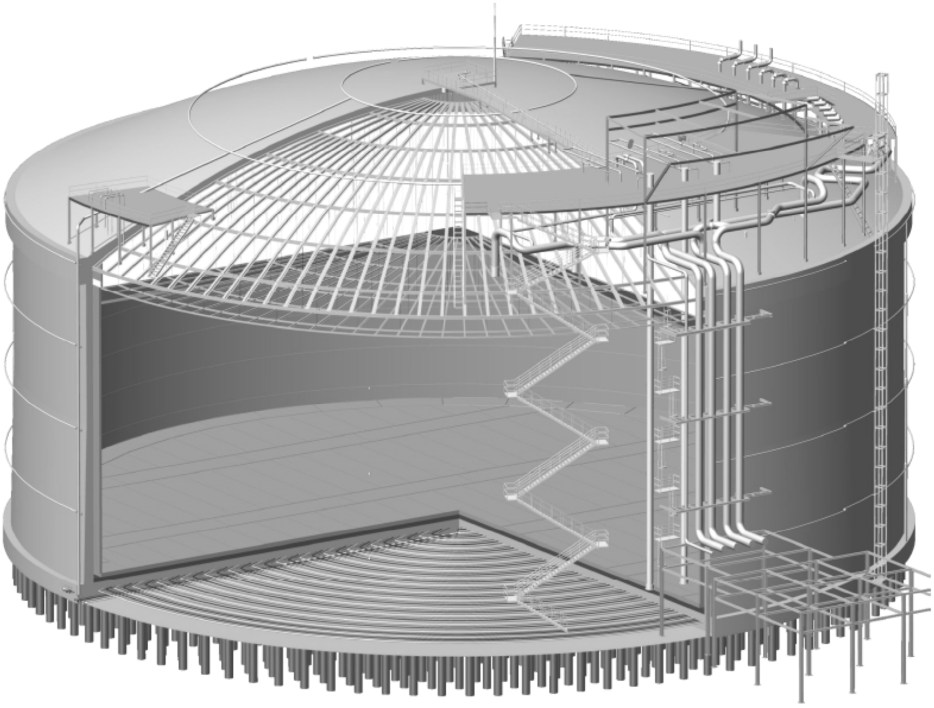

Seismic behaviour of a LNG tank foundation

MSc Thesis Jesper van Es

27 March 2014

Final Report

Cover picture:
Yang, Y.-m; (2006); *Development of the world's largest above-ground full containment LNG storage tank*; 23rd World Gas Conference; (p. 5); Amsterdam; Korea Gas Corporation.

Seismic behaviour of a LNG tank foundation

MSc Thesis Jesper van Es

Author:

Jesper van Es

Delft University of Technology

Faculty of Civil Engineering and Geoscience

Geo-engineering Section

March 2014

Seismic behaviour of a LNG tank foundation

A thesis submitted in partial fulfilment for Master of Science Degree in Geo-engineering from Delft University of Technology (Technische Universiteit Delft), Faculty of Civil Engineering and Geoscience, Geo-engineering Section, Delft, The Netherlands.

Keywords:

Geotechnical Engineering, Earthquake Engineering, Pile group interaction, Finite element analysis, Plaxis, Plaxis Embedded Piles.

Author:

Jesper van Es

Delft University of Technology

Faculty of Civil Engineering and Geoscience, Section Geo-engineering

Delft, Netherlands

Email: jespervanes@gmail.com

Graduation committee:

Prof. ir. A. F. van Tol	Technische Universiteit Delft / Deltares
Dr. ir. R. B. J. Brinkgreve	Technische Universiteit Delft / PLAXIS
Dr. ir. P. C. J. Hoogenboom	Technische Universiteit Delft
Ing. M. de Kant	Royal HaskoningDHV
Dr. ir. S. J. H. Meijers	Royal HaskoningDHV

Delft University of Technology
Civil Engineering and Geoscience Faculty
Section Geo-engineering
Address: Stevinweg 1, 2628 CN
Postal address: PO Box 5048, 2600 GA
Phone: +31 (0)15 2781880
Fax: +31 (0)88 2783328
Delft, The Netherlands

Royal HaskoningDHV
Nijmegen office
Section Infrastructure
Address: Barbarossastraat 35
Postal address: PO Box 151, 6500 AD
Phone: +31 (0)24 328 42 84
www.royalhaskoningdhv.com
info@nijmegen.royalhaskoningdhv.com

ACKNOWLEDGEMENTS

This MSc Thesis could not be completed without the support and advice from many people.

First of all, I would like to express my gratitude to Ir. J. S. van der Schrier, Ing. M. de Kant and Dr. Ir. S. H. J. Meijers who gave me the opportunity to conduct this research at Royal HaskoningDHV in Nijmegen. This research has given me the opportunity to develop myself and to expand my knowledge on this difficult and, for me, new subject of earthquake engineering. Without mentioning the people by name I like to thank all colleagues from Royal HaskoningDHV for their support and an enjoyable period.

I would also like to thank Prof. A. F. van Tol, Dr. Ir. R. B. J. Brinkgreve and Dr. Ir. P. C. J. Hoogenboom as my graduation committee. The discussions and guidance during the meetings have helped me finish this MSc Thesis.

My student time, at the TU in Delft and Saxion in Enschede, was an awesome time thanks to my ex-roommates and fellow students: Thomas Naves, Gert-Jan Kampshof and Martijn Huis in ’t Veld. Thanks guys, for the great memories and help during my MSc Thesis.

Finally, I would like to express profound gratitude to my parents, family, friends and girlfriend. My parents provided the opportunity to attend VWO, HBO and University. During this period they supported every decision I made. I would like to thank my girlfriend, who has supported me unconditionally during my study and especially this MSc Thesis.

Nijmegen, 27 March 2013

Jesper van Es

SUMMARY

The design of a piled LNG (Liquid Natural Gas) tank under seismic loading is a complex interaction between the earthquake load and the behaviour of the soil, foundation and super structure. In previous designs Royal HaskoningDHV used an uncoupled method to calculate the impact of an earthquake on the pile foundation of a LNG tank. First a dynamic model (MDOF model) is used in which the earthquake load is applied as base plate motion. These motions result in reaction forces (vertical force, shear force and overturning moment) from the super structure on the foundation. Secondly these forces are applied in a static model to assess the pile forces. This approach has two drawbacks: The base plate is supposed to be infinitely stiff and therefore the influence of wave propagations effects in the soil on the behaviour of the base plate is neglected. In addition, due to the static calculation method for pile reactions, wave propagation effects over the length of the pile are neglected. Based on these drawbacks, three research objectives were formulated in this thesis:

1. *Assess the feasibility of a 3D full dynamic model for the analysis of a LNG tank (foundation) under seismic loading;*
2. *Compare the uncoupled calculation method with a full dynamic method;*
3. *Assess the influence of wave propagation effects in the soil on the base plate.*

After an extensive literature study of the application of finite element modelling to earthquake related problems, three sub investigations were performed:

Embedded pile group effects

Embedded piles in PLAXIS were assessed on their static lateral group behaviour and their applicability for this MSc Thesis. When embedded piles are applied in situations where the lateral load is small compared to the failure load their group behaviour is acceptable. Group and side-by-side efficiency factors from PLAXIS are comparable to values found in literature ((Reese en Impe 2001) and (Mokwa 1999)). The efficiency factors for pile rows are slightly lower than the ones from literature. Based on the expected displacement/load magnitudes and their lateral pile group behaviour, embedded piles are applicable in this thesis.

Modelling of LNG liquid

Modelling of a liquid is complex and often requires excessive calculation time; therefore a simplified method is investigated. Inside a tank, distinction can be made between impulsive and convective behaviour of a liquid. This thesis focuses on the modelling of impulsive (sliding) behaviour solely, since this component ensures 90% of the resulting forces on the base slab during an earthquake event. The impulsive LNG component has a frequency of 1,85 Hz and is modelled with the aid of a frequency depended beam with mass on top and clamped to the surface (mass-spring system). An auxiliary structure is used to distribute forces, introduced by the “vibrating” beam, over the width of the base plate. Compared to the MDOF model this method shows realistic overturning moment values. However, shear force is underestimated.

Free field site response

In a free field site response analysis the influence of boundary type, boundary distance, mesh configuration and time stepping procedure is investigated. Free field boundaries are the most effective to apply at the lateral boundaries. When applied at a distance of 100 meter from the model centre, wave reflections do not influence the response in the centre. A drawback of free field boundaries for dynamic calculations is the introduction of a non-symmetrical stiffness matrix. In models consisting of more than 9,000 elements the kernel of PLAXIS 2D uses more than 32 GB of internal memory and therefore calculations are difficult to perform on common

hardware. For a proper modelling of the most important frequencies (0 – 12 Hz) the element size is limited according to (Lysmer & Kuhlmeyer R.L., 1969) to 1.08, 0.82 and 5.02 Hz for respectively the sand fill, clay and deep sand layer. The time steps are limited by Courant's condition to 0.0061 seconds; this is larger than the time steps of the input signal, which will therefore be normative.

The sub investigations, together with a global 3D model of the complete geometry are used to assess the feasibility a 3D full dynamic model in PLAXIS. For a good description of both: soil behaviour and soil-structure interaction, a model will require more than 500,000 elements. According to (Brinkgreve 2013, personal communication), models with 500,000 elements or more in combination with a dynamic calculation is currently not practically feasible. Calculation times will be up to several days or even a week and handling of output will be very slow.

The uncoupled calculation method is compared to a full dynamic calculation method in PLAXIS 2D. The comparison is based on two normative situations during a SSE earthquake event of a LNG tank in Angola. The full containment tank is founded on 1300 open ended steel piles. The soil is characterised by three layers: sandy top layer (±4 m), a thick softer clay core (±29 m) and a stiffer deep soil of sand until bedrock level.
Reaction forces from the superstructure in the dynamic model are used as input for a (pseudo) static model with the same geometry and properties. Pile forces are obtained from the different models and compared: model B1 vs B1.1 and model B2 vs B2.1 / B2.2 (see figure below).

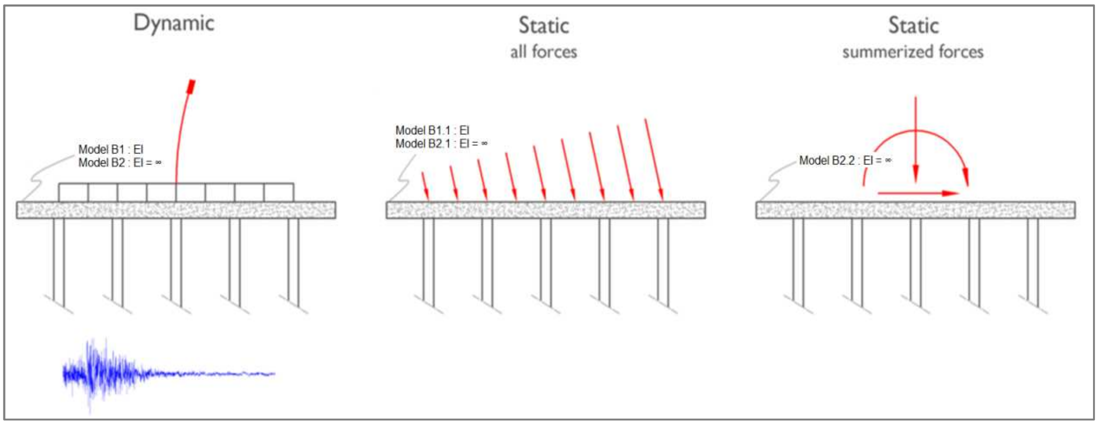

Considered models for comparison between full dynamic and pseudo static calculation method for pile forces

It can be concluded that pile forces are underestimated by the static models (B1.1, B2.1, B2.2). The pseudo static models do not show clamping forces/moments in the pile foot at the transition between the clay-and deeper sand layer. Pile forces/moments at this point are underestimated by 80-100%. Pile head forces are only 0-10% lower than calculate by the dynamic models (B1, B2).

No influences of wave propagation effects over the width of the base slab were found in the results of the dynamic calculations in PLAXIS 2D. The base slab is moving in its entirety, together with the pile heads and the top soil layer. However, wave propagation effects were found over the length of the piles. The response (displacements and accelerations) is amplified towards the surface by the thick soft clay layer. In addition there is load coupling between the construction, impulsive liquid mass and the earthquake signal. The original input signal is affected by the mass and frequency of the impulsive liquid.

CONTENTS

LIST OF SYMBOLS

General symbols

Symbol	Property	Unit
A_{pile}	Area of pile foot	$[m^2]$
$a_{g;bedrock;SSE}$	Bedrock acceleration for SSE situation	$[g]$
$a_{g;bedrock;OBE}$	Bedrock acceleration for OBE situation	$[g]$
c	Cohesion	$[kN/m^2]$
c'_{ref}	Effective cohesion at reference stress level	$[kN/m^2]$
d	Thickness (of pile, plate, embedded pile,..........)	$[m]$
E	Young's modulus/ Elasticity modulus	$[kN/m^2]$
E_{oed}	Oedometer modulus	$[kN/m^2]$
E_{50}^{ref}	Secant stiffness modules in standard drained triaxial test at reference stress level	$[kN/m^2]$
E_{oed}^{ref}	Tangent stiffness modulus for primary oedometer loading ate reference stress level	$[kN/m^2]$
E_{ur}^{ref}	Unloading/reloading stiffness at reference stress level	$[kN/m^2]$
EA	Axial stiffness	$[kN]$
EI	Bending stiffness	$[kNm^2]$
$e_{initial}$	Initial void ratio	$[-]$
F	Force	$[kN]$
$F_{\max}$	Maximum allowable base resistance	$[kN]$
$F_{r;h;group}$	Lateral capacity of pile group	$[kN]$
$F_{r;h;pile}$	Lateral capacity of specific pile	$[kN]$
$F_{r;h;pile\,row}$	Lateral capacity of pile row	$[kN]$
$F_{r;h;single\,pile}$	Lateral capacity of single pile	$[kN]$
f	Frequency	$[Hz]$
f_0	Fundamental frequency	$[Hz]$
f_{input}	Frequency used as input in formula	$[Hz]$
$f_{\max}$	Maximum frequency	$[Hz]$
f_n	Natural frequency	$[Hz]$
f_{PLAXIS}	Frequency found in PLAXIS (output)	$[Hz]$
G	Shear modules	$[kN/m^2]$
G_0	Initial shear modulus	$[kN/m^2]$
G_o^{ref}	Initial shear modulus at reference stress level	$[kN/m^2]$
G_s	Secant shear modulus	$[kN/m^2]$
G_t	Tangent shear modulus	$[kN/m^2]$

Symbol	Property	Unit
G_{ur}	Unloading-reloading shear modulus	$[kN/m^2]$
g	Gravity	$[m/s]$
H	Thickness of soil deposit	$[m]$
I	Moment of Inertia	$[m^4]$
K_0^{nc}	K_0-value for normal consolidation	$[-]$
k	Spring constant / stiffness of system	
ℓ	Length of a beam/plate	$[m]$
$M_{\max}$	Maximum moment	$[kNm]$
$M_{\min}$	Minimum moment	$[kNm]$
m	Power for stress-level dependency of stiffness	$[-]$
m	Mass	$[kg]$
$N_{\max}$	Maximum axial force	$[kN]$
O_{pile}	Circumference of the pile	$[m]$
p^{ref}	Reference stress for stiffness (default $p^{ref} = 100\ kN/m^2$)	$[kN/m^2]$
$Q_{\max}$	Maximum shear force	$[kN]$
$Q_{\min}$	Minimum shear force	$[kN]$
$q_{c;bottom}$	q_c value at the bottom of the pile	$[MPa]$
R_f	Failure ratio q_f / q_a	$[-]$
s	Special form factor	$[-]$
T_0	Fundamental period	$[s]$
$T_{bottom:\max}$	Maximum allowable skin resistance at the pile foot	$[kN/m]$
$T_{top:\max}$	Maximum allowable skin resistance at top the pile	$[kN/m]$
Δ_t	Time step in dynamic calculations	$[s]$
$\Delta_{t;\max}$	Maximum time step	$[s]$
u	Deflection of a beam	$[m]$
$u_{bending}$	Deflection due to bending (EI)	$[m]$
u_{shear}	Deflection due to shear	$[m]$
V_p	Primary or compression wave velocity	$[m/s]$
V_R	Rayleigh wave velocity	$[m/s]$
V_s	Secondary or shear wave velocity	$[m/s]$
$V_{s;layer}$	Secondary or shear wave velocity in specific layer	$[m/s]$
w	Specific weight (of pile, plate, embedded pile,……….)	$[kN/m/m]$
α_s	Pile class factor	$[-]$
β_s	Pile class factor	$[-]$

Symbol	Property	Unit
γ	Shear strain	$[-]$
$\gamma_{0.7}$	Shear strain at which G_0 is reduced to 72.2%	$[-]$
$\gamma_{cut-off}$	Cut-off shear strain at which G_t is cut-off by G_{ur}	$[-]$
γ_{sat}	Wet unit weight	$[kN/m^3]$
γ_{total}	Total shear strain	$[-]$
γ_{unsat}	Dry unit weight	$[kN/m^3]$
η_{group}	Pile group efficiency	$[-]$
$\eta_{pile\,row}$	Pile row efficiency	$[-]$
η_{pile}	Pile efficiency	$[-]$
ρ	Density	$[kN/m^3]$
υ	Poisson's Ratio	$[-]$
υ_{ur}	Poisson's ratio for unloading and reloading	$[-]$
ξ	Damping ratio	[-] or [%]
φ	Friction angle	$[^\circ]$
ψ	Dilatancy angle	$[^\circ]$
ω_n	Natural frequency	$[Rad/s]$

<u>Symbols for finite element modelling</u>

Symbol	Property
$\underline{\underline{B}}$	Strain interpolation matrix
$\underline{\underline{C}}$	Damping matrix
$\underline{\underline{D}}^e$	Elastic material stiffness matrix representing Hooke's law
$\underline{\underline{D}}^{foot}$	Material stiffness matrix of spring element at the pile foot
$\underline{F}$	Load Vector
$\underline{f}^{foot}$	Force in the pile foot spring
$\underline{f}_0^{foot}$	Initial force in the pile foot spring
$\Delta \underline{f}^{foot}$	Force increment in the pile foot spring
$\underline{\underline{K}}$	Stiffness matrix
K_s	Elastic shear stiffness
K_n, K_t	Elastic normal stiffness in horizontal directions
$\underline{\underline{L}}$	Differential operator
$\underline{\underline{M}}$	Material stiffness matrix
$\underline{\underline{N}}$	Matrix with shape functions
$\underline{u}$	Vector with displacement components

Symbol	Property
$\dot{\underline{u}}$	Vector with velocity components
$\ddot{\underline{u}}$	Vector with acceleration components
$\underline{u}^p$	Pile displacement
$\underline{u}^s$	Soil displacement
$\Delta\underline{u}_{rel}$	Relative displacement vector between embedded pile and soil
$\underline{\underline{T}}^{skin}$	Material stiffness matrix of the interface element of an embedded pile
t_s	Shear stress in axial direction
t_n , t_t	Normal stress in horizontal directions
$\underline{t}^{skin}$	Skin resistance of an embedded pile
$\underline{t}_0{}^{skin}$	Initial skin resistance of an embedded pile
$\Delta\underline{t}^{skin}$	Force increment at integration points of embedded pile
$\underline{v}$	Vectors with nodal displacements
$\underline{v}_i$	Vector with displacements in node i
x_i , y_i , z_i	Nodal displacement in x, y, z direction in node i
α_R , β_R	Rayleigh damping coefficients Alpha and Beta
α_N , β_N	Newmark time integration coefficients Alpha and Beta
γ_{xy} , γ_{yz} , γ_{zx}	Shear strain in xy, yx, zx direction
$\underline{\varepsilon}$	Vector with strain components
$\underline{\varepsilon}_0$	Vector with initial strain components
$\underline{\varepsilon}^e$	Vector with elastic strain components
$\underline{\varepsilon}^p$	Vector with plastic strain components
ε_x , ε_y , ε_z	Strain in x, y, z direction
$\underline{\sigma}$	Vector with stress components
$\underline{\sigma}_0$	Vector with initial stress components
σ_x , σ_y , σ_z	Stress in x, y, z direction
τ_{xy} , τ_{yx} , τ_{zx}	Shear stress in xy, yz, zx direction

LIST OF FIGURES

LIST OF TABLES

1 INTRODUCTION

Natural gas is an important and relative clean energy source compared to fossil fuels. The natural gas industry is growing quickly and with it the regulations for design. Liquefied Natural Gas (LNG) is natural gas that has been converted, temporarily, to liquid form for ease of storage and transport, because it takes up about 1/600th the volume of natural gas in the gaseous state. This conversion to liquid state is performed by cooling the gas to -163°C at atmospheric pressure.
The safety of LNG storage tanks is, partly due to this cooling, very important. Especially in areas that are subjected to earthquakes. Building LNG storage tanks in areas where earthquakes can occur requires that the effect of these vibrations is taken into account in the design of the LNG tank and its foundation. Damage to a tank filled with flammable content, like LNG, could cause huge losses.

Royal Haskoning DHV (RHDHV) is a company with experience of the design of LNG-tank constructions. Under the name of Protective Storage Engineers (PSE) several LNG-tanks were designed all over the world. In areas that are subjected to seismic activity they also assessed the seismic response of the construction.
This dynamic analysis is performed with the aid of a Multi Degrees Of Freedom model (MDOF model) in which the construction is schematized in several masses, springs and dampers. Due to an earthquake one of the masses is set in motion which leads to a dynamic interaction between all components. In the end all interactions in the MDOF model will lead to a base shear and overturning moment on the base slab. For the calculation of the total foundation (base slab and piles) the construction is subjected to this base shear and overturning moment in a separate static analysis.

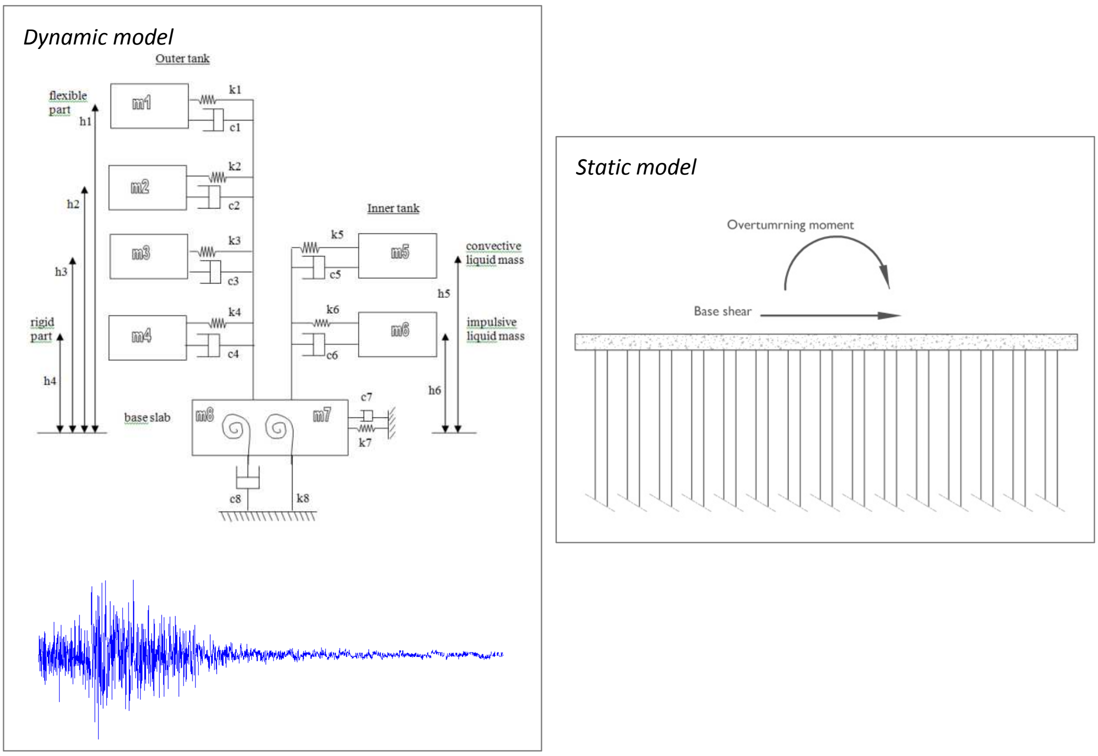

Figure 1-1 Uncoupled approach, using the MDOF model for dynamic calculations

1.1 Problem definition

As mentioned, in current designs the dynamic analysis of a LNG tank is performed with the aid of a MDOF model. This model contains a highly schematized construction of several masses, springs and dampers, and uses some basic assumptions to make the analysis more manageable. Along with the upcoming possibilities of finite element modelling questions are raised about the chosen calculation scheme for the calculation of pile forces and moments based on a static analysis with a base shear and overturning moment obtained from a dynamic analysis.
In addition there are some doubts about the assumptions made in the MDOF model regarding wave propagation effects, load structure interaction and pile group effects.

1.2 Objectives

In this thesis there are three main objectives:

1. *Assess the feasibility of a 3D full dynamic model for the analysis of a LNG tank (foundation) under seismic loading*

The goal of RHDHV is to use a 3D full dynamic model for the analysis of a LNG tank (foundation) under seismic loading. It is not yet certain whether or not it is possible to perform such an analysis based on available computer power, calculation time and handling of the model; this thesis will be the first step into realizing this goal.

2. *Compare the uncoupled calculation method with a full dynamic method*

In previous designs the pile forces and pile moments caused by an earthquake are obtained by a static calculation in which the construction is subjected to a base shear and overturning moment. This base shear and overturning moment are computed in a dynamic calculation with the MDOF model.
With the current finite element models it is possible to perform a full dynamic analysis of the construction and obtain the pile forces and pile moments directly. A comparison will made between a full dynamic analysis and a static analysis in which results of the dynamic analysis, base shear and overturning moment, will be as input.

3. *Assess the influence of wave propagation effects in the soil on the base plate*

In formerly used MDOF model the baseplate and piles are schematized to a single mass-spring-damper system. In this schematization the baseplate is assumed to be fully rigid. This means that the foundation moves as a whole and wave propagation effects over the width of the tank are neglected. With the current possibilities of finite element models for soils it is possible to account for wave propagation effects. All piles can be modelled and the baseplate can have a realistic stiffness to include the effect of wave propagation over the width of the baseplate and between the piles.

To reach the above described mean objectives the following sub objectives are defined:

4. *Assess the (embedded) pile group effects in PLAXIS and compare them with available literature.*

   The design of the LNG tank in the case study project contains about 1300 piles with relatively small centre to centre distances (< 3.5D). This implies that pile group effects will play an important role in the behaviour of the foundation. Embedded piles in PLAXIS are developed for vertically loaded piles and have some limitations when subjected to horizontal loading. Therefore a comparison is made between pile group effects in a horizontal loaded pile group as calculated with Plaxis3D and as described in literature.

5. *Schematize the liquid inside the tank to make the calculation process easier and faster*

   The liquid inside the tank has a big influence on the dynamic behaviour of the tank foundation. Modelling the liquid as a volume layer with zero shear strength and fully plastic behaviour is theoretically possible but would lead to a significant increase of calculation time in a 3D calculation. A simplified method of modelling the liquid inside the tank is required to keep handling of the model fast and tractable without significantly affecting the results.

6. *Assess the influence of boundaries, mesh properties and time stepping for dynamic calculation (free field site response analysis)*

   For a proper modelling of earthquake related problems the influence of boundaries effects, mesh configuration and time stepping procedure need to be investigated. These aspects can have a big influence on accuracy and computation time and are therefore important for the final model. A free field site response analysis will be used to assess the aspects listed above.

1.3 Delimitations

- The dynamic analysis is based only on horizontal shear waves that propagate vertically;
- Only the impulsive part of the fluid mass is considered;
- Outer tank is modelled as loads instead of real construction;
- Only two earthquake signals are discussed, one for OBE[1] and one for SSE[2];
- Liquefaction behaviour is outside the scope of this thesis;

[1] OBE = Operation Basis Earthquake , the LNG tank facility is expected to remain operational during/after an OBE event;
[2] SSE = Safe Shut-down Earthquake, it is not required that the LNG tank facility remains operational during/after a SSE event. The tank is designed to prevent catastrophic failure

2 RESEARCH APPROACH AND THESIS OUTLINE

The research approach is shown in Figure 2-1. In this scheme the research approach is coupled to the treated subjects. The thesis outline is visualised by the chapter numbers that are related to the different subjects of each phase.
The thesis consists of three phases: phase 1 represents the literature study and gathering of information for the case study project. Phase 2 consist of 3 smaller researches supporting the full dynamic model considered in Phase 3.

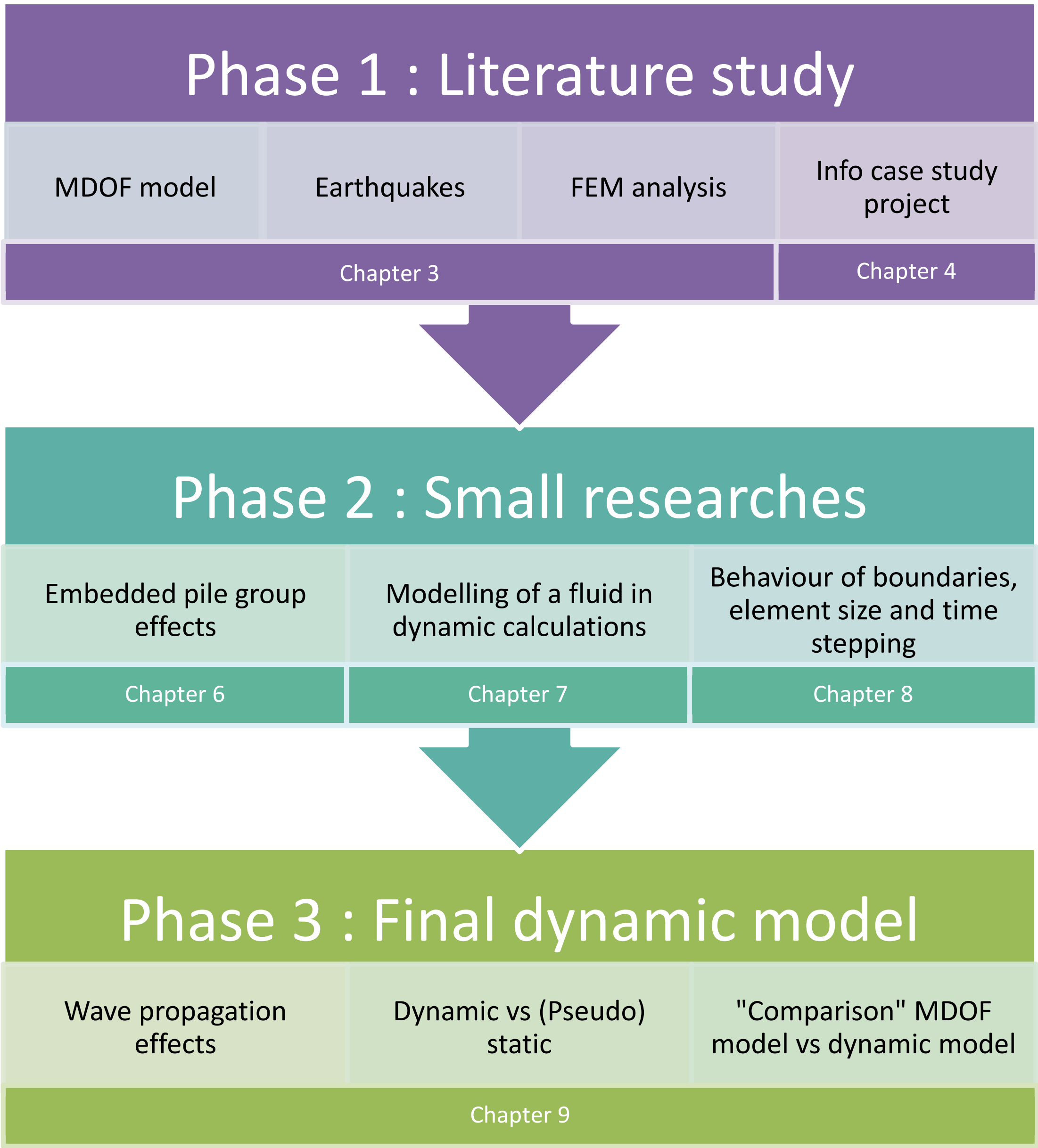

Figure 2-1 Research approach and thesis outline

2.1 Phase 1 : Literature study

In phase 1, information is gathered about different subjects as a starting for the smaller researches treated in phase 2:

- General information about earthquakes and seismic waves;
- General information about the MDOF model developed by TNO, used in previous dynamic analyses of LNG tanks. General operation of the model should be clear and strengths and weaknesses are assessed;
- General information about finite element method for modelling soil-structure interaction;
- Information in more detail about the material models available in PLAXIS;
- Information in more detail about PLAXIS embedded piles;
- General information about the Angola case. A LNG tank project performed in 2009

2.2 Phase 2 : Small researches

In phase 2, three smaller researches are conducted to investigate

- Embedded pile group behaviour.
  Embedded piles have the capability to reduce volumetric soil elements and nodes inside the finite element mesh. On the other hand their applicability in larger groups under lateral loading is doubtful. Applicability for this thesis is assessed by investigating different pile group effects.
- Modelling of a fluid
  The modelling of a fluid in PLAXIS is difficult. Modelling fluid as a soil layer leads to an enormous amount of elements and plastic behaviour. This combination will increase the computational times significantly. An alternative method for the modelling of a fluid is investigated.
- Free field site response
  Modelling of dynamic behaviour requires the application of dynamic model boundaries. Different lateral boundaries are investigated on their applicability in this thesis, together with the influence of mesh element size and time stepping procedure.

2.3 Phase 3 : Final model

The three researches performed in phase 2 are the basis for phase 3. In this phase a full dynamic calculation will be performed to achieve the stated research objectives from paragraph 1.2. Normative situation during the earthquake are considered in more detail by performing pseudo static calculations as well.

2.4 Thesis outline

The thesis is divided into 10 chapters, consisting of:

- Chapter 1: provides information about the main problem, research objectives and delimitations;
- Chapter 2: explains the approach of the research and the content of the report;
- Chapter 3: presents the theoretical background which is required for the analyses to be carried out in the following of this thesis;
- Chapter 4: provides general information about the case study project in Angola;
- Chapter 5: discusses the feasibility of a 3D full dynamic model;
- Chapter 6: investigates the pile group behaviour of embedded pile group in PLAXIS;
- Chapter 7: investigates the possibilities of a new method to model fluid behaviour in PLAXIS;
- Chapter 8: investigates the applicability of different dynamic model boundaries, together with the effect of mesh element size and time stepping procedure;
- Chapter 9: deals with the final dynamic model to achieve the stated research objectives;
- Chapter 10: contains the conclusion and recommendations that can be made based on the previous chapters.

The thesis outline is coupled to the research approach; this is visualized in Figure 2-1.

3 THEORETICAL BACKGROUND

3.1 MDOF model

Previous Dynamic analyses are performed with the aid of the Multi Degree Of Freedom (MDOF) model developed by TNO in cooperation with Royal HaskoningDHV. The model is based on the discrete substructure approach which means that the system components are represented by a limited number of discrete degrees of freedom. The model (Figure 3-1) contains 7 discrete masses that schematize the foundation, inner tank, outer tank (+ roof) and the liquid inside the tank.

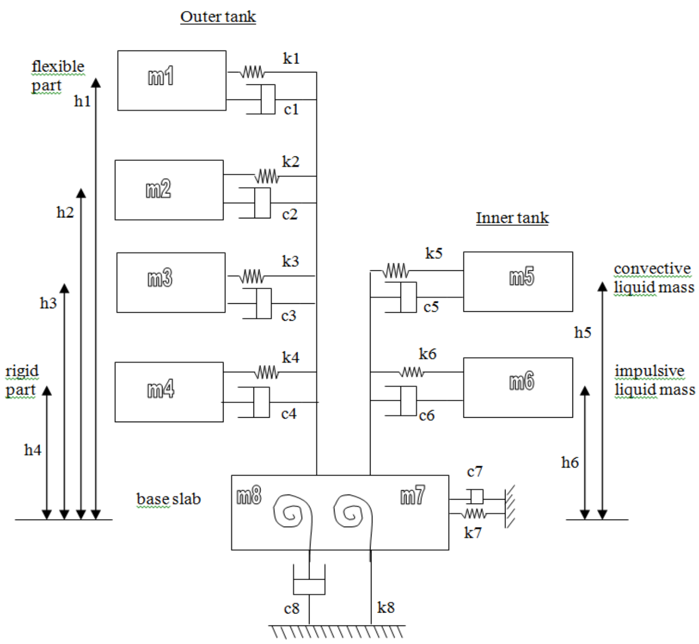

Figure 3-1 Schematic overview of MDOF model for dynamic calculations

The outer concrete tank is represented by 4 discrete masses. The dynamic characteristics of the tank masses are determined by means of a separate 3D FE-model. The inner tank and fluid are represented by 2 masses; one accounting for the combined impulsive motion of the inner tank + the fluid, and one accounting for the convective motion of the fluid (better known as sloshing mode). For the scenario with liquid in the inner tank only the dynamic characteristics of the fluid modes are calculated by means of analytical formulas available in literature. For the scenario with liquid in the annular space between the inner and outer tank wall as well the dynamic characteristic of the impulsive fluid mode are calculated by attaching the fluid mass to the outer concrete wall in the 3D static FEM-model of the outer tank. The last discrete mass represents the base slab, which is assumed to be rigid for the dynamic analysis. For the vertical direction the motion of the base slab is governed by a single translational degree of freedom. For the horizontal direction also the rotational degree of freedom is included. This rotational degree of freedom is introduced to account for the overturning causes by the lever arm of the various tank and fluid components with respect to the base slab.

The dynamic stiffness of the soil and the pile foundation is represented by a, frequency depended, spring and damper at the interface between the base slab and the fixed support.

Spring and damper properties are calculated by using Wolf's semi-infinite half space approach from (Wolf 1994).
The seismic load is first quantified as free field motion upon which the relative bas slab motions are then calculated together with the individual masses such that equilibrium is met, including soil structure interaction. The assumption is made that the tank diameter is small compared to the earthquake wave lengths, therefore horizontal and vertical motions are treated separately and no external rocking load is applied.
For the seismic load two design scenarios are considered, the OBE (Operating Basis Earthquake) and SSE (Safe Shutdown Earthquake) scenario. For each scenario 7 time traces are derived from the earthquake response spectrum for local circumstances.
The model output consists of the dynamic response of the individual masses. From this response the forces acting on each individual mass and the overall reaction forces on the foundation (vertical reaction, base shear and overturning moment) can be calculated. Extra information about the MDOF model can be found in (Galanti en Courage, Seismic analysis of storage tanks with soil structure interaction 2006) and (Paulissen 4 january 2013)

3.1.1 Tank analysis procedure

The tank analysis is implemented in MATLAB and performed in the time domain. A Fast Fourier Transformation (FFT) is used to convert the earthquake data from the time domain to the frequency domain to calculate the dynamic foundation response. An Inverse FFT is performed to convert the results back to the time domain for the tank analysis. Figure 3-2 shows the procedure for calculation of the seismic response of a tank according to (Galanti en Courage, Seismic analysis of three storage tanks in Angola 2009).

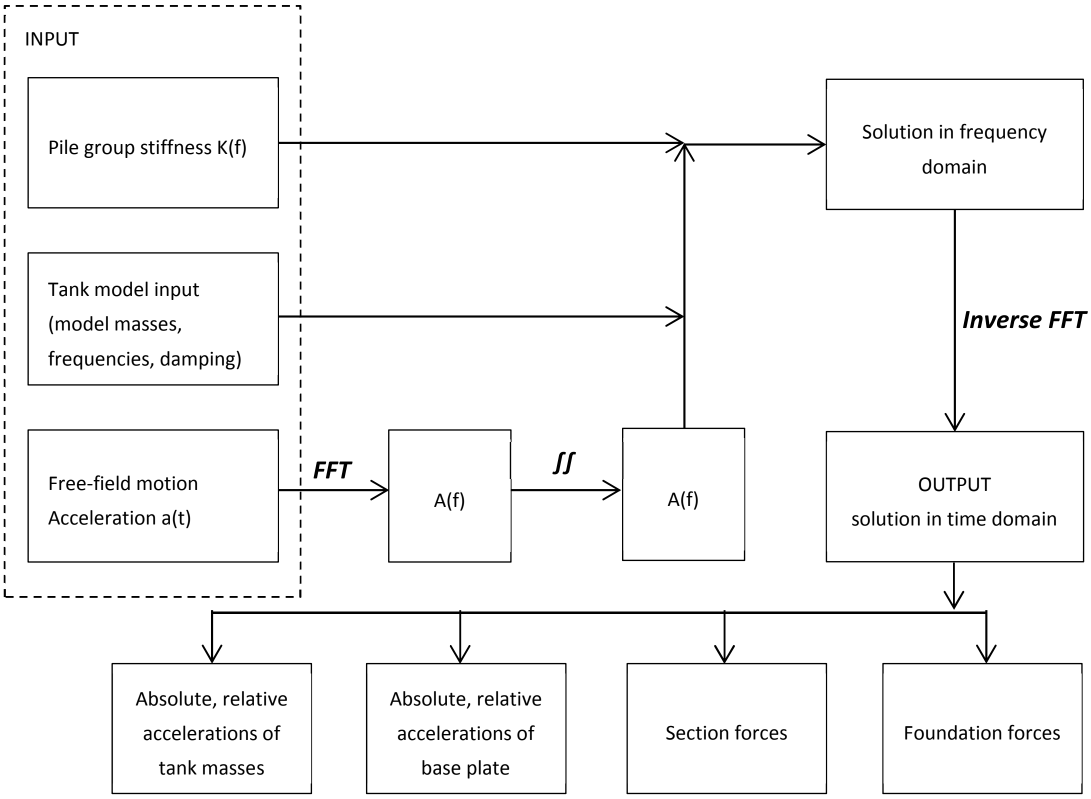

Figure 3-2 Procedure for calculation of seismic response of a tank

3.1.2 Pile (group) foundation model

The pile foundation model calculates the pile group stiffness. The group stiffness is calculated based on the dynamic stiffness of a single pile; in combination with interaction factors the stiffness of the complete group can be calculated. The model is based on the theory provide by [19] (Wolf 1994), the so called Wolf's cone model.
With the theory of Wolf's cone model the frequency dependent lumped dynamic stiffness and damping of foundations in and on layered soils can be calculated. The stiffness is linear elastic and the soil is assumed to be a semi-infinite half space with homogeneous soil layers. First the dynamic stiffness of a single floating pile is calculated by schematizing the pile as a number of rigid disks embedded in the elastic half-space. The stiffness of such a disk is calculated by the double cone model. By setting up a system of embedded rigid disks at regular intervals up to depth, which is equivalent with the length of the pile, the interaction of the pile with the soil can be described. By adding the pile stiffness + pile mass and subtracting the soil mass, which substitutes the pile, to the system the dynamic stiffness can be calculated. This process can be performed for as well horizontal, vertical and rocking motion component.
The interaction between piles (group effect) is taken into consideration by setting up a system of equations representing the pile displacements due to the pile loads in terms of a flexibility matrix. In this matrix the stiffness of a single pile is modified based on the fact that additional displacements are generated due to loading of piles in the surrounding. Specific formulas for the dynamic interaction in the horizontal and vertical directions are given in (Wolf 1994). The interaction which takes place between piles due to rocking is neglected.

Figure 3-3 shows the flow chart for calculating the pile group stiffness K(f). This figure also shows that the only input variables are the pile properties, pile group layout and the soil parameters: G, ν and ρ.

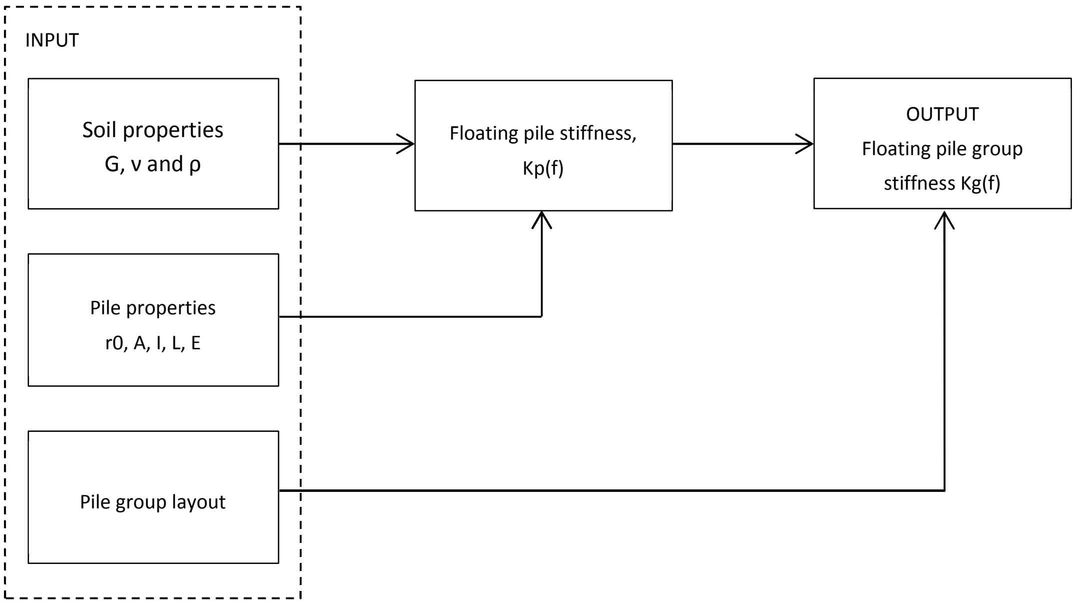

Figure 3-3 Procedure for calculation of dynamic pile group stiffness

3.1.3 Points of attention in the MDOF model

The MDOF model is a highly schematized representation of the real situation. It uses simplifications to keep the analysis manageable. This approach has the advantage that the model works fast, it requires limited modelling effort and analysis time is short. On the other hand this approach leads to some disadvantages and limitations.

Soil-structure interaction
Soil-structure interaction is the interaction between soil behaviour and the behaviour of the foundation, piles and base slab. The MDOF model uses the Wolf cone model for modelling the soil-foundation interaction. This model is only suitable for equivalent linear elastic analyses. This means that non-linear soil behaviour and plasticity is neglected.

Material behaviour of foundation piles
The MDOF does not take into account nonlinear behaviour of the foundation piles. It is possible that the will crack over at least part of the length during severe earthquake loads, this will lead to a loss of stiffness of the pile group.

Kinematic effects of foundation piles
The MDOF model does not account for a kinematic component of the pile force. This kinematic component can be caused by differential displacements between soil and piles over the length of the piles. Especially for large accelerations and liquefiable soils this effect can be significant. The wolf model calculates the dynamic stiffness and damping at the base slab level and does not account for kinematic effect of the piles.

Wave propagation effects
The MDOF model quantifies the seismic load as free field motion upon the base slab. The base slab is rigid and it therefore moves as a whole. This simplification is made based on the assumption that the tank diameter is small compared to the earthquake wave length. For large LNG tanks founded on softer soils this assumption might not be valid. In that case the seismic load is not uniformly distributed over the width of the base slab and additional forces are introduced.

Load coupling effects
Load coupling effect is the effect that mass of a structure might affect the local seismic load (accelerations, displacements) at the location of a structure.
The MDOF model quantifies the seismic load as free field motion upon which the relative base slab motion then is calculated. This approach assumes that the structure has no mass. For large LNG tanks the mass of the structure and stiffness of the pile foundation might affect the local seismic load at the location of the LNG tank. This aspect is neglected in the MDOF model.

Pre- and post-processing
For a proper dynamic calculation it is important that the methods used to calculate the input parameter match the assumptions and boundary conditions of the MDOF model. In terms of output it is important that results are used in the right way to calculate reaction forces in the piles. Due to the assumptions and schematizations in the MDOF model this input- and output process is not clear on all points.

3.2 Earthquakes

3.2.1 Earthquake origin

Earthquakes are vibrations of the earth’s surface due to suddenly release of energy in the Earth’s crust. This energy is build up gradually by stresses along plate boundaries and released suddenly as seismic waves, this is known as the elastic rebound theory (Figure 3-4 Elastic rebound theory). The stresses along the plate boundaries are induced by continental drift of the tectonic plates. The continental drift is caused by the convection currents within the Earth’s mantle forming a continuous cycle of heating and cooling of the materials it consists of.

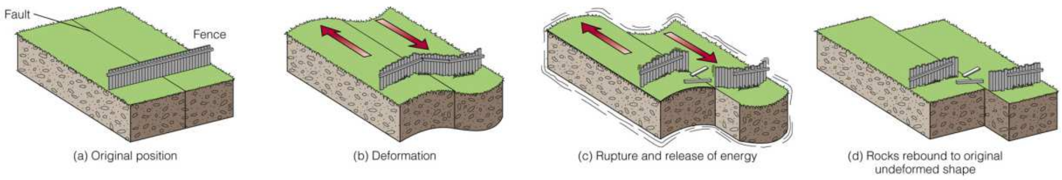

Figure 3-4 Elastic rebound theory

Earthquakes can be categorized by various criteria. In general two main categories can be distinguished: “Intra-plate” earthquakes, which are generated by faults in the interior of the plate, and “inter-plate” earthquakes that are generated due to friction along the faults between different plates (plate boundaries). Generally the inter-plate earthquakes are the strongest ones, since the build-up stresses are typically higher at these locations
Plate boundaries are categorized as divergent, convergent or transform, depending on the relative movement of the adjacent plates. Additionally, three types of fault movements can be identified, i.e. the normal, reverse fault (which are both dip-slip faults) and the strike-slip fault. The fault types are schematized in Figure 3-5.

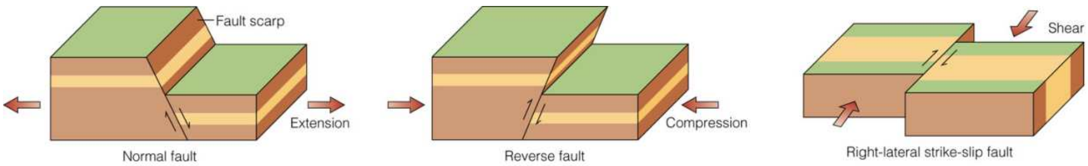

Figure 3-5 Normal fault, Reverse fault and the Strike-slip fault

The nature of faults and their activity is accounted for in probabilistic seismic hazard assessments. It is therefore why they are of interest. Additionally the distance of the site considered to the fault is of importance. For near-fault projects vertical ground motions, directivity effects and high frequency content of the seismic signal are important issues to consider in the design. While for far-fault projects horizontal ground motion is more important.

3.2.2 Seismic waves

The movement of the ground surface during an earthquake is a result of various seismic waves generated by the fault rupture. In general two basic types of waves can be distinguished: body waves and surface waves. The most important body waves are P-waves (compression- or primary waves) and S-waves (shear- or secondary waves). P and S waves are called body waves because they can pass through the interior of the earth. Surface waves are only observed close to the surface of the earth and they are subdivided into Love waves and Rayleigh waves. Surface waves are a result of interaction between body waves and the surficial earth material.

P-wave

The P-wave causes a series of compressions and dilations of the material through which it travels. The motion of an individual soil particle that is subjected to a P-wave is parallel to the direction of traveling wave.

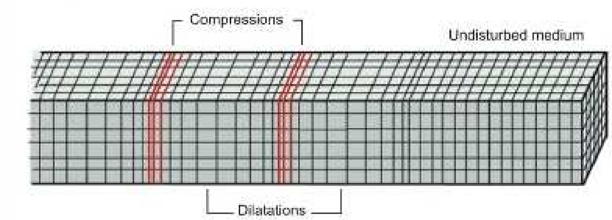

Figure 3-6 Schematization of a P-wave

Being a compression-dilation type of wave, P-waves can travel through both: solid and liquid materials. The P-wave is the fastest wave and is the first to arrive the site; its propagation speed can be obtained by the following equation:

$$V_p = \sqrt{\frac{E_{oed}}{\rho}} = \sqrt{\frac{G(2-2\upsilon)}{\rho(1-2\upsilon)}} \tag{3-1}$$

S-wave

The S-wave causes shearing deformations of the materials through which it travels. Because liquids have no shear resistance, S-waves can only travel through solids. The movement of an individual particle subjected to a S-wave can be divide into vertical and a horizontal component.

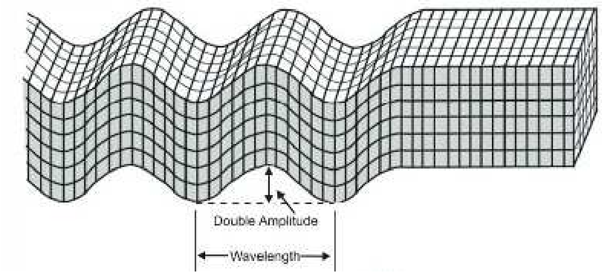

Figure 3-7 Schematization of a S-wave

The shear resistance of soil and rock is usually less than the compression-dilation resistance, therefore an S-wave travels more slowly through the ground than a P-wave. Its propagation speed can be obtained by the following equation:

$$V_s = \sqrt{\frac{G}{\rho}} \tag{3-2}$$

Love wave

Love waves are almost the same as S-waves: they are transverse shear waves but they travel close to the ground surface. Love waves are the fastest surface waves and move the ground side-to-side.

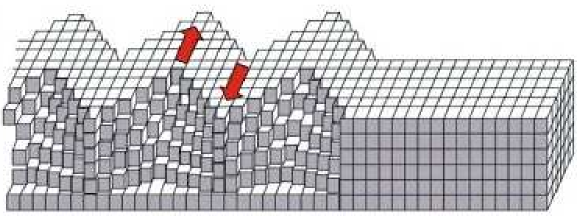

Figure 3-8 Schematization of a Love wave

Rayleigh wave

Rayleigh waves have been described as being similar to the surface ripples produced by a rock thrown into water. The Rayleigh waves a result of interaction between P-waves, vertical S-waves and the surface layer of the earth. They travel along the earth's surface with amplitudes that decrease exponentially with depth. The waves produce both: horizontal and vertical displacement of the ground.

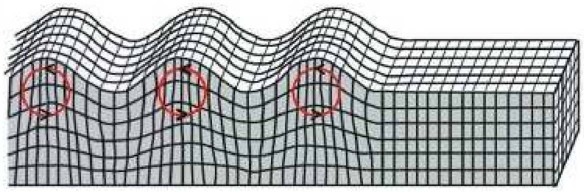

Figure 3-9 Schematization of a Rayleigh wave

The velocity of a Rayleigh wave is equal to

$$V_R = \eta \cdot V_s \tag{3-3}$$

In which

$$\eta = \frac{0.87 + 1.12\upsilon}{1 + \upsilon} \tag{3-4}$$

Wave propagation affects the seismic signal while it travels away from its source. Thereby understanding and using the principles of wave propagation make seismologists able to predict site soil response based on ground conditions along the travel path of the wave. Principles of dispersion, refraction, diffraction and filtering of wave signals are of importance in this sense. Traditionally, seismologists accounted for wave propagation by empirical local attenuation laws, which are averages found from recorded accelerograms. With increasing experience in this field specialist became able to define local seismic signals more accurately, by making use of advanced models. Nevertheless it should be noted that it is always to be recommended to check results by advanced models against these local empirical attenuation laws and simple site response analysis techniques.

3.2.3 Site amplification effects

Fault characteristics together with wave propagation effects determine the local bedrock ground motion intensity, frequency content and duration. Then to determine design ground level ground motions is to account for site amplification effects. It is noted that in this study the effects of surface waves are not considered, where it is restricted to the common engineering approach representing the seismic load by vertically propagating shear waves only.
The site amplification effects are characterized by the natural frequencies of the soil deposit, which can be estimated (Kramer 1996) based on the averaged present soil shear wave velocity and soil deposit height as:

$$f_n = \frac{v_s}{4H}\left(1+\frac{n}{2}\right), n = 0,1,2,.... \qquad (3\text{-}5)$$

Often the soil deposit parameters are taken over the top 30 meters of the deposit, but whether this common depth is appropriate is very much project dependent. Generally the top 30 meter approach is most appropriate for rather short period content of the bedrock signal, as for longer period's seismic wave lengths are much longer than 30 meters and response is likely to be affected by soil characteristics at much greater depths. From equation (3-5) the fundamental frequency and fundamental period of the soil deposit are easily derived by:

$$f_0 = \frac{1}{T_0} = \frac{v_s}{4H} \qquad (3\text{-}6)$$

It is noted that averaging the soil deposit characteristics over depth may result in inaccurate predictions of actual site amplification. A better estimate generally is obtained by performing site response analysis including the layering of the deposit.

3.2.4 Magnitude, Intensity and moment magnitude

There are three basic ways to measure the strength of an earthquake: magnitude, intensity and moment magnitude according to (Robert W. Day 2002).
Magnitude measures the amount of energy released from the earthquake. The most common magnitude scale applied in earthquake engineering practice is the Richter scale, ranging from 0 to 10. The scale was developed in 1935 by Professor Charles Richter for shallow and local earthquakes, it is therefore also known as the local magnitude scale M_L.
Intensity is based on the damage to building and reaction of people at a specific site (so it depends on distance from the epicenter and local soil conditions). The most commonly used scale for the determination of earthquake intensity is the modified Mercalli intensity scale. The intensity ranges from an earthquake that is not felt (I) up to an earthquake that result in total destruction (XII). In general, the larger the magnitude of the earthquake, the larger the area affected by the earthquake and the higher the intensity level.
Moment magnitude is a measure for the overall deformation at the fault and can be interpreted simply in terms of ground deformation. Seismic moment magnitude has become the more commonly used method for determining the magnitude of large earthquakes. This is because it tends to take into account the entire size of the earthquake. Seismic moment scales have been proposed by different researchers, e.g. (Hanks en Kanamori 1979), (Kanamori 1983) and (Yeats et al, 1997). More information regarding this earthquake measuring scales can be found in most earthquake engineering textbooks.

3.3 Finite element method

The finite element (FE) method is a computational procedure used to obtain approximate solution to engineering problems. In the finite element method a partial differential equation is numerically approximated and a continuum is discretised into a finite number of elements. The behaviour of these individual elements is in general readily understood. All elements are connected by nodes, were values of all primary variables are calculated. Each element has a number of degrees-of-freedom that correspond to the variable components, for example deformations in soil problems.
A continuum that is divided into elements is called a mesh. The elements inside the mesh usually consist of simple shapes like triangles, quadrilaterals or rectangles. In the case of 3D models this means a tetrahedral, cube or box. Full details in FE formulation in soil modelling are found in (Zienkiewicz en Taylor, The Finite Element Method 1967)

3.3.1 Displacement functions

In a three dimensional continuum a tetrahedron, with four nodal corners, is one of the most used elements for soil related problem. Figure 3-10 gives an illustration of a tetrahedron i, j, m, p in space defined by x, y and z coordinates.

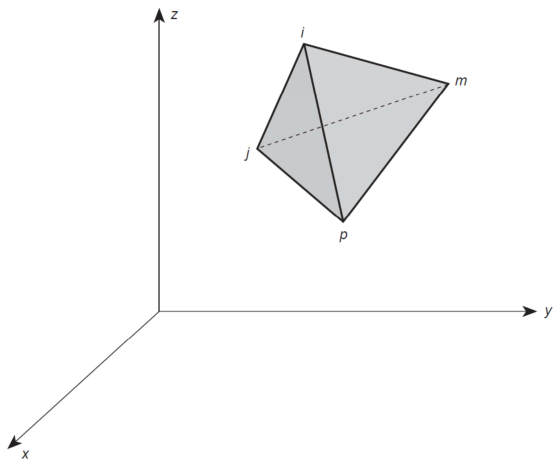

Figure 3-10 Tetrahedron i,j,m,p in three dimensional space

The displacements field u is obtained from the discrete nodal displacement values in a vector v by using the shape functions in matrix N

$$\underline{u} = \underline{\underline{N}} \cdot \underline{v} \tag{3-7}$$

In the case of a three dimensional continuum the displacements of a node have 3 components: x-, y- and z-direction. Combined they give the nodal displacement. Below this is shown for node i

$$\underline{v_i} = \begin{Bmatrix} x_i \\ y_i \\ z_i \end{Bmatrix} \tag{3-8}$$

For the complete element this will lead to a 12 component displacement vector

$$\underline{v_e} = \begin{bmatrix} v_i \\ v_j \\ v_m \\ v_p \end{bmatrix} \tag{3-9}$$

The shape functions in matrix N ensure that the displacements within an element are uniquely defined. In fact, the shape functions represent the interpolation of the primary quantity within the element.

3.3.2 Strain matrix

In a three dimensional continuum there are six strain components that are relevant. The strain matrix is defined as:

$$\underline{\varepsilon} = \begin{bmatrix} \varepsilon_x \\ \varepsilon_y \\ \varepsilon_z \\ \gamma_{xy} \\ \gamma_{yz} \\ \gamma_{zx} \end{bmatrix} = \underline{\underline{L}} \cdot \underline{\underline{N}} \cdot \underline{v} = \underline{\underline{B}} \cdot \underline{v} \tag{3-10}$$

In this formulation, B is the strain interpolation matrix which contains the spatial derivatives of the interpolation functions and L is the differential operator.

3.3.3 Elasticity matrix

In general, for elastoplastic behaviour of materials, the strain is split up into an elastic part and a part for plastic strains. This can be formulated as:

$$\underline{\varepsilon} = \underline{\varepsilon^e} + \underline{\varepsilon^p} \tag{3-11}$$

In this formulation the elastic part is in general given by the linear relation:

$$\underline{\varepsilon^e} = (\underline{\underline{D^e}})^{-1} \cdot \underline{\sigma} \tag{3-12}$$

In equation (3-12) D^e is the matrix of elastic moduli according to Hooke's law. The total stress-strain relation for elastic behaviour can be described by:

$$\underline{\sigma} = \begin{bmatrix} \sigma_x \\ \sigma_y \\ \sigma_z \\ \tau_{xy} \\ \tau_{yz} \\ \tau_{zx} \end{bmatrix} = \underline{\underline{D^e}}(\underline{\varepsilon} - \underline{\varepsilon_0}) + \underline{\sigma_0} \tag{3-13}$$

In this formulation ε_0 is the initial strain and σ_0 is the initial stress. With complete anisotropy matrix D, relating the six strain components to stress components, can contain 21 independent constants. This is due to symmetry.

3.3.4 Dynamic behaviour

The equation for time-dependent motion in a volume under the influence of a (dynamic) load is:

$$\underline{\underline{M}}\underline{\ddot{u}} + \underline{\underline{C}}\underline{\dot{u}} + \underline{\underline{K}}\underline{u} = \underline{F} \tag{3-14}$$

In this equation M is the mass matrix, C is the damping matrix, K is the stiffness matrix and F is the load vector and $\ddot{u}$, $\dot{u}$, u correspond to respectively acceleration, velocity and displacement. The last two terms of equation (3-14) ($K u = F$) correspond to the static deformation

In its simplest form the static stiffness matrix K represents a linear-elastic response. In this case the stiffness matrix K, which is build up from the element stiffness matrix K^n, can be formulated as described below:

$$\underline{\underline{K}} = \sum_{i=1}^{n} K^i \tag{3-15}$$

$$\underline{\underline{K^n}} = \int \underline{\underline{B^T}}\, \underline{\underline{D^e}}\, \underline{\underline{B}}\, dV \tag{3-16}$$

Were D^e is again the matrix of elastic moduli, B the strain interpolation matrix and n is the number of elements. A stiffness matrix that resembles the material response more accurately is obtained by including plasticity. In this case the stiffness matrix can be formulated as:

$$\underline{\underline{K^n}} = \int \underline{\underline{B^T}}\, \underline{\underline{D^{ep}}}\, \underline{\underline{B}}\, dV \tag{3-17}$$

Where D^{ep} is the elastoplastic material matrix based on the current state of stress. This elastoplastic behaviour can be described by different material models which will be treated in 3.4 Material models.

In equation (3-14), the mass matrix M is defined as the sum of all element masses (see equation (3-18)). The element mass matrix M^n is defined by equation (3-19). In this formulation N holds the shape functions and n is the number of elements.

$$\underline{\underline{M}} = \sum_{i=1}^{n} M^i \tag{3-18}$$

$$\underline{\underline{M}}^n = \rho \int \underline{\underline{N}}^T \underline{\underline{N}} \, dV \tag{3-19}$$

Matrix C, in equation (3-14), represents the material damping of the different materials. In reality damping is caused by friction or by irreversible deformations (plasticity or viscosity). With more viscosity or more plasticity, more vibration can be dissipated. Plasticity models already include these phenomena's and therefore show damping. In case this damping is not sufficient or if elasticity is assumed, matrix C can be used to take (extra) damping into account.

The damping matrix C in the finite element program PLAXIS is derived by the Rayleigh damping formulation. In this formulation C is a function of the mass and stiffness matrices. The global damping matrix in PLAXIS is formed by collecting the element damping matrices (see equation (3-20)), which are derived by equation (3-21):

$$\underline{\underline{C}} = \alpha_R \underline{\underline{M}} + \beta_R \underline{\underline{K}} = \sum_{i=1}^{n} C^i \tag{3-20}$$

$$\underline{\underline{C}}^n = \alpha_R^n \underline{\underline{M}}^n + \beta_R^n \underline{\underline{K}}^n \tag{3-21}$$

In this formulation, α_R^n and β_R^n are scalars, the so-called Rayleigh damping coefficients. In this way the damping is proportional to the mass and the stiffness per element. The coefficients α_R and β_R are related to the damping ratio. A larger α_R means that the lower frequencies are stronger damped; with a larger β_R the higher frequencies are damped stronger. The Rayleigh coefficients can be evaluated by means of the following relation between angular frequency ω and damping ratio ξ :

$$\xi = \frac{\alpha_R}{2\omega} + \frac{\beta_R}{\omega} \tag{3-22}$$

3.3.5 Time integration

In numerical dynamic calculations, the formulation of time integration is an important factor for the stability and accuracy of the calculation process. There are several different integration schemes, the most commonly used are explicit and implicit integration.

Explicit integration is relatively simple but it has some limitations in terms of time stepping. The implicit method is more difficult but also more reliable. In general the solution obtained with implicit time integration is more accurate and the calculation process more stable (Sluys 1992)

PLAXIS is using the implicit time integration scheme of Newmark (Brinkgreve, Engin en Swolfs, Manual Plaxis 3D 2012). With this method, the displacement and velocity at a point in time $t+\Delta t$ are expressed as:

$$u^{t+\Delta t} = u^{t} + \dot{u}^{t}\Delta t + \left(\left(\frac{1}{2} - \alpha_N\right)\ddot{u}^{t} + \alpha_N \ddot{u}^{t+\Delta t}\right)\Delta t^2 \tag{3-23}$$

$$\dot{u}^{t+\Delta t} = \dot{u}^{t} + \left(\left(1-\beta_N\right)\ddot{u}^{t} + \beta_N \ddot{u}^{t+\Delta t}\right)\Delta t \tag{3-24}$$

In the above equations, Δt is the time step. The Newmark coefficients α_N and β_N determine the accuracy of the numerical time integration. To find a stable solution, the following conditions must apply:

$$\beta \geq 0.5, \qquad \alpha_N \geq \frac{1}{4}\left(\frac{1}{2} + \beta_N\right)^2 \tag{3-25}$$

With the implicit time integration scheme, equation (3-14) can obtained at the end of time step $t+\Delta t$:

$$M\ddot{u}^{t+\Delta t} + C\dot{u}^{t+\Delta t} + Ku^{t+\Delta t} = F^{t+\Delta t} \tag{3-26}$$

3.4 Material models

3.4.1 General definitions

The state of stress at a point in a continuous medium may be defined by the stress components acting on three mutually orthogonal planes passing through a point. Normally these planes are taken perpendicular to the ones in the coordinate system. In this research, the Cartesian system (x, y, z) is used to describe the stress states.
For the case of a cubic body the different stress components on every plane are shown in Figure 3-11 below for the positive tensile direction.

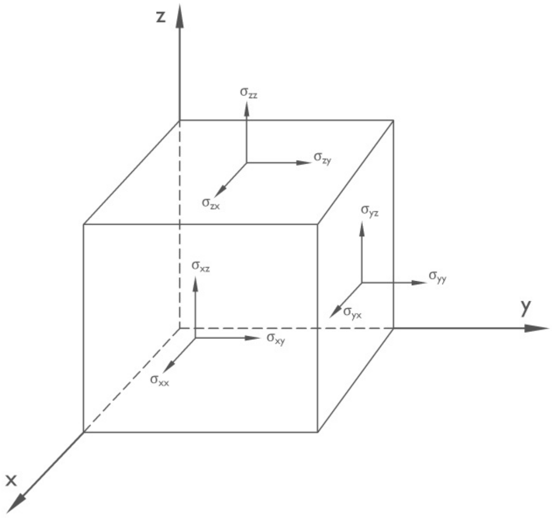

Figure 3-11 Stress components on cube in a three dimensional space

The different stress components on a plane can be combined to a stress vector τ acting on each plane of the cubic body:

$$\underline{\tau_x} = \begin{Bmatrix} \sigma_{xx} \\ \sigma_{xy} \\ \sigma_{xz} \end{Bmatrix}; \qquad \underline{\tau_y} = \begin{Bmatrix} \sigma_{yx} \\ \sigma_{yy} \\ \sigma_{yz} \end{Bmatrix}; \qquad \underline{\tau_z} = \begin{Bmatrix} \sigma_{zx} \\ \sigma_{zy} \\ \sigma_{zz} \end{Bmatrix} \tag{3-27}$$

In this formulation (for τ_x) σ_{xx} is the normal stress and σ_{xy} and σ_{xz} are the shearing stresses. The subscripts indicate the working direction of the stress components. The first letter indicates the plane on which it acts and the second describes the direction. This is similarly for the stress vectors working on the other planes. The total stress state of the cubic body can be presented by combining all stress vectors acting on the different planes. In total this formulation comprises nine stress components which are given as:

$$\underline{\underline{\sigma}} = \begin{bmatrix} \tau_x \\ \tau_y \\ \tau_z \end{bmatrix} = \begin{bmatrix} \sigma_{xx}\, \sigma_{xy}\, \sigma_{xz} \\ \sigma_{yx}\, \sigma_{yy}\, \sigma_{yz} \\ \sigma_{zx}\, \sigma_{zy}\, \sigma_{zz} \end{bmatrix} \tag{3-28}$$

These nine components can be reduced to six considering the symmetry in elastic soils without rotational stresses: $\sigma_{xy} = \sigma_{yx}$; $\sigma_{yz} = \sigma_{zy}$; $\sigma_{xz} = \sigma_{zx}$

The deformation of the cubic body is described by the strain. Every component of stress is related to an associated component of strain. If displacements in x-, y- and z-direction are respectively u, v and w the components of strain are given by:

$$\begin{aligned} &\varepsilon_{xx} = \frac{\partial u}{\partial x}\ ; && \varepsilon_{yy} = \frac{\partial v}{\partial y}; && \varepsilon_{zz} = \frac{\partial w}{\partial z} \\ &\gamma_{xy} = \gamma_{yx} = \frac{1}{2}\left(\frac{\partial u}{\partial y} + \frac{\partial v}{\partial x}\right); && \gamma_{yz} = \gamma_{zy} = \frac{1}{2}\left(\frac{\partial v}{\partial z} + \frac{\partial w}{\partial y}\right); && \gamma_{zx} = \gamma_{xz} = \frac{1}{2}\left(\frac{\partial w}{\partial x} + \frac{\partial u}{\partial z}\right) \end{aligned} \tag{3-29}$$

The total strain tensor for the cubic body can be presented by combining all strain vectors belonging to the individual planes:

$$\underline{\underline{\varepsilon}} = \begin{bmatrix} \varepsilon_{xx} & \gamma_{xy} & \gamma_{xz} \\ \gamma_{yx} & \varepsilon_{yy} & \gamma_{yz} \\ \gamma_{zx} & \gamma_{zy} & \varepsilon_{zz} \end{bmatrix} = \begin{bmatrix} \frac{\partial u}{\partial x} & \frac{1}{2}\left(\frac{\partial u}{\partial y} + \frac{\partial v}{\partial x}\right) & \frac{1}{2}\left(\frac{\partial w}{\partial x} + \frac{\partial u}{\partial z}\right) \\ \frac{1}{2}\left(\frac{\partial u}{\partial y} + \frac{\partial v}{\partial x}\right) & \frac{\partial v}{\partial y} & \frac{1}{2}\left(\frac{\partial v}{\partial z} + \frac{\partial w}{\partial y}\right) \\ \frac{1}{2}\left(\frac{\partial w}{\partial x} + \frac{\partial u}{\partial z}\right) & \frac{1}{2}\left(\frac{\partial v}{\partial z} + \frac{\partial w}{\partial y}\right) & \frac{\partial w}{\partial z} \end{bmatrix} \tag{3-30}$$

3.4.2 Stress-strain relation

The relation between stress and strain at some point in a continuum is described by:

$$\underline{\sigma} = \underline{\underline{D}}\,\underline{\varepsilon} \tag{3-31}$$

This relation, in a slightly different form, was already presented in paragraph 3.3.3. In equation (3-31) D is denoted as the stiffness matrix. It describes the stress-strain behaviour of the continuum. In general six types of stress-strain response can occur; all are presented in Figure 3-12.

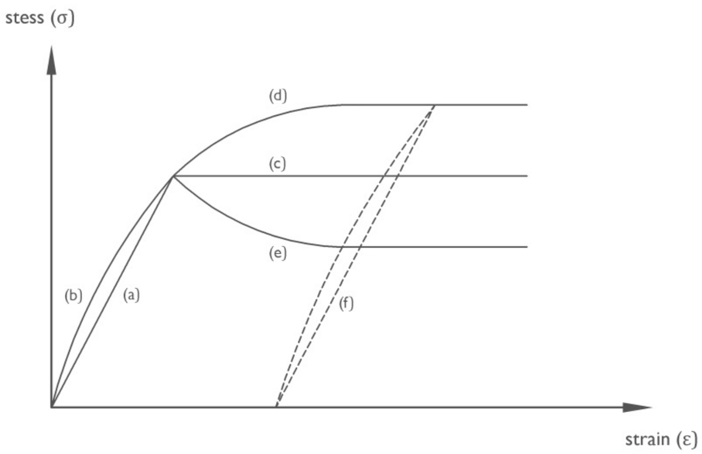

Figure 3-12 Stress-strain responses

Curves (a) and (b) represent the elastic loading phase; with the difference that (a) shows linear elastic behaviour and (b) nonlinear elastic behaviour. Curves (c), (d) and (e) represent the plastic behaviour. Curve (c) is perfectly plastic and (d) and (e) are respectively strain hardening and strain softening. The last curve, (f), shows the elastic unloading/reloading.

The behaviour of soils can be described by different soil models. In these models the response is related to material properties, loading path and stress-strain history. All models are available in the finite element program PLAXIS and are described in (Brinkgreve, Engin en Swolfs, Manual Plaxis 3D 2012). Models relevant for this thesis are described in the following paragraphs.

3.4.3 Linear elastic model

The linear elastic model is the most basic soil model. It is based on the equation of Hooke's Law for isotropic linear elastic behaviour. This means that plasticity is not included. The two elastic stiffness parameters that are used in the model are Young's modulus E (or Shear modulus G) and the Poisson's ratio ν. In general this model is not suitable to model soil behaviour in a proper way.

3.4.4 Mohr-Coulomb model

When deformation increases, the assumption of perfect linearity gives a very poor description of soil behaviour. To include nonlinearity the theory of plasticity can be included. The Mohr coulomb model is a linear-elastic perfectly-plastic model. Hooke's law is used to describe the linear elastic part while perfectly plastic material behaviour is represented by the Mohr-Coulomb failure criterion (see Figure 3-13).

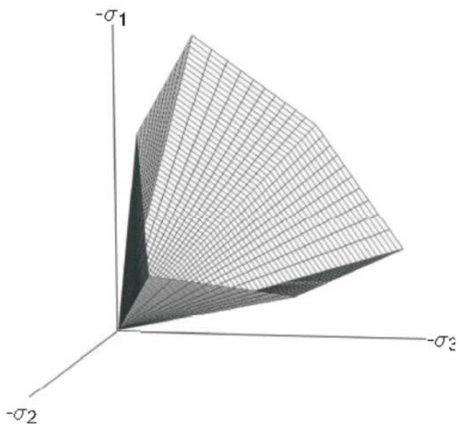

Figure 3-13 Mohr-Coulomb yield surface in principal stress space

The Mohr-Coulomb failure surface is fixed, i.e. it is fully defined by the material parameters and not affected by (plastic) straining. For stress states represented by points within the yield surface, the behaviour is purely elastic and strains are reversible. The model involves five parameters that are listed in Table 3-1 Input parameter of Mohr-Coulomb modelTable 3-1.

Parameter	Explanation
φ	Friction angle
C	Cohesion
ψ	Dilatancy angle
E	Young's modulus
ν	Poisson's ratio

Table 3-1 Input parameter of Mohr-Coulomb model in PLAXIS

In general, failure and plastic behaviour is pretty well captured in the Mohr-Coulomb model. On the other hand the stiffness behaviour before plastic yielding is modelled less accurate. Especially in situation where stress is changing significantly or in case that different stress paths are followed.

3.4.5 Hardening soil model

The hardening soil (HS) model developed by Schanz is an advanced model for simulating the behaviour of soft soils as well as harder types of soil. The model is related to the well-known hyperbolic model (Duncan & Chang, 1970) but some important aspects are added:

- Theory of plasticity is used rather than elasticity;
- Soil dilatancy is included;
- A yield cap is introduced (See Figure 3-14).

In contrast to the Mohr-Coulomb model, the yield surface of the HS model is not fixed in principle stress space. As a result of plastic straining the yield function may develop, this phenomenon is called hardening. In general we can distinguish two types of hardening: strain- and kinematic hardening. Only strain hardening is included in the HS model of PLAXIS and can be subdivided in: compression- and shear hardening. In case of compression (or cap) hardening, the cap of the yield surface is put aside due to primary compression that creates irreversible plastic strains. Additionally, shear (or friction) hardening is used to model irreversible strains due to primary deviatoric loading. Deviatoric loading corresponds to a difference of stresses in x- and y-direction. With both compression hardening and shear hardening, the elastic region is enlarged. This is shown in Figure 3-15. Inside the yield contour, resulting from previous stress/strain states, the material governs elastic behaviour. In PLAXIS this is governed by parameter E_{ur} .

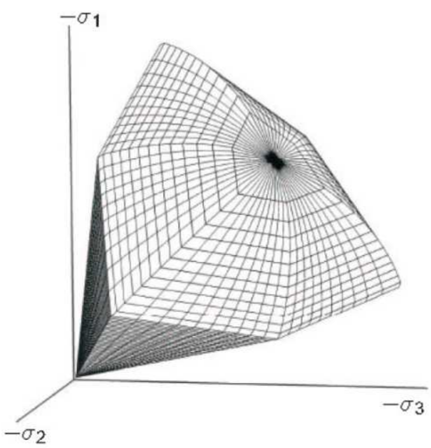

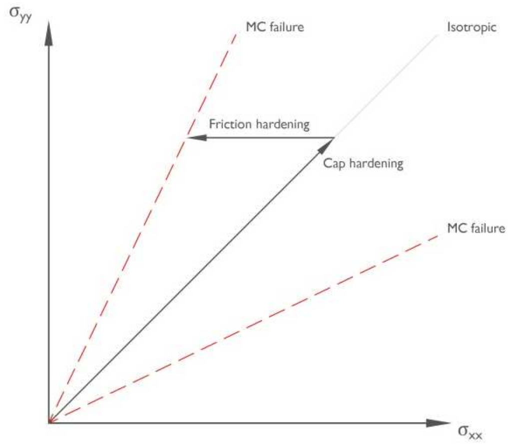

Figure 3-14 HS yield surface with cap presented in principal stress space
Figure 3-15 Cap- and friction hardening

Failure in the HS model is defined by means of the Mohr-Coulomb failure criterion, based on ultimate strength parameters c' and φ' . The failure line is schematically represented in Figure 3-15. In PLAXIS effective strength/stiffness parameters are used as input parameters for both drained and undrained analysis. For undrained situations two calculation methods can be distinguished in PLAXIS:

Undrained calculation method A: material behaviour is described by effective parameters in combination with excess pore pressure generation

Undrained calculation method B: material behaviour is described by effective stiffness parameters with undrained shear strength, this removes the stress dependent stiffness from the model.

With respect to the stiffness behaviour, the model uses a power law formulation for the stress dependency of stiffness. In PLAXIS this is for secant stiffness:

$$E_{50} = E_{50}^{ref}\left(\frac{c\cos\varphi - \sigma'_3 \sin\varphi}{c\cos\varphi - p^{ref}\sin\varphi}\right)^m \tag{3-32}$$

For E_{oed} and E_{ur} a similar relation is used. In total the HS model requires 11 input parameters. All input parameters are discussed in Table 3-2.

Parameter	Explanation
E_{50}^{ref}	Secant stiffness modules in standard drained triaxial test
E_{oed}^{ref}	Tangent stiffness modulus for primary oedometer loading
E_{ur}^{ref}	Unloading/reloading stiffness (default $E_{ur}^{ref} = 3 \cdot E_{50}^{ref}$)
m	Power for stress-level dependency of stiffness
ν_{ur}	Poisson's ratio for unloading and reloading
p^{ref}	Reference stress for stiffness (default $p^{ref} = 100\ kN/m^2$)
φ	Effective friction angle
c	Effective cohesion
ψ	Dilatancy angle
K_0^{nc}	K_0-value for normal consolidation (default $K_0^{nc} = 1 - \sin(\varphi)$)
R_f	Failure ratio q_f / q_a (default R_f =0.9)

Table 3-2 Input parameters of Hardening Soil model in PLAXIS

The HS-model shows a lot of improvements compared to the MC-model. It can be used to accurate predict displacements and failure for static types of geotechnical problems in both soft and stiffer soil types. The model does not include anisotropic strength/stiffness behaviour, time depended behaviour (creep) and its capabilities for dynamic calculations are limited.

3.4.6 Hardening soil small model

In the previous paragraph it was mentioned that in the HS model unloading/reloading behaviour is assumed to be linear elastic within the yield surface. However, the strain range in which soils can be considered truly elastic is very small. When strains increase, unloading/reloading stiffness has a nonlinear decency of strain.

In the Hardening Soil Small strain (HS-Small) model the small strain stiffness relation is implemented according to the formulation of (Benz 2006). Because this small strain approach can be included in many elasto-plastic models, it is called the 'small strain overlay model'.
The overlay model is based on the modulus reduction curve, formed by the shear modulus, G, plotted as logarithmic function of the shear strain, γ.The shape of the curve is purely related to the shear strain corresponding to 72.2% of G_0, known as $\gamma_{0.7}$. The stiffness at very small strains, G_0, and $\gamma_{0.7}$ are the only parameters that differentiate the HS-small model from the original HS model.

The small-strain stiffness is described with a simple hyperbolic law proposed by (Hardin en Drnevich 1972) and modified by [18] (Santos en Correia 2001), see equation (3-33). The basic characteristic of this hyperbolic relation is the decrease of stiffness with increasing strain due to loss of intermolecular and surface forces within the soil skeleton. This is shown below for as well the secant shear modules as tangent modulus. The tangent expression can be used in the time integration procedure and is found by differentiation with respect to strain.

$$\frac{G_s}{G_0}=\frac{1}{1+0.385\left|\frac{\gamma}{\gamma_{0.7}}\right|} \quad \Rightarrow \quad G_s=\frac{G_0}{1+0.385\left|\frac{\gamma}{\gamma_{0.7}}\right|} \tag{3-33}$$

$$\frac{G_t}{G_0}=\frac{1}{\left(1+0.385\left|\frac{\gamma}{\gamma_{0.7}}\right|\right)^2} \tag{3-34}$$

Plotting the reduction curves according to equation (3-33) and (3-34) shows that the reduction tends to zero for infinite shear strains, this is represented in Figure 3-16. In the HS-small model the tangent modulus reduction curve is cut-off by a lower limit G_{ur}, derived from the material parameters E_{ur}^{ref} and ν_{ur} (see equation (3-35)). The tangent shear modulus is derived by the material properties E_t^{ref} and ν_{ur} (see equation (3-36)). The lower cut-off of the tangent shear modulus is introduced at the unloading reloading shear modulus, $G_t = G_{ur}$

$$G_{ur}=\frac{E_{ur}^{ref}}{2\left(1+\nu_{ur}\right)} \tag{3-35}$$

$$G_t = \frac{E_t^{ref}}{2\left(1+\nu_{ur}\right)} \tag{3-36}$$

The cut-off shear strain can be calculated as:

$$\gamma_{cut-off} = \frac{1}{0.385}\left(\sqrt{\frac{G_0}{G_{ur}}}-1\right)\gamma_{0.7} \tag{3-37}$$

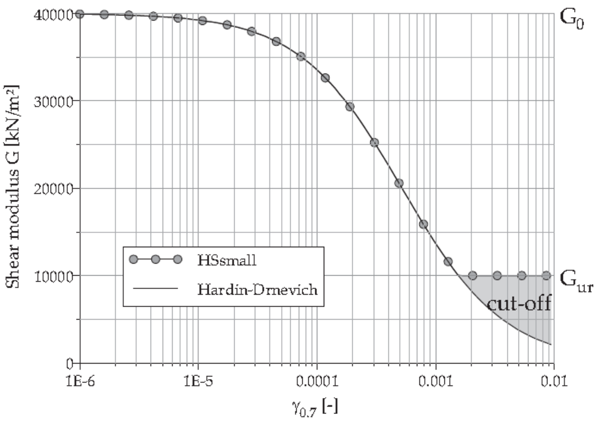

Figure 3-16 Example of a modulus reduction curve

Hysteretic behaviour in the HS-small model

The HS-small model shows hysteretic behaviour in case of cyclic loading. Strain reversals switch back to the original intermolecular structure and therefore the maximum small strain stiffness is recovered. Every time the loading direction is changed a full 180 degrees, in a hysteretic loop, the stiffness is supposed to restart at its maximum.

The inclination of the hysteretic loop, depicted in Figure 3-17, is related to the stiffness of the soil while the surface is related to the damping. The inclination can be described at any point and directly arises from the modulus reduction curve. The average value can be approximated by the secant shear modules, G_s, which is defined as the ratio of maximum shear stress over maximum shear strain.

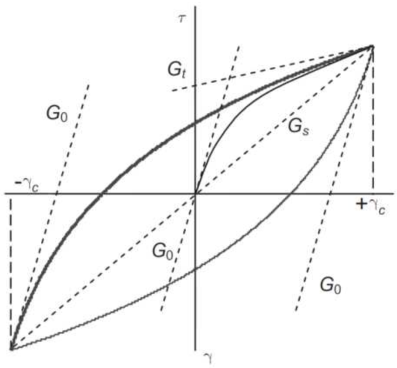

Figure 3-17 Hysteretic behaviour in the HS-small model

Under dynamic loading, unloading/reloading loops as included in the HS-small model (see Figure 3-17) introduce a hysteretic damping component. This damping can be formulated as a damping ratio according to (Kappert 2006), as presented below:

$$\xi = \frac{2}{\pi} + \frac{\gamma_{0.7}}{0.09625\pi\gamma_{tot}} - \frac{4}{\pi\ln\left(1 + \frac{0.385}{\gamma_{0.7}}\gamma_{tot}\right)} \tag{3-38}$$

The damping ratio is defined as $\xi = 1$ for critical damping, i. e. exactly the amount of damping needed to let a single degree-of-freedom system that is released from an initial excitation u_0, smoothly stop without rebounding.

According to the relation of (Hardin en Drnevich 1972) for G/G_0 as function of shear strain, this damping will be negligibly small for small motion amplitudes, which appears to be unrealistic compared to actual soil behaviour. Therefore it is recommended, according to (Brinkgreve, Bonnier en Kappert, Hysteretic damping in a small-strain stiffness model 2007), to introduce additional Raleigh damping in the model. For this Rayleigh damping 1-2% of the critical damping may be assumed to be reasonable. The same study shows that the hysteretic damping at higher shear strain levels resulting from the HS-small model to be overestimating actual material damping in clayey materials. This can be solved by adjusting G_0 closer to G_{ur}.

Concluded the HS-small model contains the following parameters:

Parameter	Explanation
E_{50}^{ref}	Secant stiffness modules in standard drained triaxial test
E_{oed}^{ref}	Tangent stiffness modulus for primary oedometer loading
E_{ur}^{ref}	Unloading/reloading at engineering strains ($\varepsilon \approx 10^{-3}$ *to* 10^{-2})
m	Power for stress-level dependency of stiffness
ν_{ur}	Poisson's ratio for unloading and reloading
G_0^{ref}	Reference shear modulus at very small strains ($\varepsilon < 10^{-6}$)
$\gamma_{0.7}$	Shear strain at which $G_s = 0.722G_0$
p^{ref}	Reference stress for stiffness (default $p^{ref} = 100\ kN/m^2$)
φ	Effective friction angle
c	Effective cohesion
ψ	Dilatancy angle
K_0^{nc}	K_0-value for normal consolidation (default $K_0^{nc} = 1 - \sin(\varphi)$
R_f	Failure ratio q_f / q_a (default R_f =0.9)

3.5 PLAXIS embedded piles

3.5.1 General

The Plaxis embedded pile model considers the pile as slender beam element, which is connected to the soil by embedded skin interfaces and embedded foot interfaces. The pile may cross the bulk soil elements at any arbitrary position and with an arbitrary inclination (see Figure 3-18). Because the embedded pile is modelled as a beam element it does not contain a volume. Instead there is a particular elastic volume around the pile (elastic zone) whose dimension is related to the pile diameter. In this elastic zone, the plastic behaviour of the soil is neglected (see Figure 3-18). This makes the embedded pile almost behave like a volume pile.

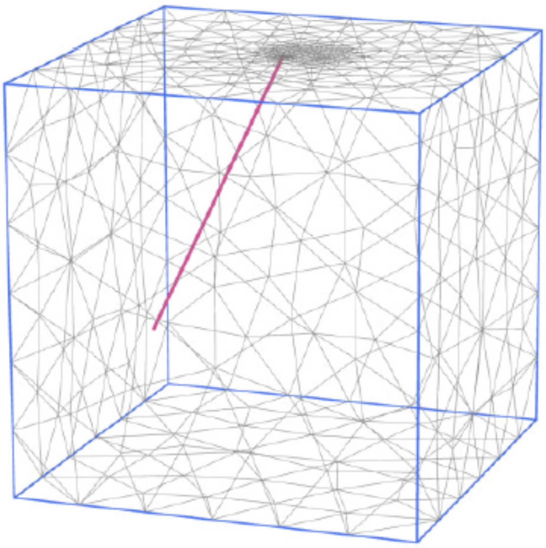

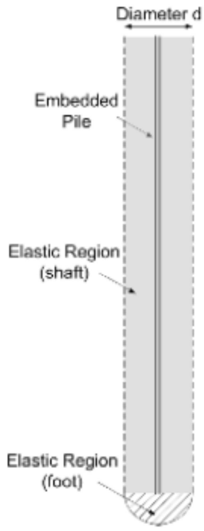

Figure 3-18 Embedded pile in 3D mesh and elastic zone around embedded pile e

Compared to the volume pile, which is created of volume elements, the embedded pile has some benefits in terms of calculation time and evaluation of output. In contrast to the volume pile, no corresponding geometry points are created. This means that the embedded pile doesn't influence the mesh that is generated from the geometry model. The mesh refinement is lower and therefore the calculation time will be shorter. Another advantage is that the embedded pile is modelled as a beam structure. This makes it possible to read out forces directly from Plaxis 3D output. In the case of a volume pile this is more difficult, because it is modelled by means of a soil volume which is assigned with a manipulated soil material. In contrast to the volume pile, pile-soil interaction of an embedded pile is modelled at the centre rather than at the circumference.
In general, the embedded pile can be considered as a simplified model of a volume pile. The following three paragraphs will provide some extra information about the pile-soil interaction, influence of coefficient R_{inter} and the required material parameters. More information can be found in the different manuals from Plaxis 3D (Brinkgreve, Engin en Swolfs, Manual Plaxis 2D 2012)

3.5.2 Pile soil interaction

During the mesh-generation stage, new nodes are generated representing the pile(beam) nodes at the intersection points between the pile and the soil elements. The special interfaces, modelling the pile-soil interaction, are created by the connection between the new pile nodes and the existing soil nodes. The special interface elements are different from the regular interface elements as used along walls and volume piles. At the position of the beam element nodes, virtual nodes are created in the soil volume element from the element shape functions. The special interface elements connects these virtual nodes with the pile (beam) nodes, and thus with all nodes of the soil volume.
An elasto-plastic model is used to describe the behaviour of the special interfaces. The interaction is split up in skin resistance (in unit of force per circumference per length) and tip resistance (in unit of force). Together they provide the bearing capacity of the embedded pile. Both, skin- and tip resistance, has a failure criteria to distinguish between elastic and plastic behaviour at the interface.
The skin resistance (t^{skin}) at the interface is represented by the following equation:

$$\underline{t}^{skin} = \underline{t}_0^{skin} + \Delta \underline{t}^{skin} \tag{3-39}$$

Where:

$\underline{t}_0^{skin}$: initial skin resistance;

$\Delta \underline{t}^{skin}$: force increments at the integration points.

The constitutive relation between the skin friction increments and the relative displacement increments is formulated as:

$$\Delta \underline{t}^{skin} = \underline{\underline{T}}^{skin} \cdot \Delta \underline{u}_{rel} \tag{3-40}$$

Where:

$\Delta \underline{t}^{skin}$: force increments at the integration points;

$\underline{\underline{T}}^{skin}$: material stiffness matrix of the interface element;

$\Delta \underline{u}_{rel} = \underline{u}^p - \underline{u}^s$: relative displacement vector between the pile and the soil.

Equation (3-40) can be rewritten to the 3D local coordinate system (t, n, s) as presented in equation (3-41).

$$\begin{bmatrix} t_s \\ t_n \\ t_t \end{bmatrix} = \begin{bmatrix} K_s & 0 & 0 \\ 0 & K_n & 0 \\ 0 & 0 & K_t \end{bmatrix} \begin{bmatrix} u_s^p - u_s^s \\ u_n^p - u_n^s \\ u_t^p - u_t^s \end{bmatrix} \tag{3-41}$$

Where:

t_s : shear stress in axial direction;

t_n and t_t : normal stress in horizontal directions (remain elastic);

K_s : elastic shear stiffness;

K_n and K_t : elastic normal stiffness in horizontal directions;

u^p : displacement of the pile;

u^s : displacement of the soil.

By default the values for K_s, K_t and K_n are defined such that the stiffness of the embedded interface elements does not influence the total elastic stiffness of the pile-soil structure:

$$K_s >> G_{soil}$$
$$K_n = K_t = \frac{2(1-\upsilon)}{1-2\upsilon} K_s \qquad (3\text{-}42)$$

Figure 3-19 gives a visualization of the constitutive relation presented in equation (3-41).

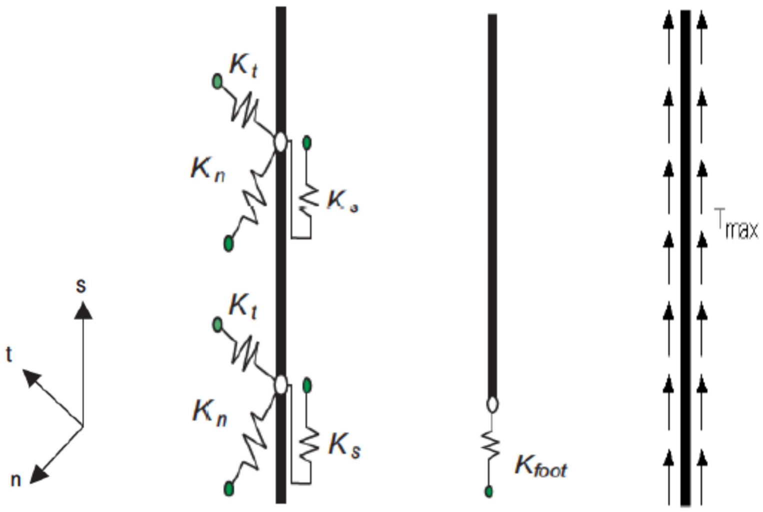

Figure 3-19 Stiffness relations along the pile

In the material dataset T_{max} is one of the input variables. The value of T_{max} defines the behaviour of the interface and the value of the shear force t_n at a particular point. For the interface to remain elastic the shearforce t_s at a particular point is given by:

$$|t_s| < T_{max} \qquad (3\text{-}43)$$

For plastic behavior the shear force t_s is given by:

$$|t_s| = T_{max} \qquad (3\text{-}44)$$

The skin resistance T_{max} in Plaxis 3D can be model in three ways:
- Constant/Linear over the length;
- Multi-linear, to take account of inhomogeneous or multiple soil layers;
- Layer dependent, to relate skin resistance to the strength properties.

In addition to the skin resistance, the foot resistance is defined by a non-linear spring at the pile foot (see Figure 3-19). The spring connects the pile foot to the surrounding soil. The force acting on the spring is represented by:

$$\underline{f}^{foot} = \underline{f}_0^{foot} + \Delta \underline{f}^{foot} \tag{3-45}$$

Where:

$\underline{f}_0^{foot}$: initial force at the foot;

$\Delta \underline{f}^{foot}$: force increments at the foot.

The constitutive relation between the force increments at the foot and the relative displacement increments is formulated as:

$$\Delta \underline{f}^{foot} = \underline{\underline{D}}^{foot} \cdot \Delta \underline{u}_{rel} \tag{3-46}$$

Where:

$\Delta \underline{f}^{foot}$: force increments at the foot;

$\underline{\underline{D}}^{foot}$: material stiffness matrix of spring element at the foot;

$\Delta \underline{u}_{rel} = u_{foot}^{p} - u_{foot}^{s}$: relative displacement vector between the pile foot and the soil.

Equal to the situation of the shaft resistance there is a failure criterion for the foot resistance which is formulated with the aid of input value F_{max}:

$$F_{axial}^{foot} \leq F_{\max} \quad \text{(compression)} \tag{3-47}$$

$$F_{axial}^{foot} = 0 \quad \text{(tension)} \tag{3-48}$$

The pile-soil interaction parameters in the embedded pile material data set involve only the pile bearing capacity (skin resistance and base resistance). This means that the material dataset does not include the stiffness response of the pile in the soil (or p-y curves). The stiffness response is the result of the pile length, equivalent radius, bearing capacity and stiffness of the soil layers in which the pile is located.

To ensure a realistic bearing capacity, as specified, a zone without any soil plasticity is specified around the beam. The size of this elastic zone is based on the pile's diameter or equivalent radius R_{eq}. Because of the elastic zone, the embedded pile almost behaves like a volume pile. However, pile-soil interaction is modelled at the pile centre.

In addition to displacement differences and shears forces in axial direction along the pile, the pile can undergo transverse forces, due to lateral displacements. These transverse forces are not limited in the special interface element (t_n and t_t equation (3-41) remain elastic) that connects the pile to the soil, but they are limited due to failure of the surrounding soil (outside elastic zone). In general embedded piles are not meant to be used as laterally loaded piles because they don't show accurate failure loads when subjected to lateral loads. However, at small loads and displacement their behaviour seems reasonable for use in situations with lateral loads.

3.5.3 Influence of R_{inter} on the behaviour of pile soil interaction

The skin resistance in Plaxis 3D is the shear resistance of the interface in axial direction of the pile. Like explained before, the skin resistance is based on the input value T_{max} which can be described by a constant/linear, multi-linear or layer dependent model. Within this third option, the skin resistance directly relates to the strength parameters of the surrounding soil and the strength reduction factor R_{inter}. This means that the value of R_{inter} has direct influence on the pile-soil interaction in case of axially loaded piles.
In the case of earthquake movements the most important deformations are in lateral direction. It is therefore important to known the influence of R_{inter} on the lateral pile-soil interaction. An explanation can be provided by the stiffness of the embedded interface element in lateral directions (K_t and K_n in equation (3-41) and Figure 3-19) and the information provide in (Brinkgreve, Engin en Swolfs, Manual Plaxis 2D 2012). K_n and K_t denote the elastic normal stiffness (against perpendicular displacement differences) of the embedded interface elements, whereby the normal stresses t_n and t_t will always remain elastic. Initially K_n and K_t are only relate to the Poisson's ratio and not to the strength parameters of the soil. R_{inter} only affects the strength parameters for plastic behavior; this means that R_{inter} doesn't has any influence on the lateral pile-soil interaction.

3.5.4 Input-parameters for embedded piles

Properties and model parameters for embedded piles are entered in separate material data sets. In general a data set for an embedded pile contains: a pile type, pile material, geometric properties and the interaction properties witch the surrounding soil (pile bearing capacity). It should be taken into account that, in contrast to what is common in finite element modeling, the bearing capacity of an embedded pile is an input parameter rather than a result of the calculations.

The embedded pile is modeled as a slender beam element and there are, beside the geometric parameters, five input parameters required (see Table 3-3)

Parameter	Explanation
γ	*Unit weight of the pile*
E	*Young's modulus*
Pile type	*Massive circular pile / circular tube / massive square pile*
D	*Diameter of pile (only for massive circular or circular tube pile)*
W	*Width (massive square pile)*
Thickness	*Wall thickness (circular tube)*
A	*Cross-sectional area*
I_3, I_2	*Moment of inertia around respectively the third and second axis*
$T_{\max}$	*Maximum skin resistance*
$F_{\max}$	*Maximum allowed base resistance*

Table 3-3 Input parameter PLAXIS embedded pile

From the above described geometric properties an equivalent radius R_{eq} is determined, which will specify the elastic zone. The equivalent radius R_{eq} is specified as:

$$R_{eq} = \max\left\{\sqrt{A/\pi}, \sqrt{2I_{avg}/A}\right\} \text{ where } I_{avg} = (I_2 + I_3)/2 \qquad (3\text{-}49)$$

4 CASE STUDY PROJECT

In this thesis the focus is on the soil-structure interaction of a LNG tank under seismic loading. For calculation purposes there is chosen a case project, the already mentioned "Angola project" The project included the development of a LNG plant and marine terminal, the project is finished in 2010. Besides two LNG tanks, the project included one LPG tank, one Propane tank, one LPG Butane tank and a condensate tank. This thesis is focussing on the LNG tanks.
In this chapter all relevant information about the project is provided that is needed in the next phases of this thesis.

4.1 Project location

As the name suggest, the project is in Angola. The project site is located along the west coast in the delta of the Congo River near the town of Soyo. The general location of the site is shown in Figure 4-1 below.

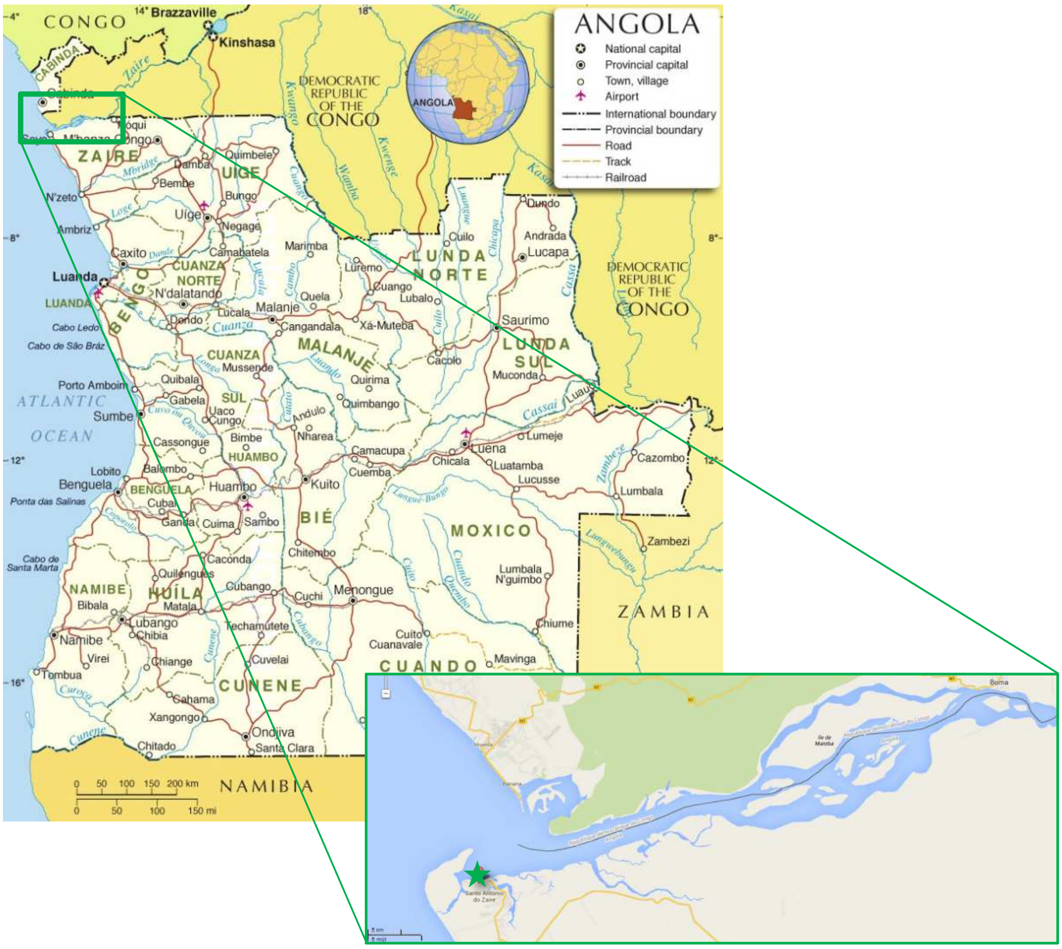

Figure 4-1 Project location

4.2 LNG tank geometry

The LNG tank considered in this thesis is a full containment tank, consisting of open-top inner tank and concrete outer tank. The steel inner tank contains the cold liquid, the concrete outer tank provides primary vapour containment and secondary liquid containment. In the unlikely event of a leak, the outer tank contains the liquid and provides controlled release of the vapour. Both tanks in the Angola project have the same design and are founded on about 1300 piles. Figure 4-2 provides a generalized cross section of the LNG tanks.

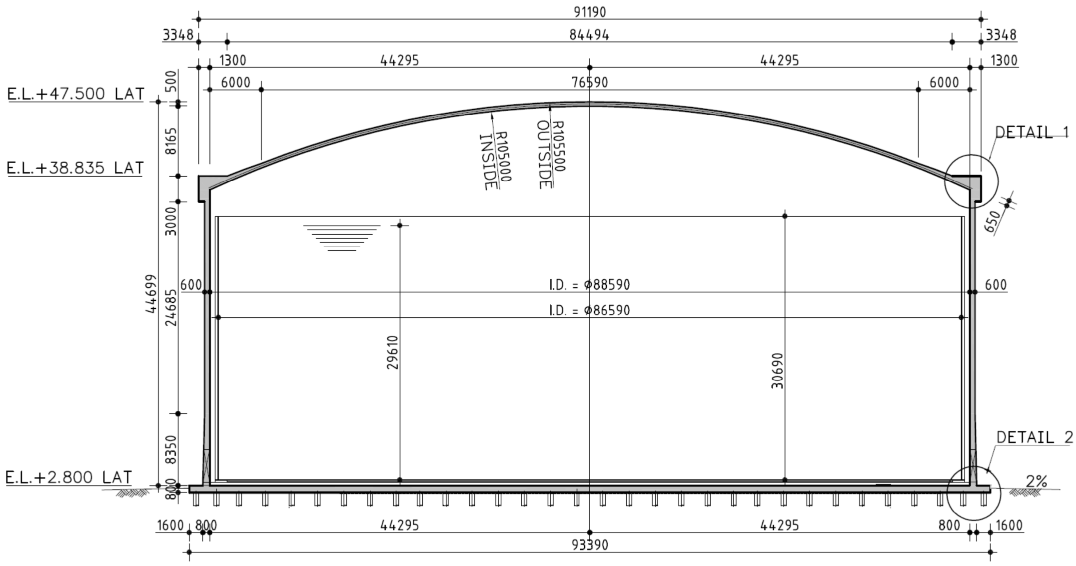

Figure 4-2 Cross section of LNG tank

The diameter of the LNG tank is about 90 meters. The concrete storage structure for the LNG tank consist of a piled foundation (steel piles, diameter 610 mm), a reinforced concrete base slab (thickness 800), a (horizontally and vertically) pre stressed concrete wall (thickness varying from 800 mm to 600 mm) and a thin reinforced concrete dome (thickness varying from 450 mm to 500 mm). More detailed information about the tank and dimension can be found on the drawing in Appendix A.

4.2.1 Construction properties

From geotechnical perspective all constructions above ground level will be modelled as elastic materials without any plastic behaviour. This also applies for the material behaviour of the steel foundation piles. However, their geotechnical bearing capacity in axial direction is limited. More about this subject is explained in paragraph 3.5. Table 4-1 shows the parameters that are used for the modelling of the base slab and Table 4-2 shows the used parameters for the foundation piles. Only the basic parameters are given at this moment because the more advanced parameters are not yet determined. The properties for the concrete outer tank are not provided at this moment. Probably the outer tank will be modelled as two surface loads located at the connection with the base slab.

Parameter	Explanation	Value	Unit
Type	*Isotropic plate*		
EA	*Axial rigidity/stiffness*	24.0 E6	[kN/m]
EI	*Bending stiffness*	1.28 E6	[kNm2/m]
d	*(Equivalent) Thickness, based on EI and EA*	0.80	[m]
w	*Specific weight*	20.0	[kN/m/m]
v (nu)	*Poisson's ratio*	0,20	[m]

Table 4-1 Base plate properties

Parameter	Explanation	Value	Unit
E	*Elasticity modulus*	2.1 E8	[kN/m2]
γ	*Gamma, specific weight of steel*	78	[kN/m3]
Pile type	*Predefined Circular tube*		
D	*Outer diameter*	0.61	[m]
t	*Wall thickness*	0.017	[m]
$T_{top;max}$	*Maximum skin resistance at the top of the pile*	0	[kN/m]
$T_{bottom;max}$	*Maximum skin resistance at the bottom of the pile*	145	[kN/m]
F_{max}	*Maximum base resistance of the pile*	2650	[kN]

Table 4-2 Embedded pile properties

4.3 Seismic activity

The LNG site is located on the central West Coast of Africa on the Atlantic passive margin of the African tectonic plate. The Atlantic margin of the African plate is now characterized by a low rate of seismic activity, which is typical of passive plate margins. However, large earthquakes are known to have occurred in rifted passive margins through reactivation of relict structures in a modern stress field (Johnston 1994). The regional maximum horizontal compressive stress in West Africa is oriented in northeast-southwest direction (Zoback en Zoback 1989).
In regions of low and diffuse seismicity, not associated with a specific source (such as West Africa), the seismic hazard is most of the time quantified by a probabilistic seismic hazard analysis (SHA). Such an analysis is performed for the Angola project by MMI Engineers.
In a probabilistic SHA, earthquake ground motions for the site are estimated considering the uncertainty in the location of an earthquake, its size and the intensity of ground vibrating. In the Angola project, real events from the past, area sources and fault sources are combined in a probabilistic analysis that have led to the design response spectra for an operating basis earthquake (OBE) and a safe shutdown earthquake (SSE). The response spectra are presented in Figure 4-3 below. The response spectra are representative for soil type A according to NEHRP 1996, which means bed rock level.

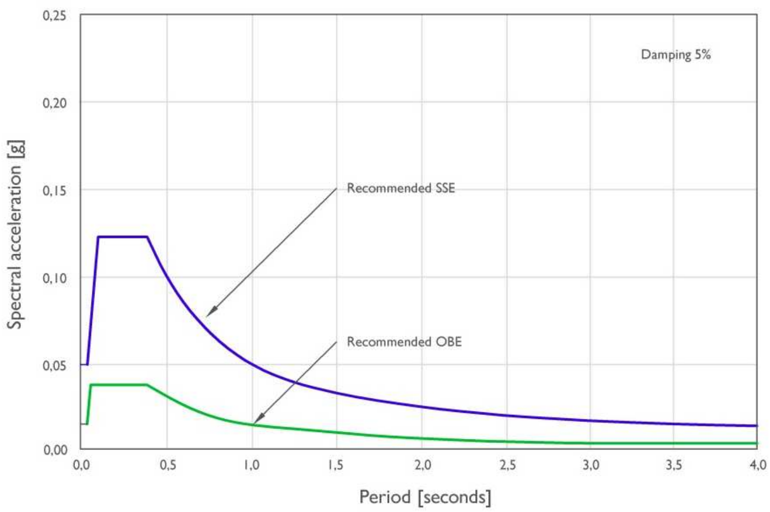

Figure 4-3 Design response spectra used for OBE and SSE

The OBE earthquake has a mean return period of 1/500 year, which is equivalent to a probability of exceedance of 10% in 50 year. The peak acceleration of the OBE earthquake is $a_{g;bedrock;OBE}$ = 0.02 g. The SSE earthquake has a mean return period of 2500 year, which is equivalent to a probability of exceedance of 2% in 50 years. This earthquake can be related to a peak bedrock acceleration of $a_{g;bedrock;SSE}$ = 0.05 g.

The values for peak bedrock acceleration show the low level of seismic activity in this region. More information about the composition of the site response spectra for both, OBE and SSE situation, can be found in Appendix B.

4.4 Geotechnical characterisation

The soil structure on the project site is characterized by three layers: a manmade sandy top layer, a softer clayey core and a stiffer deep soil of sand. The layers are assumed to be straight and continuous; this isn't realistic compared to a real situation, but it is representative for the goals in this thesis.

To account for the dynamic behaviour, all soil layers are modelled with the hardening soil small strain model (see 3.4.6 Hardening soil small model). Although this model has not been designed specifically for dynamic application, it does have capabilities to describe dynamic soil behaviour to some extent. The small-strain stiffness formulation involves degradation of the shear stiffness with the shear strain, and it takes into account that the high small-strain stiffness is regained upon load reversal. When subjected to cyclic shear loading the model shows hysteresis. This feature provides damping in dynamic calculations (Brinkgreve, Bonnier en Kappert, Hysteretic damping in a small-strain stiffness model 2007).
The parameters that are used to describe these layers during the different analyses are based on soil survey executed. Because previous analyses only required limited soil parameters several empirical correlations are used to determine proper parameter sets for the hardening soil small strain model. Important correlations were found from (Brinkgreve, Engin en Engin, Validation of emperical formulas to derive model parameters for sands 2010) for sands, from (Vardanega en Bolton 2011) for clays and from (Benz 2006) regarding small strain soil behaviour.
All soil parameters that are used to describe the different layers are summarized in Table 4-3.

Parameter	Sand Fill *Loose - Medium dense*	Clay *Medium stiff*	Sand *Medium Dense-Dense*	Unit
γ_{unsat}	18	15	18	[kN/m3]
γ_{sat}	20	15	20	[kN/m3]
$E_{50;ref}$	20000	3000	40000	[kN/m2]
$E_{oed;ref}$	20000	1500	40000	[kN/m2]
$E_{ur;ref}$	60000	15000	120000	[kN/m2]
power (m)	0,5	0,9	0,5	[-]
P_{ref}	100	100	100	[kN/m2]
e_{init}	0,5	0,5	0,5	[-]
c'_{ref}	0	$S_{u;inc}$ = 1.591 Y_{ref} = -2.00	0	[kN/m2]
ϕ'	32		34	[°]
ψ'	2		4	[°]
$\gamma_{0,7}$	1,66E-04	9,00E-04	1,33E-04	[-]
$G_{0;ref}$	78261	37500	156522	[kN/m2]
ν_{ur}	0,15	0,2	0,15	[-]

Table 4-3 Soil parameters

5 FEASIBILITY OF A 3D FULL DYNAMIC MODEL

The feasibility of a full dynamic 3D model is mainly depending on computational time. With the current finite element packages, in this thesis PLAXIS, the dynamic behaviour of soil and soil-structure interaction is described in such a way that a full dynamic 3D model appears to be within the capabilities in terms of modelling. The question is whether these models are practicable on the basis of computational time and post processing.

In the Angola case a LNG tank with a diameter of 90 meters, founded on nearly 1,300 closely spaced piles (foundation level -36 m. below surface) has to be modelled. Proper modelling of such a big structure in dynamic analyses would require a very large model to exclude boundary effects due to reflection of seismic waves. A large model indirectly means: a mesh consisting of many elements. This certainly applies to a model with the 1,300 closely spaced foundation piles. For a good description of their behaviour, different piles must be separated by at least two finite elements. This means that even more elements are needed.
For a good description of both: soil behaviour and soil-structure interaction, a model will require more than 500,000 elements. According to (Brinkgreve 2013, personal communication), models with 500,000 elements or more in combination with a dynamic calculation is currently not feasible. Calculation times will be up to several days or even a week and handling of output will be very slow. This is not desirable, especially for this thesis. Aspects such as minimum required number of time steps, maximum element size and plastic behaviour of the soil are neglected in the foregoing. These aspects will lead to even longer computation times and difficulties in handling of the output.

There are however a number of alternatives that can be applied to model the problem in PLAXIS 3D and reduce calculation time:

- Model half the tank
  A symmetry axis can be placed through the centre of the tank, in this way only halve the geometry should be modelled. Despite a halving of the number of elements it seems not a viable solution. A model will still require a mesh consisting of about 500,000 elements for a good description of soil behaviour and soil-structure interaction. This is not feasible. Besides this there is the possible influence of wave reflections from the lateral symmetry boundary, even if only horizontal shear wave parallel to the lateral boundary are applied.

- Model a cross-section of the tank (semi 2D)
  A “strip” of the base plate could be modelled. This semi 2D model should only contain one or two pile spacings in out of plane direction. In this way it is possible to judge wave propagation effects in the soil and between the piles. Elements inside the mesh can probably be reduced to less than 10% of a full 3D model. On the other hand there are uncertainties about the influence of wave reflections from the lateral symmetry boundaries, even if only horizontal shear wave parallel to the lateral boundary are applied.

- Replace piles by soil layer
  All piles can be replaced by a soil layer with equivalent stiffness. This will lead to a significant reduction of the number of elements inside the mesh which means that the calculation process is faster and the handling of the model is more convenient. For investigation of the actual pile-soil behaviour, parts of the equivalent soil layer can be replaced by the real pile geometry. Figure 5-1 on the next page shows a schematization of the described model. The feasibility of this possible solution has not been investigated yet.

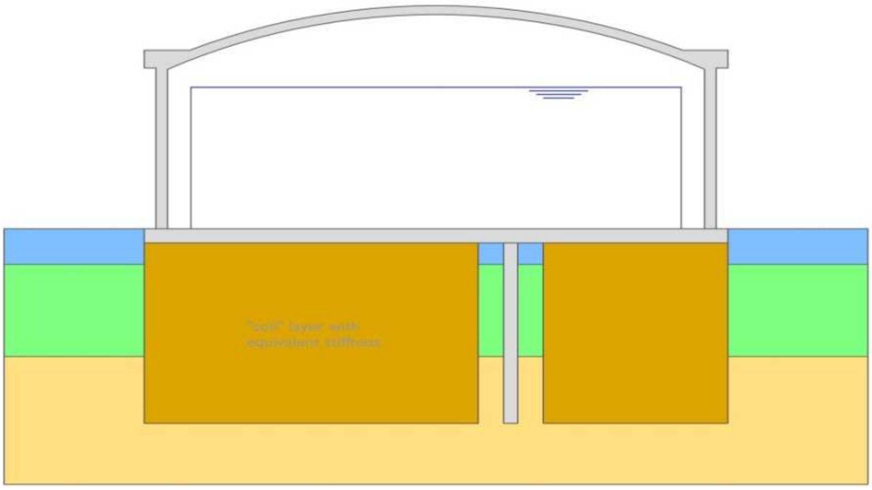

Figure 5-1 Schematization of model with piles replaced by soil layer with equivalent stiffness

Due to the complexity, long computation times and difficulties in handling of the output a full 3D dynamic model is no longer part of this thesis. There are a number of simplifications possible to continue the analyses in a 3D space. However, due to the uncertainties in required elements (indirectly calculation time), the unclear influence of wave reflections from the lateral symmetry boundaries and the limited advantages compared to a 2D calculation there is chosen to perform the dynamic analyses in PLAXIS 2D. This software has already proven its capabilities for full dynamic calculations.

Although a full dynamic 3D model is practically not feasible at this moment, the company of Royal HaskoningDHV still like to investigate different aspects of a LNG tank under seismic loading in a 3D model. This because of the continuous development of PLAXIS and still growing computing power an integral model can become feasible in the near feature. In this thesis the subjects: embedded pile group effects and modelling of the fluid are therefore investigated in as well PLAXIS 2D as 3D. The remaining two main objectives are investigated with the aid of a 2D model.

In general three distinct models can be applied in a 2D analysis. All types are schematized in the figures below and have their advantages and limitations are described on the next page.

Symmetric 2D model

A symmetrical 2D model is based on a symmetry axis in the centre of the baseplate. This means that only half of the structure is modelled in a 2D plane. For a dynamic analysis, as conducted in this thesis, a symmetrical 2D model is not an option because of boundary effects. The structure is modelled against the lateral symmetry boundary of the model and calculation results will probably be influenced by wave reflections from this boundary. Besides this the model implies a non-cylindrical wall that is infinitely long in out-of-plane direction.

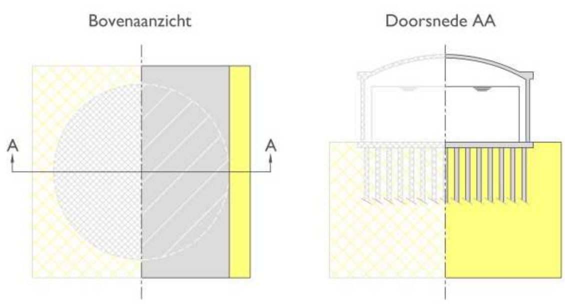

Axisymmetric 2D model

In an axisymmetric geometry the baseplate is again modelled with a symmetry axis in the centre of the baseplate. The symmetry is supposed to be in radial direction around this axis. This type of model is again not suitable for seismic calculations due to the location of the model boundary and the possible influence of wave reflections. Besides this it is difficulties to apply non-axial symmetric loads (horizontal shear waves) in an axisymmetric model. In general a 2D axisymmetric model is only used for axial problem, such as an axially loaded pile.

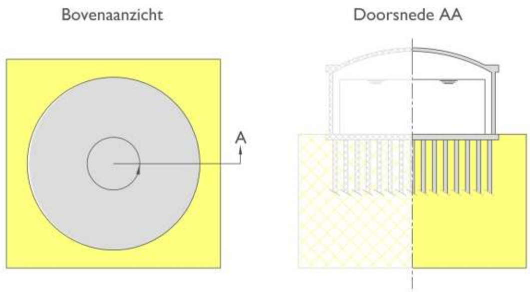

Complete 2D model (plane)

In a "complete" 2D model an actual section of the construction is modelled. For the objectives defined in this thesis a complete 2D model is the best solution. The complete diameter of the tank is taken into account which means that wave propagation effects over the length of the tank can be assessed.

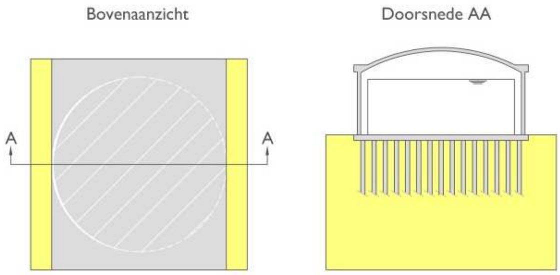

A disadvantage is that this model implies a non-cylindrical wall that is infinitely long in out-of-plane direction.

6 STATIC EMBEDDED PILE GROUPS EFFECTS

In general, horizontal (soil) movement is the most important movement during an earthquake for LNG- and other liquid storage tanks. Horizontal (soil) movement can cause movement of the liquid inside the tank which will lead to severe forces on the tank wall, base plate and foundation. Due to the large amount of piles (closely spaced) under the considered tank and the importance of horizontal (soil) movement, more knowledge about the behaviour of embedded pile groups in PLAXIS 3D and embedded pile rows in PLAXIS 2D is valuable. If PLAXIS will be used for a full dynamic three dimensional model, calculation time will be an important issue. Embedded piles have the ability to reduce calculation time but there are still limitations. Embedded piles do not show accurate failure loads for lateral behaviour (Brinkgreve, Engin en Swolfs, Manual Plaxis 2D 2012). It is therefore important to verify the behaviour of the embedded pile for the used application.

6.1 Analysis in PLAXIS 3D and PLAXIS 2D

The goal of this small investigation is to assess the applicability of embedded pile(s) (rows) for this thesis. This is done by verifying the group behaviour of static laterally loaded pile groups by comparing results from PLAXIS with results found in literature. Group behaviour is assessed at displacement levels that are identical to the displacements found in the Angola case.
It is expected that the lateral pile loads in the Angola case are far removed from the actual failure load, this applies to both static- and dynamic phase, and therefore embedded piles can be applied.

6.1.1 Situation and input parameters

Pile group behaviour of laterally loaded embedded piles is checked in a static situation. Different geometries (pile lines and pile groups) are subjected to a lateral load applied as point displacement at the pile head. After the analysis of a single pile, the problem is scaled up to larger pile lines and groups. The situation can be schematized by the following picture:

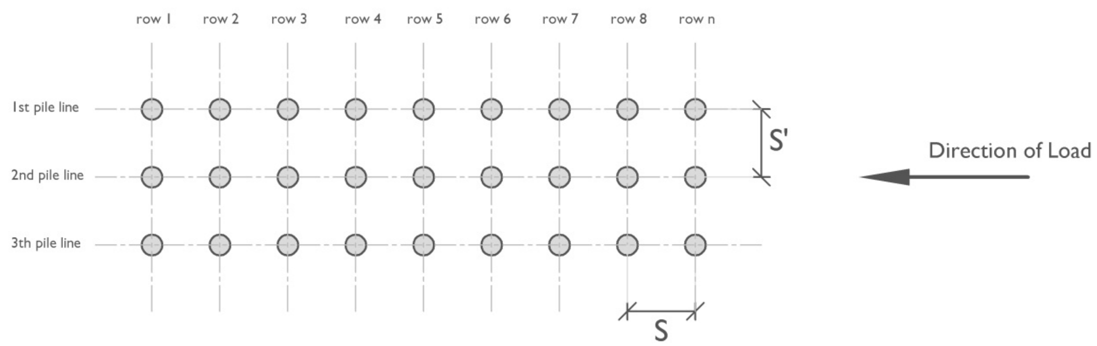

Figure 6-1 Situation

All piles will be subjected to a point displacement of the same value that is applied at the same moment in time. In essence the pile group can therefore be seen as a group of piles that are connected at the head by a stiff plate (same pile-head movement) with the exception that in this analysis the interaction between the plate and the soil is neglected.
In total three different pile spacings (centre-to-centre) are considered: 1.5 D, 2.0 D and 3.0 D. The values are easy to model and include the ranges of pile spacings that are used in the Angola case. For pile groups, the spacing is applied for both, the pile rows and pile lines.

The first analysis considers the case of single pile and is a reference analysis. After this, the geometry is scaled up to one pile line with varying rows and finally pile groups consisting of 3 pile lines and varying pile rows are considered. In total 7 geometries are considered with 3 different pile spacings.

Soil conditions

The analyses are performed in a very basic soil profile consisting of only one soil layer. Group behaviour of embedded piles is supposed to be depending on the way of how they are modelled in PLAXIS and not on the soil conditions. Results are compared to literature results representative for comparable soil conditions and pile spacings.

There is chosen to model medium dense sand with properties comparable to the medium dense sand found in the “Angola” case. The soil is modelled with the Hardening Soil Small strain (HS Small) model, more information about this model can be found in paragraph 3.4.6. This model has been chosen because of the dynamic analyses that will be performed in the following of this thesis. Table 6-1 provides an overview of the soil-parameters that are used.

Soil : Medium dense sand (HS Small)			
γ_{unsat}		18	[kN/m^3]
γ_{sat}		20	[kN/m^3]
$E_{50;ref}$		45 E+3	[kN/m^2]
$E_{oed;ref}$		50 E+3	[kN/m^2]
$E_{ur;ref}$		135 E+3	[kN/m^2]
power (m)		0.5	[-]
e_{init}		0.5	[-]
c'_{ref}		0.5	[kN/m^2]
ϕ'		34	[°]
ψ'		4	[°]
$\gamma_{0,7}$		0.2 E-3	[-]
$G_{0;ref}$		1.45 E+5	[kN/m^2]

Table 6-1 Sand properties

Pile properties

The piles are open ended steel piles (D = 610 mm), equal to those in the Angola case. The length, 10 meter, is chosen randomly, again under the assumption that the group behaviour of embedded piles is supposed to be depending on the way of how embedded piles are modelled in PLAXIS. All pile properties are shown in Table 6-2.

Pile properties of embedded piles in PLAXIS 3D and 2D			
E	*Young’s modulus*	2.1 E8	[kN/m2]
γ	*Unit weigth of the pile material*	78	[kN/m3]
Pile	*Predefined from the list provided by PLAXIS*		
type	*Circular tube*		
D	*Pile diameter*	0.61	[m]
t	*Wall thickness of the piles*	0.017	[m]
$T_{top;max}$	*Maximum skin resistance at the pile top*	0	[kN/m]
$T_{bottom;max}$	*Maximum skin resistance at the pile bottom*	287	[kN/m]
F_{max}	*Maximum base resistance of the pile*	2190	[kN]

Table 6-2 Pile properties for embedded pile (row)

The parameters $T_{top;max}$, $T_{bottom;max}$ and F_{max} are determined by the length of the pile in combination with an adopted q_c-value of 15 MPa at the bottom of the pile. This leads to the following values based on a plugged pile:

$$T_{bottem;\max} = \alpha_s \cdot q_{c;bottom} \cdot O_{pile} = 287 \text{ kN} \tag{6-1}$$

$$F_{\max} = \frac{1}{2} \cdot \alpha_p \cdot \beta_s \cdot s \cdot q_{c;bottom} \cdot A_{pile} = 2190 \text{ kN} \tag{6-2}$$

In these equations:

α_s	= pile class factor;
$q_{c;mbottom}$	= q_c-value at bottom of the pile;
O_{pile}	= circumference of the pile;
α_p	= pile class factor;
β_s	= form factor;
s	= special form factor;
A_{pile}	= surface of the pile.

With the values for $T_{top;max}$, $T_{bottom;max}$ and F_{max} the ultimate (axial) bearing capacity of the embedded pile is defined according to:

$$N_{pile} = F_{\max} + \frac{1}{2} \cdot L_{pile} \cdot (T_{top,\max} + T_{bottom,\max}) = 2190 + \frac{1}{2} \cdot 10 \cdot (0 + 287) = 3625 \text{ kN} \tag{6-3}$$

This means that in contrast to what is common finite element calculations and other calculation programs, the bearing capacity of an embedded pile in PLAXIS is a input value rather than the result of a finite element calculation. The values for $T_{top;max}$, $T_{bottom;max}$ and F_{max} can be chosen different in the following analyses. They especially determine the axial behaviour of the pile. The lateral stiffness response is the result of the pile length, equivalent radius, bearing capacity and stiffness of the soil layers in which the pile is located (see Paragraph 3.5).

Only difference in input parameters between PLAXIS 3D embedded piles and PLAXIS 2D embedded pile rows are the interface stiffness factors: ISF_{AXIAL}, $ISF_{LATERAL}$ and ISF_{BASE}. These factors influence the interface stiffness that are important for realistic load displacement behaviour. Default values for the interface stiffness factors are valid for bored piles that are loaded statically in the HS small model. For different situations it is recommended to determine a new set of ISF values by validating with 3D calculations, measurements or codes of practice.

6.1.2 Boundaries

It is important that the model boundaries are far enough from the piles. They should lie so far that they do not affect the outcome of the calculations. The boundaries of all models are checked by looking to the deformation contour of the soil and the horizontal effective stress in the direction of the load at ground level. The boundary check is in this case described for the situation of a single pile in PLAXIS 3D. It contains the following two steps:

1. Check boundary at active (earth pressure) side;
2. Check boundary at passive (earth pressure) side;

Boundary at active side

The boundary at the active side is checked by separated analyses, in which different distances are used for the boundary at the active side. In total 13 analyses are performed with boundary distances varying between 1 and 20 meters. At this stage the boundary at the passive side (30 meters) is supposed to be far enough away. If step 2 shows that the passive boundary was too close, the analysis will be performed again. The same counts for the boundary at the sides, these are set at 12 meters.

The mesh in all analyses is generated as medium and the embedded pile is refined with a factor of 0.1. The accuracy of values compared to mesh density/element size is not investigated yet; this will follow in the next paragraph.

The boundary is checked by looking to the deformation contour and horizontal effective stress at ground level. The following criteria are applied:

- Deformation at ground level close to boundary is smaller than 1% of applied horizontal displacement at the pile head;
- Horizontal effective stress at ground level close to boundary is limited ($1 > \sigma'_{xx} > -1$ [kN/m2])

In Figure 6-2 he deformation contours for U_{xx} are shown for different boundary distances. Only the values that are smaller than 1% of the prescribed displacement (0,05 m) are shown. It is clear that from about 9 meters the boundary is far enough away.

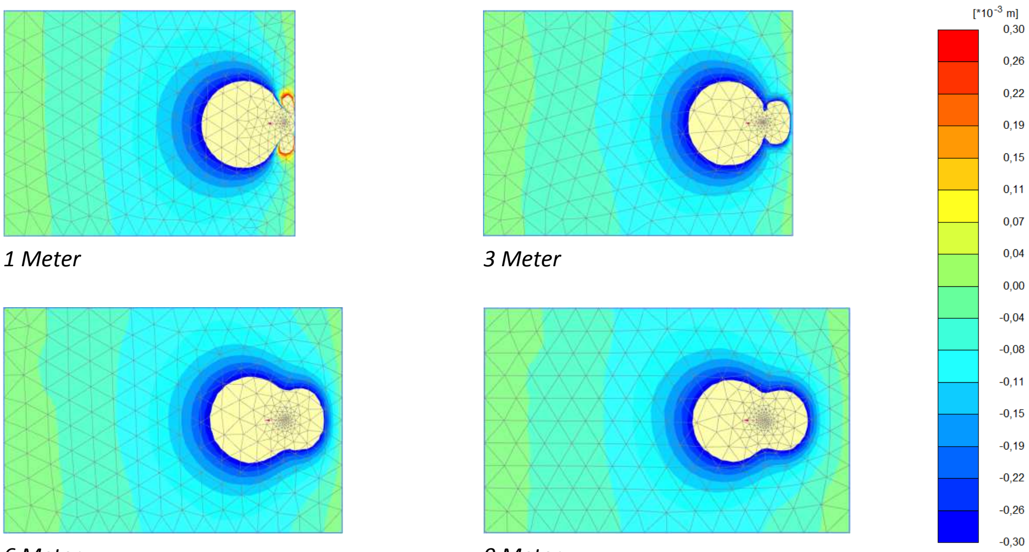

1 Meter *3 Meter*

6 Meter *9 Meter*

Figure 6-2 Deformation contours of Uxx for active boundary

Looking to the horizontal effective stresses (sigma’ xx) in Figure 6-3 this assumption is confirmed. There is only minimal increase of the lateral effective stress in x-direction at the boundaries so they lay far enough away.

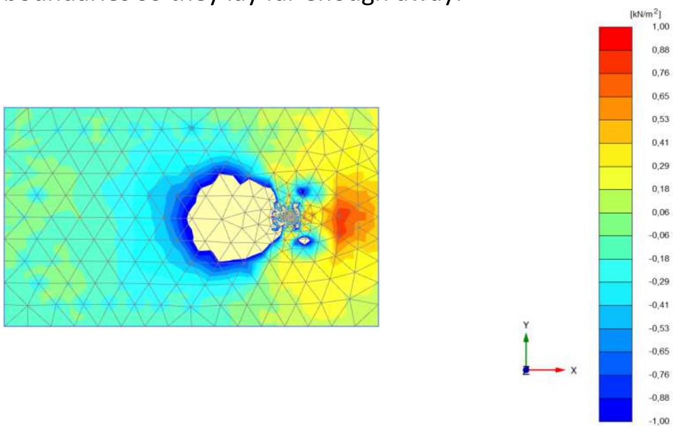

Figure 6-3 Horizontal effective stress in direction of the load (xx)

Based on the deformation contours and plot of the horizontal effective stress in x-direction the active boundary is chosen at 9 meter for the situation of a single pile.

Boundary at passive side

The boundary at the passive side is checked using the same scheme as used for the active boundary. The only difference is the boundary distances that are used. In total there are performed 14 analyses with boundary distances varying between 2 and 30 meters.
In all analyses the boundary at the active side is chosen at 9 meter, which is determined in the previous step. The boundary at the sides is set at 12 meter. The mesh is generated as medium and the embedded pile is refined with a factor of 0.1. The accuracy of values compared to mesh density/element size is not investigated yet; this will follow in the next paragraph.

The boundaries are again investigated by looking to the deformation contours (Uxx) and the lateral effective stress in x-direction at the boundary. From Figure 6-4 it is clear that the boundary does not affect the results from about 18 meters.

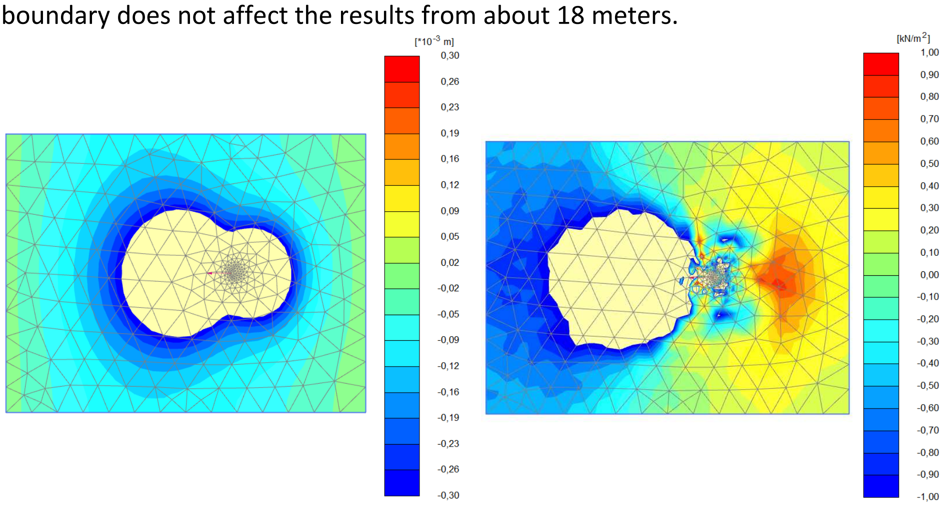

Figure 6-4 Deformation (U_{xx}) and effective stress (σ'_{xx}), with passive boundary at 18 m

Based on the deformation contours and plot of the horizontal effective stress in x-direction the passive boundary is chosen at 18 meter for the situation of a single pile.

Boundary at the sides (out of plane direction)

The boundaries at both sides in out of plane direction are set at 12 meter from the centre of the pile. Based on the results for the active- and passive boundary this seems to be far enough away. Probably it is even possible to reduce this distance to about 10 meters. However, this is not considered further because it will not lead to significant reduction in the number of elements and therefore the computation time.

For now the boundaries are set at:
Active boundary – 9 meter
Passive boundary – 18 meter
Boundary at sides – 12 meter

These boundaries only apply for the situation of a single pile. More piles lead to larger deformation contours and therefore the boundaries will lie further away.

6.1.3 Mesh coarseness and element size

The influence of mesh coarseness is investigated by linking the number of elements in the mesh to the lateral force (Fx) needed to achieve the prescribed displacement. The analysis of a single pile is performed 5 times with different mesh coarseness's (the 5 predefined options in PLAXIS). The results are shown in Figure 6-5. It is clear that the force stabilize when the number of elements increases.

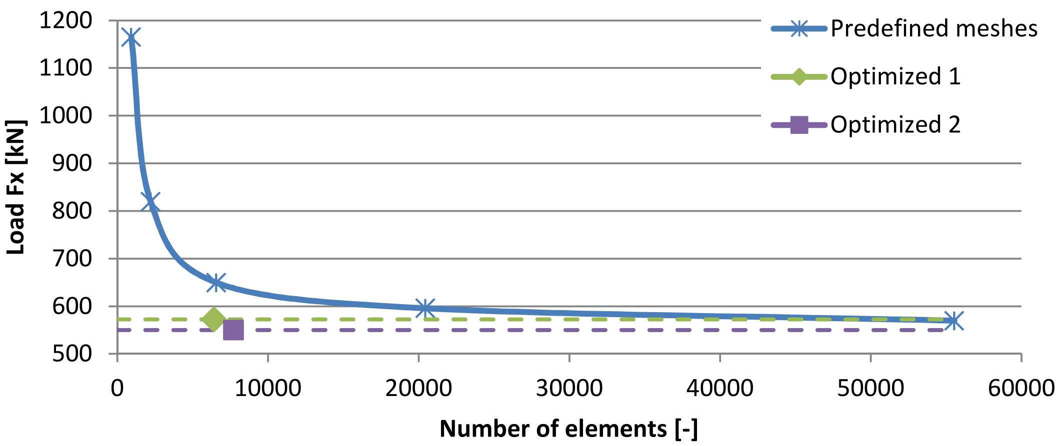

Figure 6-5 Result versus number of elements

The results of the predefined mesh option are compared with two optimized meshed:

- *Optimized mesh 1:* The embedded pile is refined by a factor of 0.1 and the mesh is generated as coarse. In this way there is enough refinement around the pile without creating an unnecessary amount of elements close to the boundaries (see Figure 6-6).
- *Optimized mesh 2*: A volume element is created around the pile which is refined with a factor of 0.1 in combination with a refinement of the embedded pile with a factor of 0.1. Again the mesh is generated at coarse (see Figure 6-6).

Both optimizations show a huge improvement of the result compared to the number of elements. Biggest difference between the both methods is the number of elements that are created around the pile at half its length (See Figure 6-6). This may have effects for especially pile groups were interaction between different piles is important.

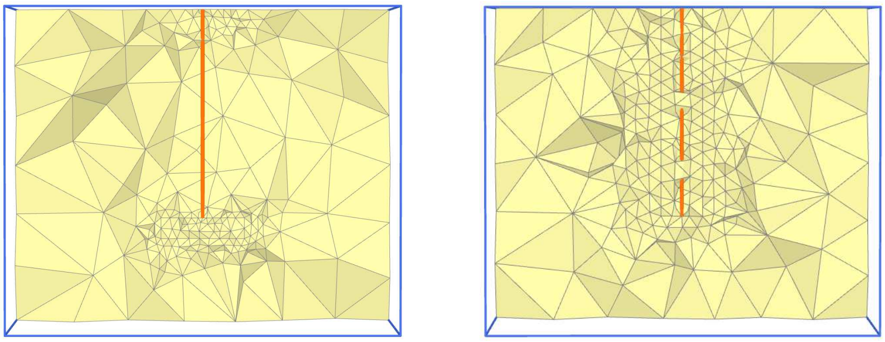

Figure 6-6 Difference between optimized mesh 1 and optimized mesh 2

The element size is an important aspect in the zone around the embedded pile. An embedded pile element can cross bulk soil elements at any point, this is important to know especially when closely spaced piles are modelled. If soil elements are big compared to the pile distance it is possible that different embedded piles cut through the same soil element. This is not desirable for the accuracy of the calculations. In general it is useful to ensure that there are at least 2 soil elements between two different piles. Because of this aspect, and uniformity, optimized mesh 2 will be used during all investigations in PLAXIS 3D.

6.1.4 Expected results

The expected result of the investigation is a reduction in lateral pile capacity as the number of piles in the group increases. This inefficiency of a pile in a group can be subscribed to the so called: “shadow effect” and/or “edge effect” (see Figure 6-7). The essence of shadow effect is that passive wedges of the ground behind individual piles within a tightly packed pile group show overlap, if there is overlap between piles in the same row than it is called “edge effect”. Due to this overlap less soil can be mobilized in a passive way and therefore mainly the piles in the middle of the group react less effective on lateral pile loading.

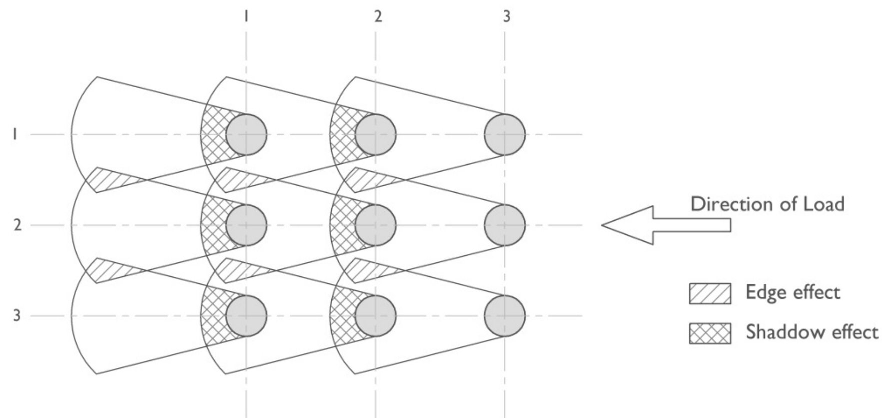

Figure 6-7 edge- and shadow effect

In literature there are several methods available that describe how to deal with lateral loading and pile group effects. In the past decades a lot of research (theoretical analysis's, lab tests and practical full scale test) on at the head lateral loaded piles was performed. Most of this research is summarized in (Reese en Impe 2001). This book mainly focusses on p-y curves, p-multipliers and pile group efficiency.

P-y curves

p-y curves include the relationship between the pile deflection y and the mobilized soil resistance p. This relationship is mainly determined by the lateral stiffness E_{py} which varies with the properties of a particular soil and with depth. It is therefore that a p-y curve only provides information (spring characteristics) about one point along a pile. A typical example of a p-y curve can be found in the figure below:

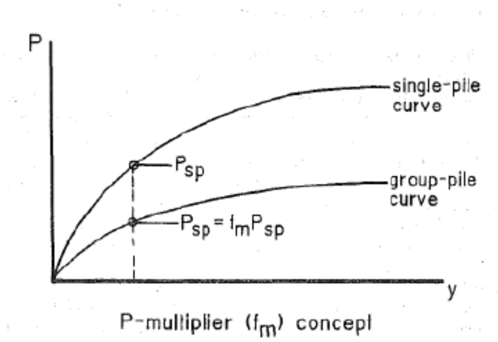

Figure 6-8 py-curve and p-multiplier

The lateral stiffness response of embedded piles in PLAXIS is the result of pile length, equivalent radius, stiffness (pile and soil layers) and bearing capacity. This means that it does not include the lateral stiffness response of the pile in the soil (p-y curves). To check whether or not the lateral pile-soil response is modelled correctly there will be made use of p-multipliers and pile efficiency.

P-multipliers and pile efficiency

As mentioned before: Inside a group, laterally loaded piles behave less efficient due to the shadow effect and edge effect. This inefficiency can be presented in p-y curves with so called "p-multipliers". Modification of a p-y curve can be performed as shown in Figure 6-8 with p-values multiplied by (fm). For the values of (fm) we can find a lot of solution determined by different methods.

It is difficult to determine the mobilized soil resistance in PLAXIS. Therefore in this case the efficiency of piles in different rows, determined from calculations in Plaxis, is compared to the multipliers (efficiency factors) determined by Reese & van Impe for pile capacity of piles in different rows. Reese and van Impe (Reese en Impe 2001) summarized test results (laboratory – and field tests) of different researchers (Cox 1984, Franke 1988, Prakash 1962, Schmidt 1981/1985, Wang&Reese, and Shibata) and made formulas based on fitting. These formulas describe the efficiency of piles in different rows. They made distinction between leading rows, trailing rows and side by side piles. The formulas are valid for different soil types, pile diameters and penetration depths. It is only important that all results were back-calculated to a reference deflection of 1/50th of the pile diameter.

The formulas for different rows are presented below, starting with the formula for leading rows;

$$e = 0.7\left(\frac{s}{D}\right)^{0.26} \text{ voor } 1 \leq \frac{s}{D} \leq 4.0 \text{ and } e = 1.0 \text{ voor } \frac{s}{D} \geq 4.0 \qquad (6\text{-}4)$$

all trailing rows:

$$e = 0.48\left(\frac{s}{D}\right)^{0.38} \text{ voor } 1 \leq \frac{s}{D} \leq 7.0 \text{ and } e = 1.0 \text{ voor } \frac{s}{D} \geq 7.0 \qquad (6\text{-}5)$$

They efficiency of piles that are standing side-by-side can be described by:

$$e = 0.64\left(\frac{s}{D}\right)^{0.34} \text{ voor } 1 \leq \frac{s}{D} \leq 3.75 \text{ and } e = 1.0 \text{ voor } \frac{s}{D} \geq 3.75 \qquad (6\text{-}6)$$

In Figure 6-9 below, the different formulas of Reese & van Impe are plotted together with the original data on which the formulas are based. The legend below the graph gives an explanation of the original data. The original data for the side-by-side efficiency is not added in the graph.

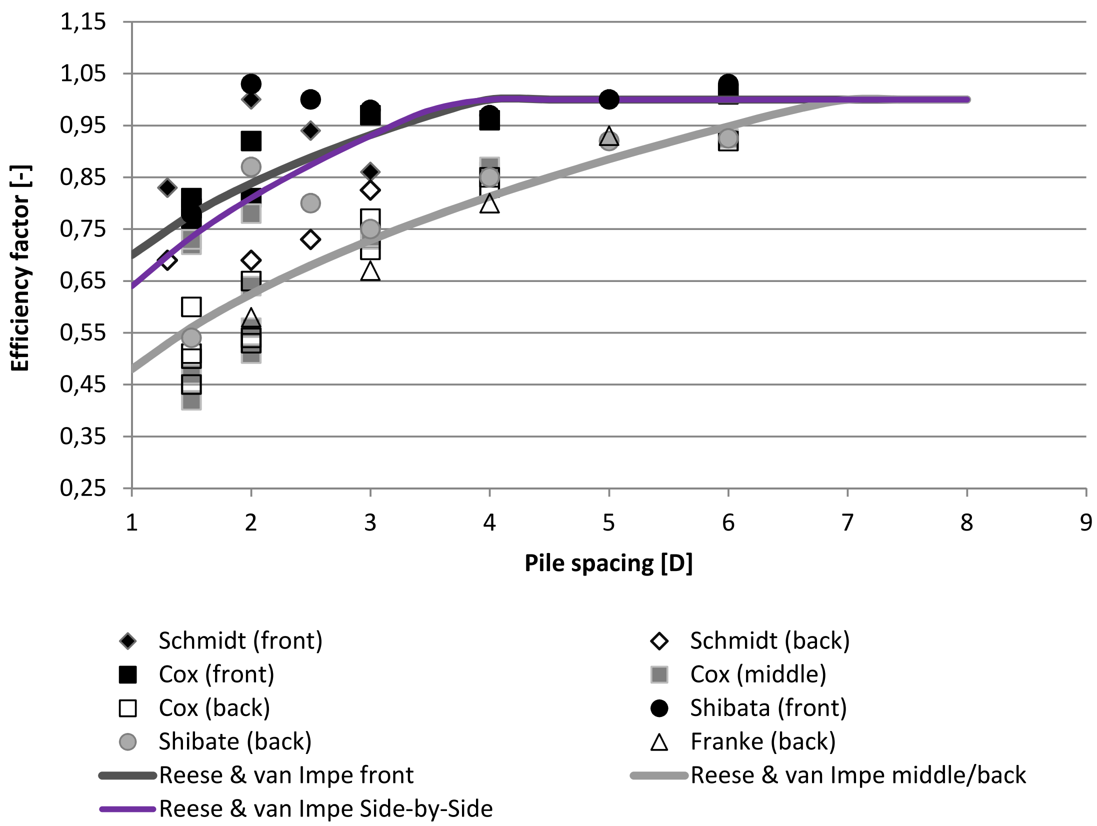

Figure 6-9 Efficiency factors according to Reese & van Impe

6.2 Results

In total 21 analyses are performed on 7 different geometries (3 pile lines and 4 pile groups) are analysed with different pile distances: 1.5 meter (2.46 D) – 2 meter (3.28 D) – 3 meter (4.92 D). Soil and piles are modelled according to the properties presented in Table 6-1 and Table 6-2. Piles are loaded by a prescribed displacement of 0.05 m. at the top of the pile.
The results of the PLAXIS analyses are checked on group efficiency, pile-row efficiency and side-by-side efficiency. This means that the accuracy of the internal pile forces/moments is not considered but only the distribution of the total force over the different piles.

6.2.1 Group efficiency

Group efficiency of piles is based on the aspect of "shadow -" and "edge effect". Piles in the middle of closely spaced pile groups are less efficiency and therefore the lateral capacity of a pile group will be lower than expectations based on the capacity of single piles. The group efficiency of embedded pile groups in PLAXIS 3D is performed according to the relation described by Poulos and Davis (Poulos en Davis 1980) :

$$\eta_{group} = \frac{F_{r;h;group}}{n \cdot F_{r;h;single\,pile}} \tag{6-7}$$

In this equation:

η_{group}	: Efficiency factor
n	: Number of piles
$F_{r;h;group}$	: Lateral capacity (Q12 in PLAXIS 3D) of pile group at specific displacement
$F_{r;h;single\,pile}$	: Lateral capacity (Q12 in PLAXIS 3D) of single pile at specific displacement

For the group efficiency factor there are a lot of solution based on different theories and (scale) tests determined by multiple researchers. For the investigation of group efficiency in this thesis there is made a distinction between pile groups and pile lines. In case of a pile group, there is both shadow - and edge effect, while pile lines are only influenced by the shadow effect. This leads to various efficiency factors.
In Figure 6-10 efficiency factors for pile groups and pile lines are depicted together with the results from PLAXIS 3D. The efficiency factors are provided by Prakash and Saran (1967), Brown and Reese (1985), Shibata et al (1989), McVay et al (1995) and Rollins et al (199 8). All data is collected from (Mokwa 1999).

The calculated efficiency factors for pile lines from PLAXIS (according to equation (6-7)) are made visible by the green dots. The numbers behind the triangles are corresponding to the number of piles in the line, so 2 = 1x2 line, 3 = 1x3 line, and so on. The red triangles are representing the pile groups, again the number corresponds to the number of piles in the group: 3 = 3x1 group, 6 = 3x2 group and so on.

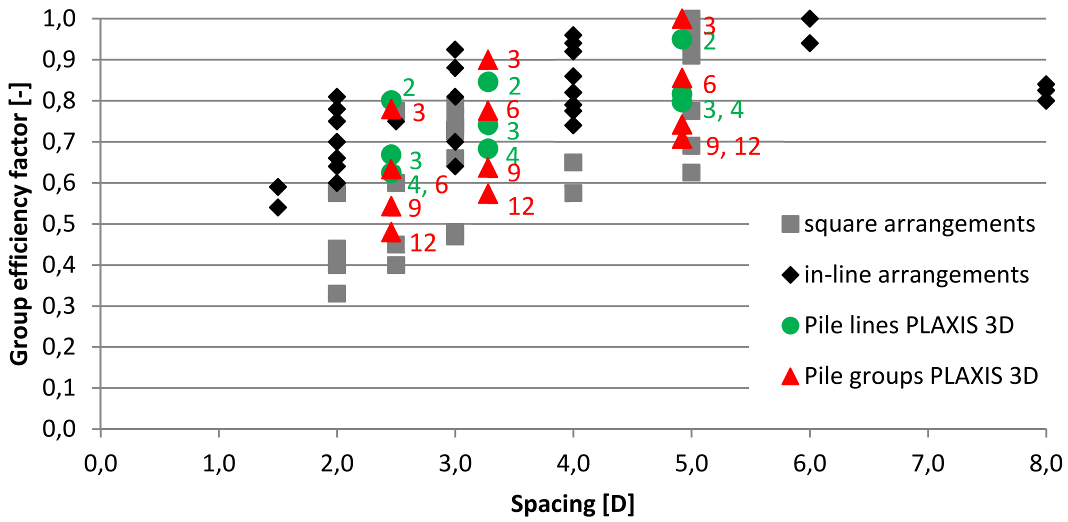

Figure 6-10 Group efficiency, result from PLAXIS compared to factors from (Mokwa, 1999)

The values found in PLAXIS for both, the pile lines and pile group are in range with the values from literature. It is good to see that PLAXIS 3D distinguishes between pile lines and piles groups. This means that distinction is made between pile row efficiency and side-by-side efficiency, typical 3D effects. Pile lines are only affected by the shadow effect while pile groups are affected by both, shadow – and edge effect. Passive wedges show more overlap and piles can therefore mobilize less soil, they react less efficient.

6.2.2 Pile-row efficiency

Besides the efficiency of the whole pile group, also the efficiency of piles in a specific row is assessed. The row efficiency is calculated by dividing the lateral force in the pile heads (Q12 in PLAXIS 3D) of piles in a specific row by the lateral force in the pile head of a single pile, this is presented in equation (6-8).

$$\eta_{pile\,row} = \frac{F_{r;h;pile\,row}}{F_{r;h;single\,pile}} \tag{6-8}$$

In this equation:

$\eta_{pile\,row}$: Row Efficiency factor

$F_{r;h;pile\,row}$: Lateral force (Q12 in PLAXIS 3D) of pile in a row at specific displacement

$F_{r;h;single\,pile}$: Lateral force (Q12 in PLAXIS 3D) of single pile at specific displacement

The lateral reaction forces that were found in the pile head are summarized in Table 6-3 on the next page. All values for pile groups (3x2, 3x3 and 3x4) are the average values of 3 piles in a row, this means one middle pile and two edge piles.

	Pile distance and pile row number											
	1.5 m = 2,46 D				2.0 = 3.28 D				3.0 = 4.92 D			
	1	2	3	4	1	2	3	4	1	2	3	4
Single pile	747											
1x2	706	491			790	474			774	524		
1x3	731	416	351		768	473	420		752	566	513	
1x4	714	451	366	355	724	480	427	410	792	541	536	511
3x1	657				745				757			
3x2	577	370			729	430			763	516		
3x3	571	348	300		676	393	360		727	493	444	
3x4	554	338	283	259	661	403	330	320	725	520	451	420

Table 6-3 (Average) pile head forces per row (Q_{12} in PLAXIS) in [kN]

With the help of Table 6-3 and Figure 6-11 the conclusion can be made that piles react less efficient when they are placed in trailing rows. This is a confirmation of the expectations based on the shadow effect. The first row of a pile group is the most efficient and behaves almost like a single pile; the capacity is still a little bit lower because of the edge effect acting on especially the middle pile. For pile lines the force in the front pile exceeds the one found in a single pile. There is no unambiguous explanation for this "over-efficiency". Some results from literature show similar behaviour.
The situation of a 1x8 pile line is added to show the stabilization of pile efficiency. From approximately the fourth trailing row the reaction forces in the pile heads are substantially identical what means that their efficiency is equal.

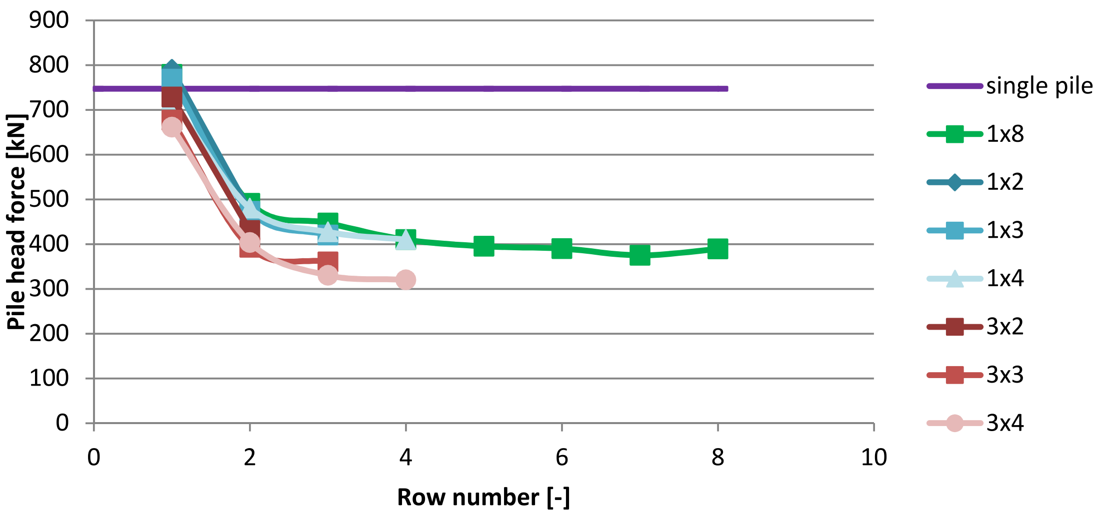

Figure 6-11 Pile force in different rows

The actual efficiency of different pile rows in PLAXIS 3D is determined according to the values presented in Table 6-3 and implemented in formula (6-8). A comparison is made with the efficiency factors described by (Reese en Impe 2001). These efficiency factors are, like described in paragraph 6.1.4, obtained from previously conducted research in both laboratory and field tests. (Reese en Impe 2001) made a distinction between front rows and trailing rows and described the efficiency by formula (6-4) and (6-5). All results from (Reese en Impe 2001) and PLAXIS 3D are presented in Figure 6-12 on the next page.

In the Figure 6-12 the symbols are representing the results from PLAXIS 3D. The triangles are corresponding to the front rows, while the dots, squares and stars are corresponding to the different trailing rows. Colours are corresponding with a pile geometry, which can be found in the legend below the graph.

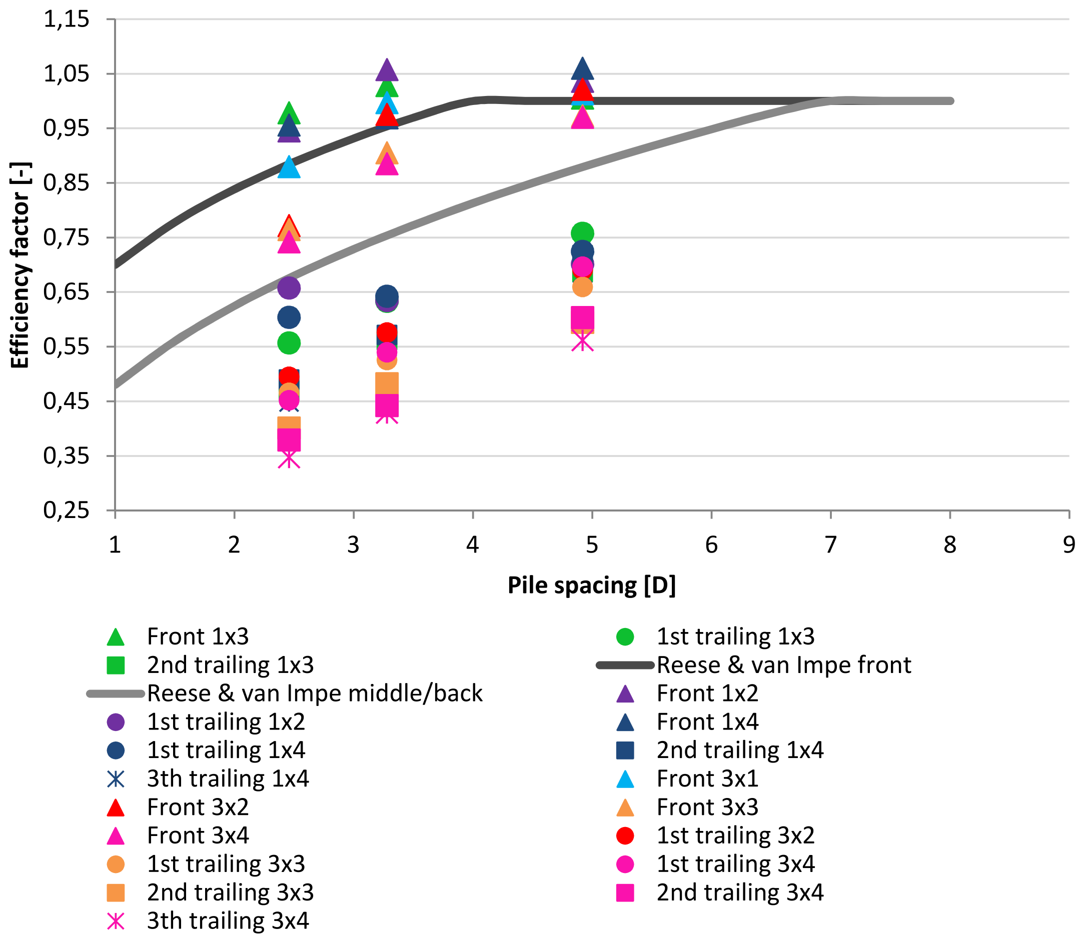

Figure 6-12 Efficiency factor for pile rows from PLAXIS compared to (Reese, 2001)

Efficiency factors from PLAXIS 3D are lower than the values for pile row efficiency determined by (Reese en Impe 2001), this is shown in Figure 6-12. Especially the efficiency factors based on the pile groups (red, orange and pink) show a big difference. This can be declared by the calculation method. Efficiency factors are calculated with the average pile head force in a row, so the edge-effect is included. Results for pile lines (purple, green and blue) do not include this effect and are therefore more in line to the efficiency according to (Reese en Impe 2001). This is a logical result because most of the results that have been used by (Reese en Impe 2001) consist of pile rows instead of pile groups.
Another effect that can have influence is the displacement magnitude that was applied at pile head level. In PLAXIS 3D a pile head displacement of 0.05 m. was applied, which is equal to 1/12.5 D. The results summarized by (Reese en Impe 2001) were back calculated to a reference deflection of 1/50 D. Therefore an additional analysis in PLAXIS has been performed on the pile line geometries with a spacing of 2 m = 3.28 D. In this additional analysis a displacement of 0.015 m. = 1/41 D was applied at the pile head. With this smaller displacement, efficiency was only 1-3% higher compared to the original results presented in Figure 6-12. This means that at almost identical deflection the efficiency factors in PLAXIS 3D are still lower than the values

presented by (Reese en Impe 2001). This especially applies for the trailing rows at larger spacing. Another deviation is that PLAXIS 3D shows a different efficiency for the first three trailing rows while (Reese en Impe 2001) suggest that all trailing rows have the same efficiency.

The results from PLAXIS 3D are therefore also compared to efficiency factors summarized and presented in (Mokwa 1999). In this study group efficiency and row efficiency of pile groups is investigated. Full scale - and centrifuge test from Cox et al (1984), Brown and Reese (1985), Morisson and Reese (1986), McVay et al (1995/1998) and Rollins et al (1998) are considered. Most of these tests were performed in sand on 3x3 pile group geometries with varying pile distance. The top displacement is not known for all test results, but in most cases it lies in the range of 0.1 - 0.3 pile diameters. All efficiency factors from (Mokwa 1999) are presented by the grey crosses in Figure 6-13, together with the design lines for row efficiency determined by (Mokwa 1999) and the efficiency factors for pile row calculated from the PLAXIS 3D pile group results.

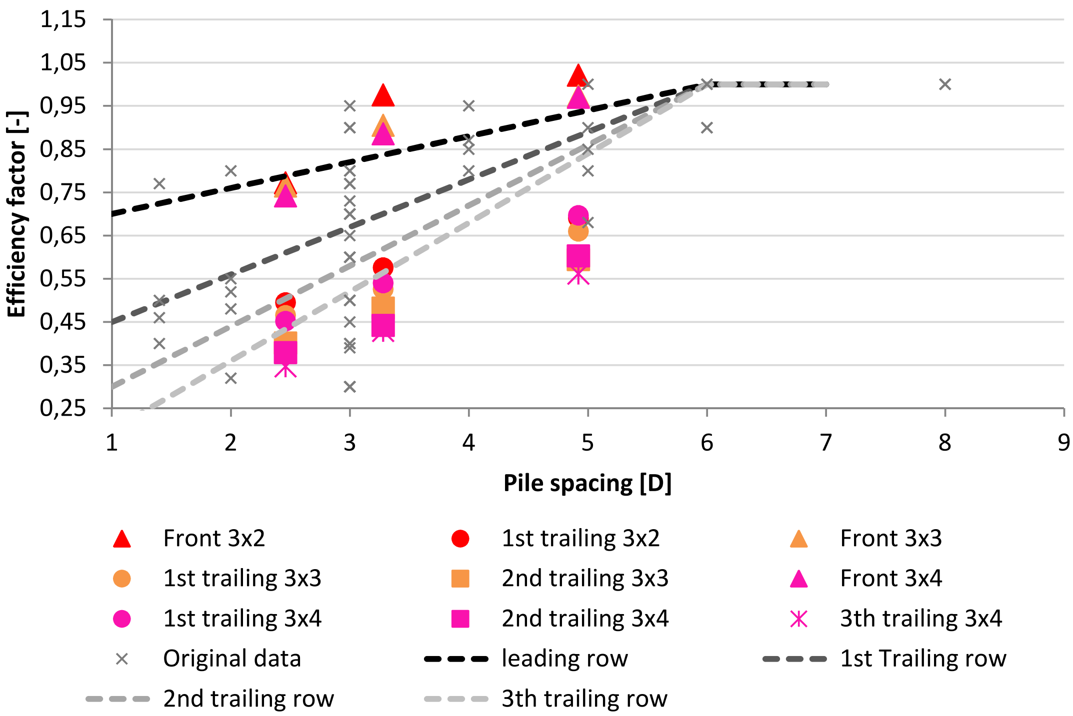

Figure 6-13 Pile row efficiency factors for medium dense-dense sands from (Mokwa, 1999)

Again the efficiency factors obtained from PLAXIS 3D are a little conservative for especially the trailing rows at larger piles distances. While the front rows show values that are in line with, or even above, the design line from (Mokwa 1999), the first trailing rows in PLAXIS show significant lower efficiency than expected by PLAXIS 3D.
At this time, it is difficult to indicate an obvious reason for these lower efficiency factors. A number of aspects, which are ignored so far, will need further investigated. For example: variation of soil properties (especially friction angle), variation of material models (elasticity/plasticity) and variation of pile properties.

6.2.3 Side-by-side efficiency

In Table 6-3 only the average pile loads per pile row are displayed for the four different pile groups. This doesn't show the inefficiency of piles in the middle of a row due to the edge-effect. PLAXIS 3D however clearly shows that piles are less effective in a closely spaced row. This is already shown in the previous paragraph (6.2.1) with the difference in efficiency of pile groups and a pile lines. To investigate the side-by-side efficiency even beter a separate analysis of a 8x1 pile row is performed. The situation is presented in Figure 6-14 below:

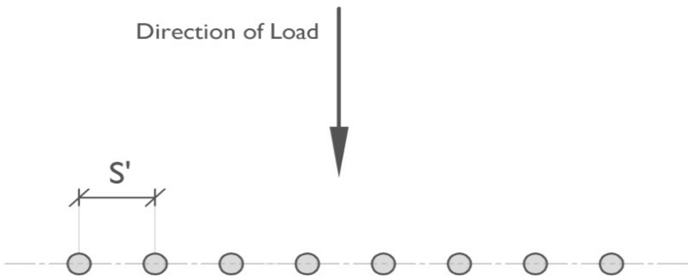

Figure 6-14 Situation for analysis of side-by-side efficiency

Again the load is applied as a prescribed displacement at pile head level. All piles are subjected to the same displacement at the excact same moment. The group can therefore be seen as a piled raft, without interaction of the raft with the soil. Efficiency of side-by-side piles are determined by equation (6-9) below:

$$\eta_{pile} = \frac{F_{r;h;pile}}{F_{r;h;\text{single}\,pile}} \tag{6-9}$$

In this equation:

η_{pile} : Efficiency factor of the considered pile

$F_{r;h;pile}$: Lateral force (Q12 in PLAXIS 3D) in considered pile at specific displacement

$F_{r;h;\text{single}\,pile}$: Lateral force (Q12 in PLAXIS 3D) in a single pile at specific displacement

The loads in the pile heads are presented in Table 6-4. There are especially differences between the two side piles and the piles in between them. Efficiency factors are approximately 0.97 for the piles on both edges and 0.84 for the piles in the middle.

	Side	Middle	Middle	Middle	Middle	Middle	Middle	Side
Force	758	647	660	672	647	647	679	743
Efficiency	*0.98*	*0.83*	*0.85*	*0.87*	*0.83*	*0.83*	*0.88*	*0.96*
Average	*0.97*	*0.84*	*0.84*	*0.84*	*0.84*	*0.84*	*0.84*	*0.97*

Table 6-4 Efficiency factors side-by-side piles

In Figure 6-15 the efficiency factors calculated from the results of PLAXIS 3D are compared to those who are recommended according to (Reese en Impe 2001). The equation for the efficiency of side-by-side piles by (Reese en Impe 2001) was already presented in Paragraph 6.1.4 by equation (6-6).
The efficiency factors of the side piles in PLAXIS 3D are almost equal to the solution of (Reese en Impe 2001), the middle piles show a lower efficiency as expected by the formula of (Reese en Impe 2001). This deviation can be declared on the fact that (Reese en Impe 2001) do not distinguish side and middle piles. From the PLAXIS 3D results also an average efficiency factor is calculated for side-by-side piles (orange squares). These average values deviates only by ± 8% compared to the values suggested by (Reese en Impe 2001).

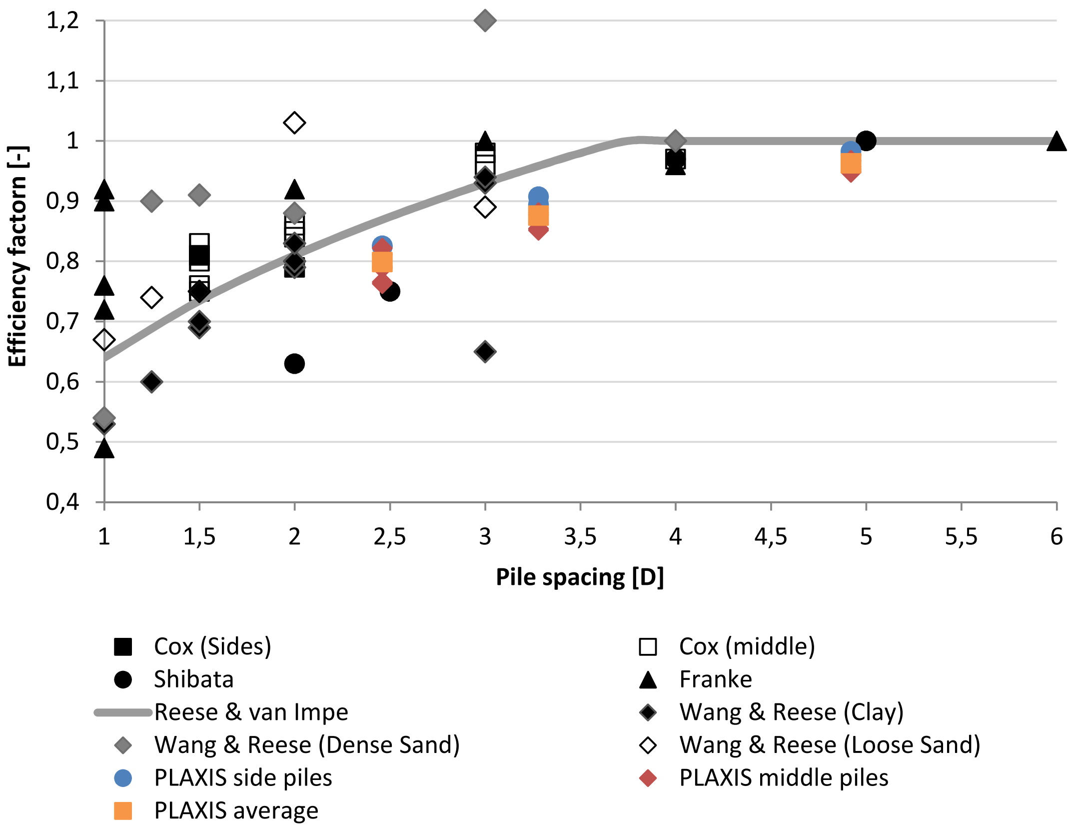

Figure 6-15 Efficiency factor for side-by-side piles from PLAXIS compared to (Reese, 2001)

During calculations it was found out that mainly the side by side efficiency is effected by the configuration of the mesh. Different meshes were investigated with 2,3,4 or even more elements between the piles but there was not a clear trend in results compared to element size, number of element (between the piles) or pile refinement. Only firm conclusion that can be drawn is that two successive embedded piles must be separated by at least two volumetric soil elements. All results in this chapter are calculated with a mesh configured according to "optimzed mesh 2" as presented in paragraph 6.1.3. It is recommended to investigate the influence of the mesh configuration on the operation, accuracy and efficiency of 3D embedded piles further. However, this is beyond the scope of this thesis.

6.3 Conclusions

In the previous three paragraphs the embedded piles in PLAXIS 3D are assessed on their lateral (group) behaviour. As already indicated by PLAXIS (Brinkgreve, Engin en Swolfs, Manual Plaxis 3D 2012) the behaviour of embedded pile becomes less accurate close to their lateral failure load. This is because lateral embedded piles response is based on elastic behaviour. Both, the elastic zone and the special interface element, are not limited by plastic behaviour in lateral directions. However, horizontal forces are limited due to the failure conditions of the surrounding soil. This ensures pretty realistic behaviour for small loads and displacements, relatively far from failure loads.

Based on the research performed in this thesis, the following conclusions can be made regarding embedded piles and their behaviour in a group:

- Group efficiency factors calculated from the results in PLAXIS 3D are acceptable compared to values found in literature (Reese en Impe 2001). There are only small deviations between both. PLAXIS 3D also distinguish between pile lines and piles groups. This means that distinction is made between pile row efficiency and side-by-side efficiency.

- Values for row efficiency differ a little bit from results found in literature. Compared to values presented by (Reese en Impe 2001) PLAXIS 3D shows lower values for especially the trailing rows. On the other hand it should be stated that PLAXIS 3D distinguish between different trailing rows while (Reese en Impe 2001) uses one efficiency factor for al trailing rows. However, efficiency factors obtained from (Mokwa 1999) for medium to dense sands make a distinction between different trailing rows. Compared to these, the efficiency factors from PLAXIS 3D are very similar with regard to the front rows. Again the trailing rows (especially the first) show values which are considerably lower than expected according to the literature. An obvious reason can yet not be found, therefore further investigation is recommended.

- The efficiency factors of side-by-side piles in PLAXIS are comparable to values expected from literature (Reese en Impe 2001). There are only deviations in the range of 8%. It is positive that PLAXIS 3D distinguishes between side- and middle piles. In literature it is often suggested to use one and the same factor for side- and middle piles.

- During calculations it was found out that mainly the side by side efficiency is effected by the configuration of the mesh. Different meshes were investigated with 2,3,4 or even more elements between the piles but there was not a clear trend in results compared to elment size, number of element (between the piles) or pile refinement.

In general it can be concluded that pile group effects are taken into account by PLAXIS 3D embedded piles. Values are in line with results from literature for pile spacings and pile head displacements comparable to the Angola case. It is therefore concluded that embedded piles can be used in the Angola case.
However it is recommended to investigate the behaviour of embedded piles even further. Import aspects are: behaviour during dynamic loading; Influence of mesh configuration; Influence of soil model (elasticity, plasticity); Influence of soil parameters and Influence op pile parameters.

7 MODELLING OF FLUID INSIDE THE TANK

The dynamic behaviour and response of a liquid inside a storage tank under lateral excitations has been the subject of extensive research. One of the first researchers who addressed the problem was Housner (Housner 1963). The motion of liquid inside the tank results in hydrodynamic pressure loading on the tank wall(s) and base Housner assumed that the response of a tank could be split into two hydrodynamic components; both are schematically represented in Figure 7-1.

Impulsive component
The impulsive part is the lower part of the fluid mass inside a tank. Under dynamic loading, the lower part of the liquid moves synchronously with the inner tank as an added mass and is subjected to the same acceleration levels as the inner tank.

Convective component
The convective component is formed by the upper part of the liquid due to sloshing of the liquid at the free surface. Under lateral excitation, oscillations of the fluid occur and this results in the generation of pressures on the walls of the inner tank.

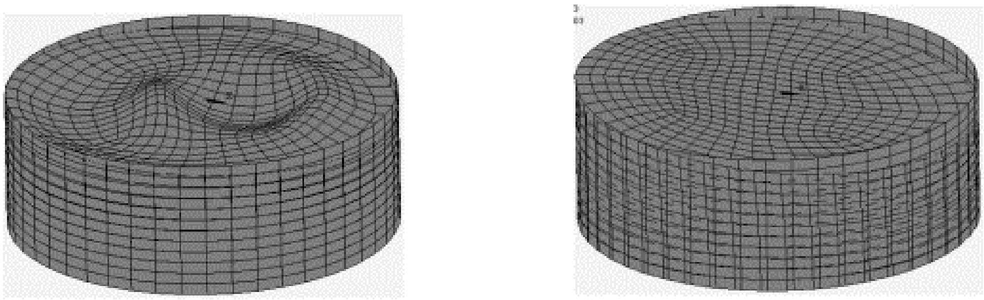

Figure 7-1 convective fluid part (sloshing) and impulsive fluid part (sliding), source:

Both components are characterised by their own natural frequencies. For the Angola case the impulsive component has a natural frequency of approximately 2 Hz and the convective part vibrates at a frequency of approximately 0,1 Hz. In the Angola case the impulsive component is the most important one. According to previous calculations of Protected Storage Engineers (PSE) this component ensures approximately 90% of the total base shear and 91% of the total overturning moment caused by the total liquid during a seismic event.

In the final model, the liquid inside the tank will be modelled as a linear mass-spring-system represented by a mass on top of a beam. The system is calibrated based on the dynamic properties of the impulsive fluid mass. The mass on the beam is equal to the impulsive fluid mass in the tank and the system (mass + beam) should have the same natural frequency as the impulsive liquid. This way of modelling will require only two beam elements instead of a huge volume cluster, which means an enormous reduction of elements, nodes and therefore calculation time.

In this chapter the modelling of the impulsive liquid part is considered in as well PLAXIS 2D as PLAXIS 3D, this with a view to the future. First some theory will be treated followed by the explanation of calculations performed in PLAXIS 2D and PLAXIS 3D. The last part: “spreading of the fluid mass” is only considered in a 2D situation because of the time aspect.

7.1 Theory

Theory is exactly the same for the 2D and 3D situation with exception of the moment of inertia. In the 3D situation the moment of inertia is based on a square cross-section, while it is defined based on a rectangular cross-section in the 2D situation. The system of a single beam with mass on top can be schematized as shown in Figure 7-2.

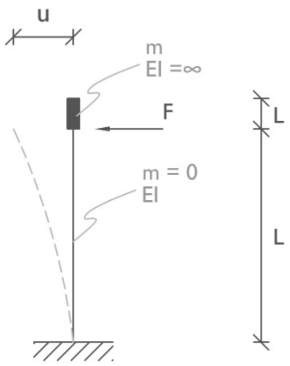

Figure 7-2 Spring-mass system with beam and a mass on top

The frequency of a single beam clamped to the surface is based on (Avitabile 2012):

$$f = \frac{1}{2\pi} \cdot \omega_n = \frac{1}{2\pi} \cdot \sqrt{\frac{k}{m}} = \frac{1}{2\pi} \cdot \sqrt{\frac{F/u}{m}} \tag{7-1}$$

In which:

f	: Frequency
ω_n	: Natural frequency;
k	: "Spring" constant;
F	: Force at top of beam (see Figure 7-2);
u	: Static deflection of the beam (see Figure 7-2);
m	: Mass of beam and mass on top of the beam.

The static deflection of a beam in PLAXIS is based on two components: deflection due to the point load at the top of the beam (bending) and deflection due to shear in the cross-section of the beam. Deflection due to bending can be determined by the general rules presented below.

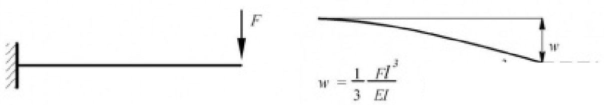

$$u_{bending} = \frac{F\ell^3}{3EI} \tag{7-2}$$

In which:

ℓ	: length of the beam;
E	: Elasticity modulus;
I	: Moment of inertia.

Deflection due to shear in the section of the beam is defined by equation (7-3).

$$u_{shear} = \frac{F\ell}{\kappa GA} = \frac{12F\ell}{5EA} \qquad (7\text{-}3)$$

In which:

κ	: Shear correction factor, defined as $5/6\,G$ (Manual Plaxis 2D 2012)
G	: Shear modulus, defined as $(1/2)\cdot E$ (Manual Plaxis 2D 2012)

Equations (7-1), (7-2) and (7-3) can be combined and written to the complete formulation for the frequency of a single beam with mass on top. This equation is presented below:

$$f = \frac{1}{2\pi}\cdot\sqrt{\frac{\left(\dfrac{F}{\left(\dfrac{F\ell^3}{3EI}+\dfrac{12F\ell}{5EA}\right)}\right)}{m}} = \frac{1}{2\pi}\cdot\sqrt{\frac{F}{\left(\dfrac{mF\ell^3}{3EI}+\dfrac{12mF\ell}{5EA}\right)}} \qquad (7\text{-}4)$$

The only free variables in this expression are the elasticity modulus (E), moment of inertia (I) and the area (A). The last two are linked together by the fact that the moment of inertia in PLAXIS 3D is based on a rectangular cross-section. By assuming a square cross-section, which is a special case of a rectangular cross-section where b=h, there are only 2 free variables left. This is shown in the formula below:

$$I = \frac{1}{12}bh^3 = \frac{1}{12}(bh)h^2 = \frac{1}{12}(bh)(hh) = \frac{1}{12}A^2 \qquad (7\text{-}5)$$

The situation in PLAXIS 2D is only slightly different. Again moment of inertia (I) and the area (A) are linked together, now based on the fact that the moment of inertia in PLAXIS 2D is based on a rectangular cross-section with b=1. In this case area A = h ($A = bxh = 1xh = h$) and therefore moment of inertia is defined as:

$$I = \frac{1}{12}bh^3 = \frac{1}{12}\cdot 1\cdot h^3 = \frac{1}{12}h^3 \qquad (7\text{-}6)$$

A known frequency, mass and length combined with a chosen elasticity modulus (E) or moment of inertia (I) leaves only one free variable. For a chosen value of moment of inertia (I) equation (7-4) can be rewritten to equation (7-7) to calculate the elasticity modulus E in case of a 3D situation. For a 2D situation equation (7-8) is used.

$$E = (f\cdot 2\pi)^2\cdot\frac{12m\ell}{A}\cdot\left(\frac{\ell^2}{3A}+\frac{1}{5}\right) \qquad (7\text{-}7)$$

$$E = (f\cdot 2\pi)^2\cdot\frac{12m\ell}{h}\cdot\left(\frac{\ell^2}{3h^2}+\frac{1}{5}\right) \qquad (7\text{-}8)$$

7.2 Free vibration analysis in PLAXIS

The theory which has been treated in the previous paragraph is used in a free vibration analysis in PLAXIS 3D and PLAXIS 2D model. In these models a specific fluid volume with a given frequency is modelled as a beam with mass on top by using the formulas from paragraph 7.1. The beam is brought out of its equilibrium by an external force at the top, which is then released. In the time that follows the beam will start to vibrate in his natural frequency which has to be equal to the frequency initially chosen in the formula.

First analyses are based on a randomly chosen volume of water (bxdxh = 6x6x5 m^3). The volume has a mass of 180.000 kg and its centre of gravity is located 2,5 meter above the ground. The beam and mass that represent the fluid have a chosen moment of inertia; this means that the elasticity modulus is supposed to be the only free variable. Respectively equation (7-7) and (7-8) can be used in a 3D or 2D situation.
After the analyses of this "random" situation there is looked in the possibility of spreading the liquid mass over a bigger area. In this way the force distribution over the base slab in the final model will be more realistic. This part of "spreading the liquid load" is based on the situation of the Angola case and is only performed in PLAXIS 2D.

7.3 PLAXIS 3D

In Table 7-1 below an overview of all parameters and their units that are used in equations (7-4) and (7-7) is given. In this example the frequency is chosen as 5 Hz.

General input			
Parameter	**Value**	**Unit**	**Explanation**
d	0.1	[m]	Width of the beam
I	8.333E-06	[m4]	Moment of inertia of the beam
Input formula 1.6			
Parameter	**Value**	**Unit**	**Explanation**
f	5	[Hz]	frequency of the system
m	180000	[kg]	mass on top of the beam
l	2.5	[m]	length of the beam
A	0.01	[m2]	Cross-sectional area of the beam
E	1.11E+14	[N/m2]	Elasticity modulus of the beam

Table 7-1 Input parameters for frequency formula

The cross-section in PLAXIS 3D is based on a square area of a slender beam (d/l < 0,1). This precondition is chosen to ensure that the contribution of the "shear part" to the deflection is minimal (< 1%), results will verify this.
In total there are seven different frequencies evaluated in the range of 1 – 15 Hz. This is sufficient to ensure the reliability of the method. The frequency of the impulsive part of a liquid natural gas has a value in the range of 1-3 Hz.

7.3.1 Geometry

There is tried to keep the model geometry as small as possible to keep analyses (and handling of the output) fast and simple.

Dimensions

The dimensions of the model are 5, 40, 3,5 meter(s) (x; y; z), this means a narrow but long model (see Figure 7-3). The model can be narrow because there is only movement in x-direction, the y-direction can almost be neglected. For meshing purposes it is better to keep a normal width because this will lead to more effective element shapes. The limited depth can be justified based on the chosen material properties for the soil layer and on the way that model boundaries are defined. Boundaries are modelled as viscous (earthquake) boundaries. The distance is judged and they don't affect the results of the vibrating beam in the middle of the model.

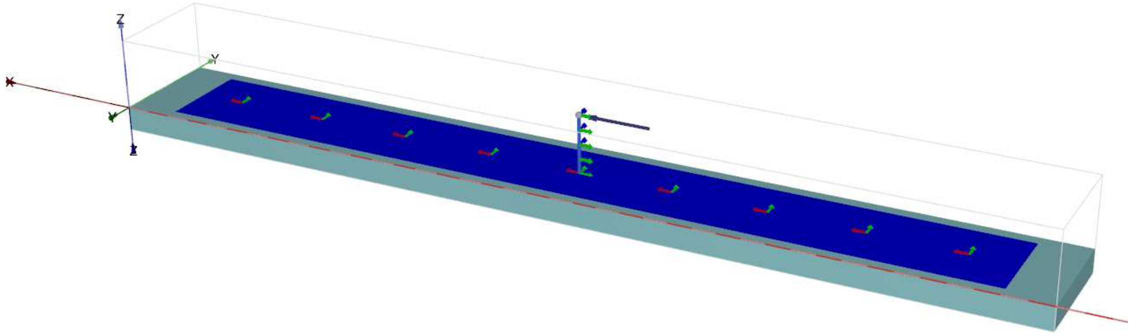

Figure 7-3 overview of PLAXIS 3D model

7.3.2 Model elements

The model contains in total four elements: a soil layer, a plate element and two beam elements. In first instance this seems quite a lot of elements for such an analysis, but for a proper modelling of the beam a few tricks and additional model elements were needed.

Soil layer and plate element

The soil layer is necessary because PLAXIS 3D can't perform any calculations without a soil layer. For this analysis the soil layer is almost superfluous because the plate element has the exact same properties and it secures the rigid connection of the beam with the ground. Both, soil layer and plate are modelled as linear elastic materials that have properties equal to concrete. In this way displacements and rotations in the plate and soil layer are negligible small and won't affect the results of the vibration analysis. The properties of the soil layer and plate element are given in the tables below:

Parameter	option	value	unit	explanation
material model	Linear elastic			
drainage type	Non-porous			
γ_{unsat}		25	[kN/m3]	saturated unit weight
E		2.1 E11	[kN/m2]	elasticity modulus
v (nu)		0.2	[-]	Poisson's ratio

Table 7-2 Parameters soil layer (concrete)

property	option	value	unit	explanation
d		0.5	[m]	Thickness of plate
Ƴ		25.00	[kN/m3]	unit weight
Isotropic	yes			
E1		2.10E+11	[kN/m2]	elasticity modulus
v (nu)		0.2	[-]	Poisson's ratio

Table 7-3 Parameters plate element

Beam element

Two elastic beam elements are used to model the impulsive fluid mass. The first beam element has a length equal to the height of the centre of gravity of the fluid mass it represents. The other parameters are determined based on the fact that the beam is slender ($d/l < 0{,}1$) and has a square cross-section or they are calculated by equations (7-4) and (7-7) presented in paragraph 7.1. The second beam element represents the mass of the fluid. Its dimensions are very small (length beam 2 = 0,04* length beam 1) to ensure it does not affect the deflection, and therefore frequency of beam element 1. Table 7-4 gives an overview of the used parameters for different frequencies.

Parameter	Values							Unit
Beam element 1								
Frequency	1	2.5	5	7.5	10	12.5	15	[m]
A	0.01	0.01	0.01	0.01	0.01	0.01	0.01	[m2]
γ	1.00E-04	1.00E-04	1.00E-04	1.00E-04	1.00E-04	1.00E-04	1.00E-04	[kN/m3]
E	4.45E+09	2.78E+10	1.11E+11	2.50E+11	4.45E+11	6.95E+11	1.00E+12	[kN/m2]
I	8.33E-06	8.33E-06	8.33E-06	8.33E-06	8.33E-06	8.33E-06	8.33E-06	[m4]
Beam element 2								
Frequency	2.5	2.5	2.5	2.5	2.5	2.5	2.5	[m]
A	0.01	0.01	0.01	0.01	0.01	0.01	0.01	[m2]
γ	1.80E+07	1.80E+07	1.80E+07	1.80E+07	1.80E+07	1.80E+07	1.80E+07	[kN/m3]
E	4.45E+12	2.78E+13	1.11E+14	2.50E+14	4.45E+14	6.95E+14	1.00E+15	[kN/m2]
I	8.33E-06	8.33E-06	8.33E-06	8.33E-06	8.33E-06	8.33E-06	8.33E-06	[m4]

Table 7-4 Parameters beam elements

7.3.3 Calculations

The calculations in PLAXIS 3D consists of three phases for every frequency analysis:

0. Initial;
1. Building;
2. Loading;
3. Free vibration

In Phase 2 (loading) the top of the beam is loaded with a horizontal force in x-direction of -100 kN. This force is randomly chosen and its goal is to bring the beam out of balance so it can vibrate in the next phase. In phase 3 (Free vibration) the applied force from phase 2 is released and then the system is allowed to vibrate for 2.5 seconds. These 2.5 seconds are sufficient as the lowest frequency is 1. This means one cycle per second, so 2.5 cycles in total. This is sufficient to determine the frequency of the system in a proper and reliable way without introducing unnecessary long calculation times.

7.3.4 Results

Deflection

The deflections calculated by hand and calculated in PLAXIS 3D are almost identical. Differences lie in the range of only 0 – 0,30 % (see Table 7-6). This is sufficiently precise.
Due to the chosen dimensions of the cross-sectional area (0,1 x 0,1 m.) the d/l ratio is smaller than 0,1 which means that we have to deal with a slender beam. The advantage of a slender beam is that the deflection is almost completely determined by the $U_{x;1}$ component (deflection due to bending). The shear component $U_{x;2}$ (as presented in Table 7-6) has only a influence of 0,1% on the total deflection. This means that by a “good chosen” cross-sectional area the shear componenet can be neglected in the formula for frequency. The formula for frequency can therefore be simplified:

$$f = \frac{1}{2\pi} \cdot \sqrt{\frac{F}{\left(\frac{mF\ell^3}{3EI}\right)}} = \frac{1}{2\pi} \cdot \sqrt{\frac{3EI}{m\ell^3}} \tag{7-9}$$

Thertefore the formula for elasticity modulus becomes:

$$E = \frac{(f \cdot 2\pi)^2 \cdot m\ell^3}{3I} \tag{7-10}$$

A comparison is made between the elasticity modulus calculated by equation (7-7) and equation (7-10). There is only a minor difference of 0,1% (see Table 7-5).

Parameter	Frequencies							Unit
f	1.0	2.5	5.0	7.5	10.0	12.5	15.0	[Hz]
E_beam	4.45E+12	2.78E+13	1.11E+14	2.50E+14	4.45E+14	6.95E+14	1.00E+15	[N/m2]
E_beam	4.44E+12	2.78E+13	1.11E+14	2.50E+14	4.44E+14	6.94E+14	9.99E+14	[N/m2]
Error	0.10%	0.10%	0.10%	0.10%	0.10%	0.10%	0.10%	

Table 7-5 comparisons of elasticity modulus determined by different formulas

In all frequency analyses equation (7-7), which include bending due to shear, is used to calculate the elasticity modulus. In further analyses also equation (7-10) can be used under the strict requirement that the beam is slender.

Parameter	Frequencies							Unit
	1	2.5	5	7.5	10	12.5	15	
Relevant input for deflection check								
F	100	100	100	100	100	100	100	[kN]
lengte_beam	2.5	2.5	2.5	2.5	2.5	2.5	2.5	[m]
Ebeam	4.45E+09	2.78E+10	1.11E+11	2.50E+11	4.45E+11	6.95E+11	1.00E+12	[kN/m2]
Ibeam	8.33E-06	8.33E-06	8.33E-06	8.33E-06	8.33E-06	8.33E-06	8.33E-06	[m4]
Abeam	0.01	0.01	0.01	0.01	0.01	0.01	0.01	[m2]
Deflection check								
$U_{x;1;hand}$	1.41E-02	2.25E-03	5.62E-04	2.50E-04	1.41E-04	9.00E-05	6.25E-05	[m]
$U_{x;2;hand}$	1.35E-05	2.16E-06	5.40E-07	2.40E-07	1.35E-07	8.64E-08	6.00E-08	[m]
$U_{x+total;hand}$	1.41E-02	2.25E-03	5.63E-04	2.50E-04	1.41E-04	9.01E-05	6.25E-05	[m]
$U_{x+total;PLAXIS}$	1.41E-02	2.25E-03	5.64E-04	2.50E-04	1.41E-04	9.02E-05	6.27E-05	[m]
Error	0.05%	0.06%	0.20%	0.09%	0.13%	0.20%	0.30%	
Check frequency of the system								
f_{input}	1	2.5	5	7.5	10	12.5	15	[Hz]
f_{PLAXIS}	1	2.4	4.8	7.2	9.6	11.6	14	[Hz]
Error	0.00%	4.00%	4.00%	4.00%	4.00%	7.20%	6.67%	

Table 7-6 Deflection and frequency results

Frequency

Frequency results are based on the input values that are determined by equations (7-4) and (7-7) presented in paragraph 7.1.. The results of the frequency analyses are presented in 3 figures and a table:

Figure 7-4	: Shows the top-deflection of the beam in the time for the lower frequencies. Lower frequency beams have a smaller value of EI, so top-deflection is larger.
Figure 7-5	: Shows the top-deflection of the beam in the time for the higher frequencies. Higher frequency beams have a larger value of EI, so top-deflection is smaller;
Figure 7-6	: Shows the frequencies that are found by PLAXIS 3D in different analyses, based on the top-deflection graphs depicted in Figure 7-4 and Figure 7-5;
Table 7-6	: Shows the input frequencies, the output frequencies and the error between them.

The table and figures show that especially the obtained values for the lower frequencies (1-10 Hz) lie close to the input frequencies. The frequencies in the range of 10-15 Hz deviate a little more. This can be caused by the number of time steps that are available per cycle. In all analysis the defaults values for numerical control parameters are used. This means 250 time steps for a free vibration of 2,5 seconds. This results in a constant time step of 0,01 seconds. In the 1 Hz analyses this means 100 steps per cycle compared to 6,67 steps in the 15 Hz analyses. If the 15 Hz analysis performed on default settings (250 steps = 6,67 steps per cycle) is compared to an analysis with 3 times more steps (750 steps = 20 steps per cycle), a significant difference is encountered.

The analysis with 750 steps is more accurate, this is shown in Figure 7-7. The error of the frequency that is found in the PLAXIS analysis with 750 steps is only 1,33% (14,8 Hz) compared to 6,67% (14 Hz) in the one with 250 steps.
Further study to the minimum amount of steps required per cycle is not performed since the analysis for lower frequencies (expected frequencies for liquid natural gas) already shows accurate results. It is still recommended to check the number of steps with the frequencies that are to be expected in the final model.

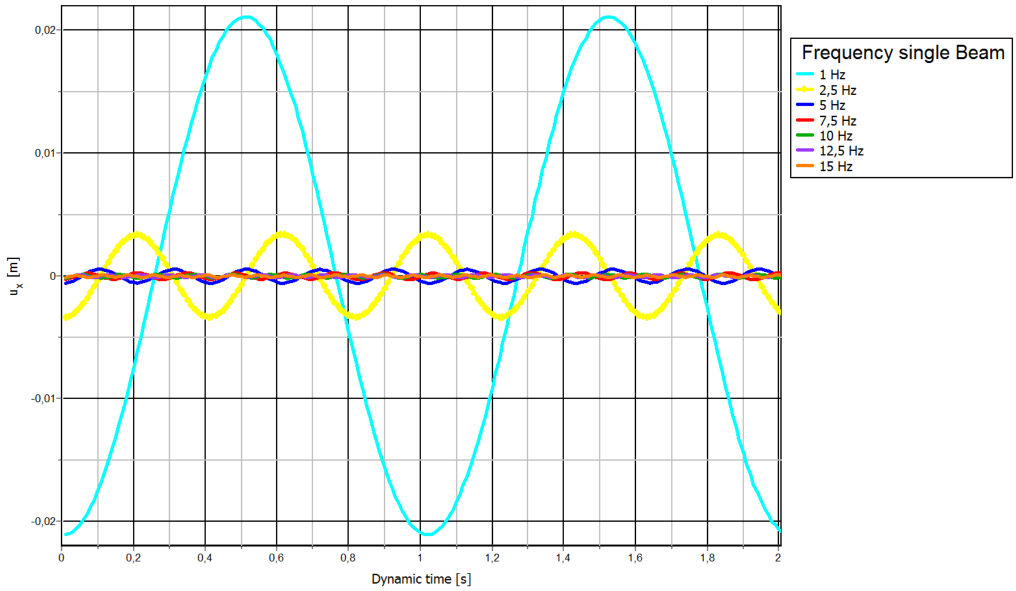

Figure 7-4 Top-deflection against time (lower frequencies)

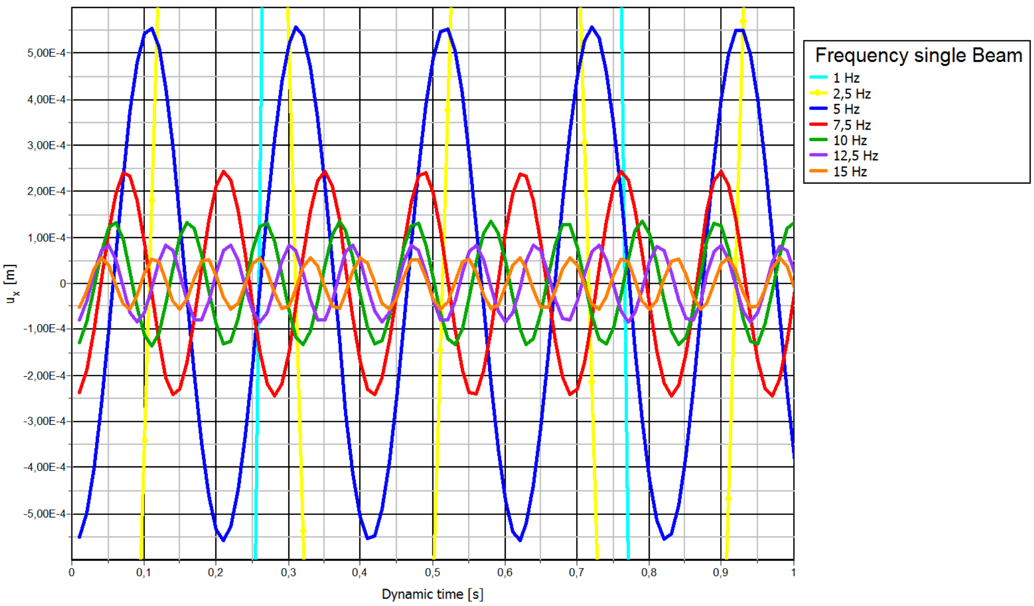

Figure 7-5 Top-deflection against time (higher frequencies)

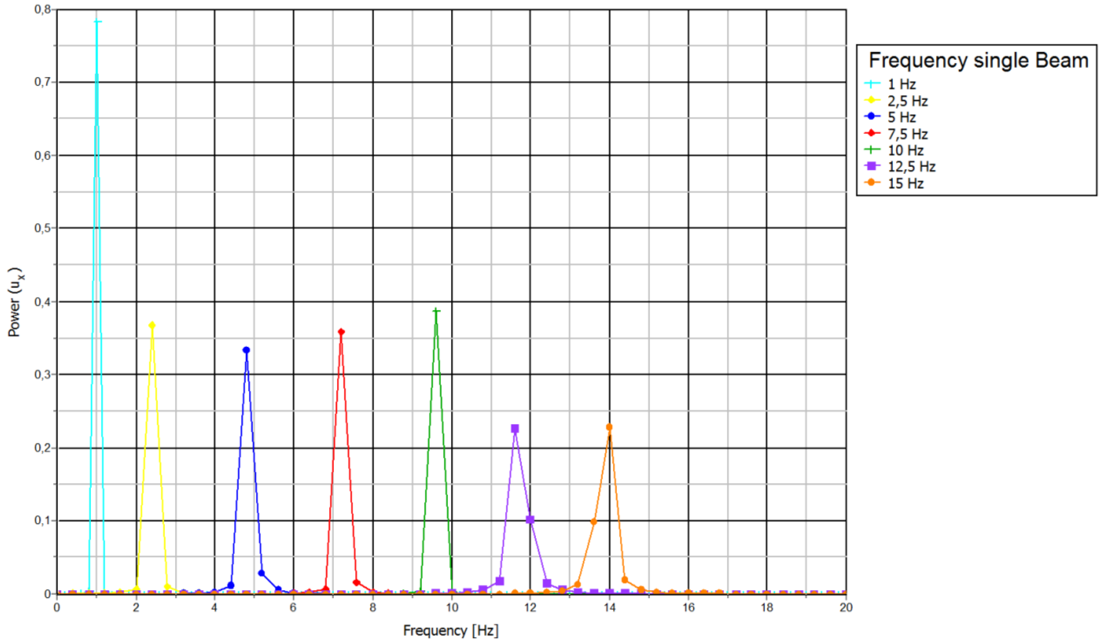

Figure 7-6 Frequency results

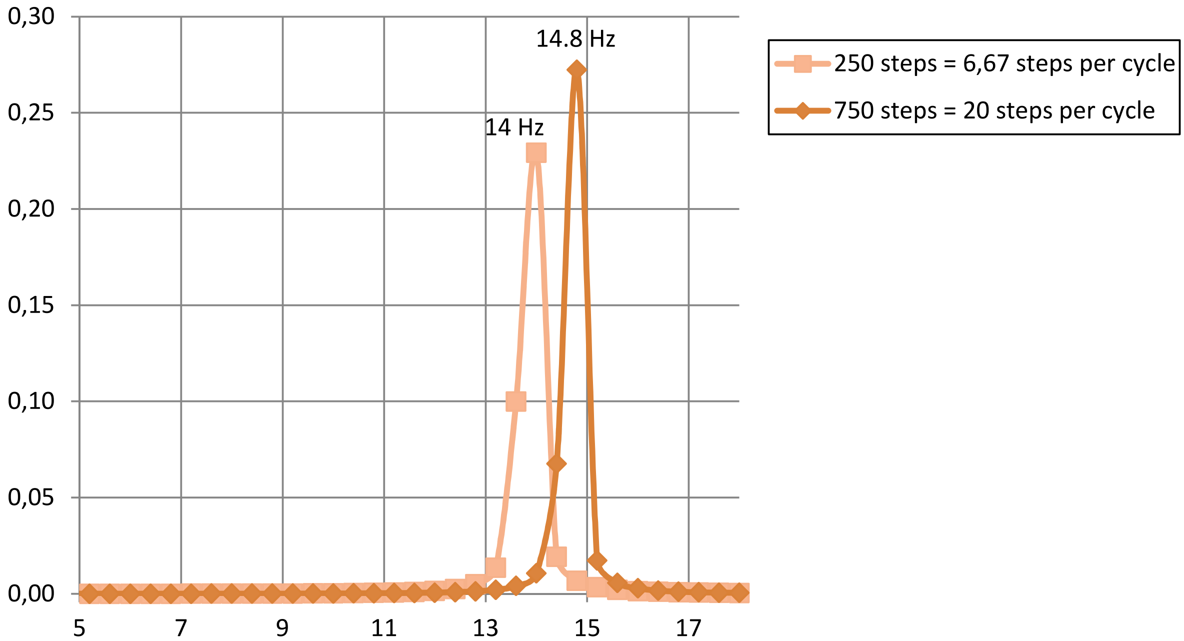

Figure 7-7 frequency by different number of steps per cycle for 15 Hz

7.4 PLAXIS 2D

The analyses performed in PLAXIS 2D are equal to those performed in PLAXIS 3D. In contrast to the analyses in 3D, the cross-section in PLAXIS 2D is based on a rectangular area. Again the requirement for a slender beam (d/l < 0.1) is met. This precondition is chosen to ensure that the contribution of the "shear part" to the deflection is minimal (< 1%). Because theory is already proven in PLAXIS 3D for a large range of frequencies the analyses in 2D are only focussing on the lower (more important) frequencies. In total there are five different frequencies evaluated in the range of 1 – 10 Hz. This is sufficient to ensure the reliability of the method in PLAXIS 2D. The frequency of the impulsive part of a liquid natural gas has a value in the range of 1-3 Hz.

In Table 7-7 below an overview of all parameters and their units (used in equations (7-4) and equation (7-7)) is given. In this example the frequency is chosen as 5 Hz.

General input			
Parameter	**Value**	**Unit**	**Explanation**
d	0.1	[m]	Width of the beam
I	8.333E-05	[m4]	Moment of inertia of the beam
Input formula 7.4			
Parameter	**Value**	**Unit**	**Explanation**
f	5	[Hz]	frequency of the system
m	180000	[kg]	mass on top of the beam
l	2.5	[m]	length of the beam
A	0.1	[m2]	Cross-sectional area of the beam
E	1.11E+13	[N/m2]	Elasticity modulus of the beam

Table 7-7 Input parameters for frequency formula

7.4.1 Geometry

It has been tried to keep the model geometry as small as possible to keep analyses and handling of the output fast and simple.

Dimensions

The dimensions of the model in PLAXIS 2D are 10 by 2.55 meter(s) (x, y), this is depicted in Figure 7-8. In PLAXIS 2D the model can be very small because it is possible to connect the beam directly on the model boundary. Due to the direct connection of the beam on the model boundary, the boundary fixities and the material properties the distance of the boundary is not important anymore.

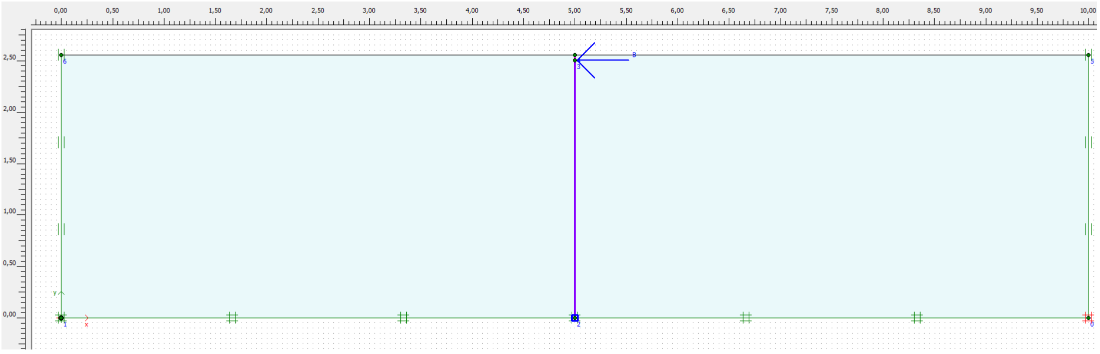

Figure 7-8 overview of PLAXIS 2D model

7.4.2 Model elements

The model in PLAXIS 2D contains only three elements: a soil layer and two plate elements. Compared to the 3D model a few things are changed.

PLAXIS 2D does not have the option to model beam elements; therefore the beam is replaced by a plate element. A plate element has a fixed width of 1 m. in out of plane direction but its height can be varied by the input parameters. Compared to a beam element in PLAXIS 3D (square cross-section), a plate element in PLAXIS 2D has a rectangular cross-section. The difference between the 3D and 2D model is depicted in Figure 7-9 in a three dimensional space.

Another difference between the 2D and 3D model is the absence of the soil layer and horizontal plate. In PLAXIS 2D a plate can be connected directly on the model boundaries. The connection type can then be defined by adjusting the boundary fixities.

The soil layer, recognizable by the light-blue colour in Figure 7-8 is just a dummy layer. It is only used for meshing purposes. During calculation this layer is deselected and therefore properties of this soil layer are not important.

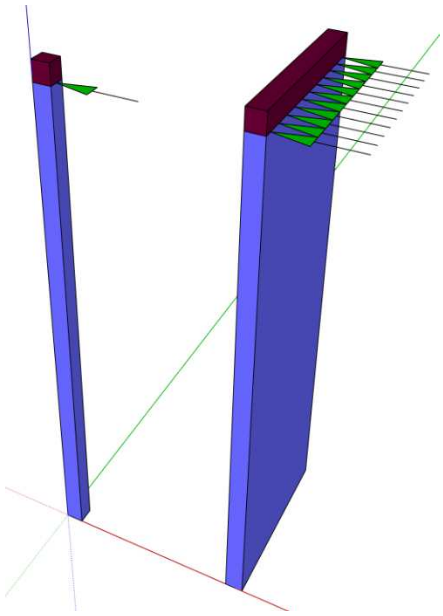

Figure 7-9 PLAXIS 3D vs PLAXIS 2D

Plate elements

In PLAXIS 2D the impulsive fluid mass is modelled by two elastic plate elements. The first plate element has a length equal to the height of the centre of gravity of the fluid mass it represents. The other parameters are determined based on the fact that the plate is slender (d/l < 0,1) and has a rectangular cross-section or they are calculated by equations (7-4) and (7-8) presented in paragraph 7.1. The second plate element represents the mass of the fluid. Its dimensions are very small (length plate 2 = 0,02* length beam 1) to ensure that they don't have effect on the deflection and therefore frequency of plate element 1. Table 7-8 gives an overview of the used parameters for different frequencies.

Parameter	Values				Unit
Plate element 1					
Frequency	1	2.5	5	7.5	[m]
A	0.1	0.1	0.1	0.1	[m2]
γ	0	0	0	0	[kN/m3]
EA	4.446E+7	2.778E+8	1.111E+9	2.501E+9	[kN/m2]
EI	3.705E+4	2.315E+5	9.262E+5	2.084E+6	[m4]
Plate element 2: weight					
Frequency	1	2.5	5	7.5	[m]
A	0.1	0.1	0.1	0.1	[m2]
γ	3.600E+4	3.600E+4	3.600E+4	3.600E+4	[kN/m3]
EA	4.45E+10	2.78E+11	1.11E+12	2.50E+12	[kN/m2]
EI	3.705E+7	2.315E+8	9.262E+8	2.084E+9	[m4]

Table 7-8 input parameters plate elements

7.4.3 Calculations

The calculations in PLAXIS 2D consists of four phases for every frequency analysis:

0. Initial;
1. Building;
2. Loading;
3. Free vibration

In Phase 2 (loading) the top of the beam is loaded with a horizontal force in x-direction of -100 kN. This force is randomly chosen and its goal is to bring the beam out of balance so it can vibrate in the next phase. In phase 3 (Free vibration) the applied force from phase 2 is released and then the system is allowed to vibrate for 2.5 seconds. These 2.5 seconds are sufficient as the lowest frequency is 1. This means one cycle per second, so 2.5 cycles in total. This is sufficient to determine the frequency of the system on a proper and reliable way without introducing unnecessary long calculation times.

7.4.4 Results

The results are checked in two ways:

- Static deflection at the top of the beam
- Frequency of the beam

Deflection

The deflections calculated by hand and calculated in PLAXIS 2D are identical. Differences are smaller than 0.01% (see Table 7-9). This is sufficiently precise.

Parameter	Frequencies				Unit
	1	2.5	5	7.5	
Relevant input for deflection check					
F	100	100	100	100	[kN]
Length	2.5	2.5	2.5	2.5	[m]
EI	3.705E+4	2.315E+5	9.262E+5	2.084E+6	[m4]
Check of top deflection					
$U_{x;1;hand}$	1.406E-02	2.249E-03	5.624E-04	2.499E-04	[m]
$U_{x;2;hand}$	1.350E-05	2.159E-06	5.399E-07	2.399E-07	[m]
$U_{x+total;hand}$	1.407E-02	2.252E-03	5.629E-04	2.502E-04	[m]
$U_{x+total;PLAXIS}$	1.41E-02	2.25E-03	5.629E-04	2.502E-04	[m]
Error	0.02%	0.02%	0,00%	0.01%	
Check frequency of the system					
$frequency_{input}$	1	2.5	5	7.5	[Hz]
$frequency_{PLAXIS}$	1	2.5	5	7.5	[Hz]
Error	0.00%	0.00%	0.00%	0.00%	

Table 7-9 Deflection and frequency results

Due to the chosen dimensions of the cross-sectional area (1 x 0.1 m.) the d/l ratio is smaller than 0.1 which means that the plate is considered to be slender. Deflection of a slender element is almost completely determined by bending, therefore the shear componenet ($U_{x;2;hand}$) can be neglected in the formula for frequency. Equations (7-4) and (7-8) can be simplified as already shown in paragraph 7.3.4 by equations (7-9) and (7-10).

Frequency

The input frequencies for equations (7-4) and (7-8) are compared to the frequencies found in the PLAXIS 2D analyses. Results are presented in 2 figures and a table:

Figure 7-10	: Shows the top-deflection of the beam in the time for all frequencies. Lower frequency beams have a smaller value of EI, so top-deflection is larger.
Figure 7-11	: Shows the frequencies that are found by PLAXIS 3D in different analyses, based on the top-deflection graphs depicted in Figure 7-10;
Table 7-9	: Shows the input frequencies, the output frequencies and the error between them.

The table and figures show that the obtained values for all the frequencies are equal to input frequencies. In the 2D analyses only the "lower" frequencies (1-7.5) are evaluated because the impulsive fluid is expected to have a frequency in the range of 1-3 Hz.
In all analyses 250 time steps are used to describe a free vibration time of 2.5 seconds. In the case of a frequency of 7.5 Hz a single cycle is therefore describe by 13 time steps, this is considered to be sufficient.

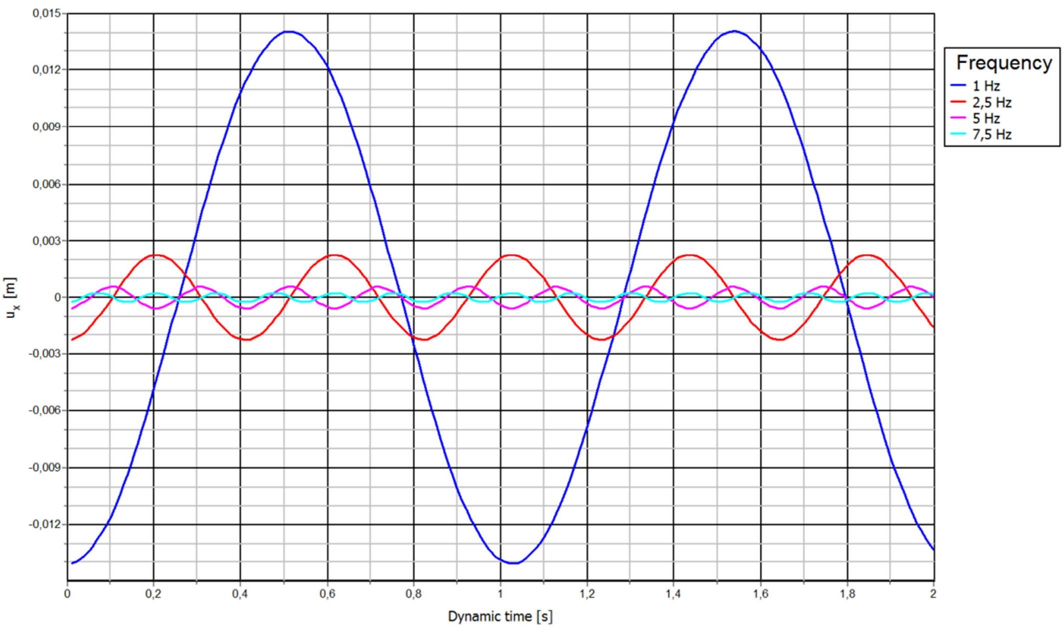

Figure 7-10 Top-deflection against time

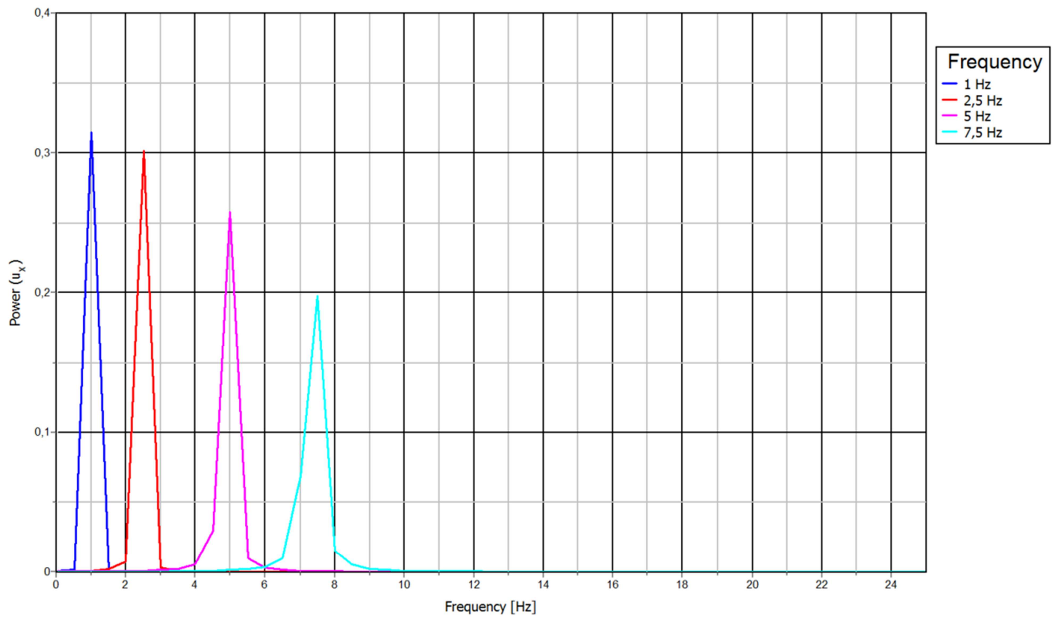

Figure 7-11 Frequency results

7.5 Spreading of the fluid mass

The beam-mass systems described in the previous paragraphs for as well the 3D as the 2D situation seem to perform properly based on frequency. For a proper modelling of the fluid in the final model it is also important that the force distribution in the base slab and foundation piles, introduced by the beam-mass system, is realistic compared to the real situation. The use of a single beam means that locally very large forces/moments are introduced which is unrealistic compared to the actual situation. In the case of a sliding liquid body inside a tank, an overturning moment is introduced by the transfer of mass over the width of the base slab. A base shear is the results of the LNG mass that is pressing against the wall (see Figure 7-12). It is therefore important to spread the vertical load and to prevent the introduction of moments in the base slab. In this way the base slab can be modelled in a realistic way without affecting the force distribution in the foundation piles. The modelling of a realistic base slab is also favourable for the assessment of wave propagation effects.

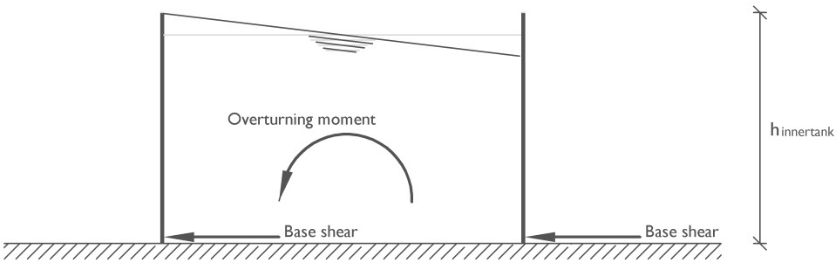

Figure 7-12 Overturning moment and base shear due to moving liquid mass

In this chapter a realistic force distribution in the base slab and foundation piles is created with the aid of an auxiliary structure. For a proper assessment of the operation of the auxiliary structure, the initial model is set up without soil layers and foundation piles. In the following paragraphs, the theory will be explained first, followed by the discussion of the PLAXIS 2D model and its results.

7.5.1 Theory

The theory to control the frequency of the beam (3D) or plate (2D) is exactly the same as described in paragraph 7.1. An auxiliary structure of horizontal and vertical supports is added to distribute the vertical and horizontal forces over the base slab without introducing any moments. Figure 7-13 gives an overview of the complete auxiliary structure used to model the fluid.

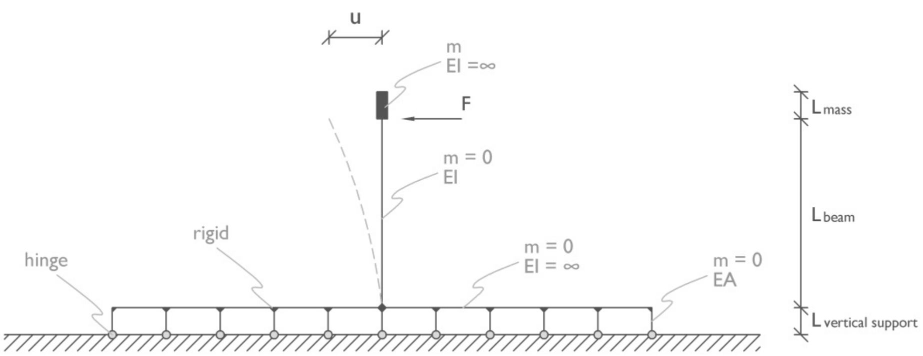

Figure 7-13 Spring-mass system with auxiliary structure

The horizontal plate is supposed to be infinite stiff, in this way all forces and moments introduced by the vibrating beam are equally distributed over the vertical supports. The vertical supports are acting as vertical springs. Due to the hinged connection with the base plate al moments are transferred as horizontal and vertical forces to the base plate. Important aspect of the construction is the stiffness ratio between the vibrating beam/plate, horizontal- and vertical support(s). The following principles should be maintained:

- Horizontal support is very stiff compared to the vibrating beam/plate and vertical supports, this to ensure an equal distribution of the forces over all the vertical supports;
- Vertical supports are stiff compared to vibrating beam, in this way they will not influence the frequency of the system.

7.5.2 PLAXIS 2D

The above described theory is used in a PLAXIS 2D model. The main goal is to create a realistic force distribution in the base slab and foundation piles that is representative for the actual situation. The model is based on a cross-section of the actual situation in Angola, as presented in Figure 4-2 and APPENDIX A.

Geometry and dimensions

The geometry of the model is based on the situation in the ANGOLA case. A cross-section over the complete tank diameter is modelled. To ensure fast analyses and post processing the calculations are performed with a relative simple and small model.

The dimension of the model in PLAXIS 2D are 160 by 16.9 meter (x, y). The model is relative wide to ensure that boundary effects don't affect the results in the middle of the model. The complete geometry is depicted in Figure 7-14 below.

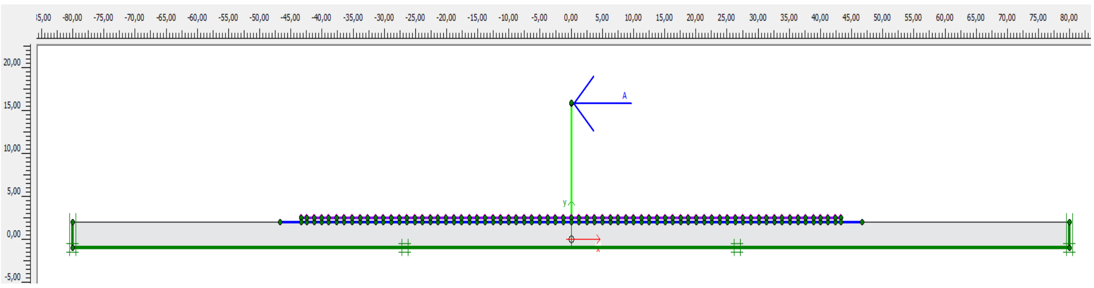

Figure 7-14 Model geometry

Model elements

Only two types of elements are used: elastic volumetric elements representing a concrete base layer and different plate elements to model the vibrating beam and the horizontal- and vertical supports. As described in the previous paragraph; the vibrating beam will ensure a proper modelling of the frequency of the fluid while the support structure will ensure a proper distribution of the forces over the base plate.

Vibrating beam/plate

The properties of the "vibrating" plate element are determined according to the formulas presented in paragraph 7.1 in combination with geometry of the cross-section from Figure 4-2 and the material properties of LNG and the inner tank.

At this moment the complete LNG mass in the cross-section together with mass of the inner tank, top girders and stiffeners is seen as impulsive mass. This is very conservative and an upper limit assumption which will lead to a high stiffness for the vibrating beam. If the auxiliary is able to work properly with these upper limit parameters, it is very likely that it will also be able to work properly in the final situation. As a result of the high stiffness of the vibrating beam, the stiffness of the horizontal support is required to be even higher. This is considered to be the most critical point of this auxiliary structure. PLAXIS uses a single stiffness matrix to calculate the complete model. In case of large differences in stiffness the matrix can lead to unrealistic results or an unstable, or even an insoluble stiffness matrix.

The density of liquid natural gas is determined to be 470 kg/m3. The centre of gravity of the LNG mass is located at 14.8 meter above the base slab; this is therefore also the length of the vibrating plate. It is known that this is not according to requirements of the code (American Petroleum Institute 2002), but it is a good first approximation to investigate the behaviour and potential of the auxiliary structure.

All relevant input for the formula (7-4) and the final input for PLAXIS are shown in Table 7-10.

General input				
Parameter	Value		Unit	Explanation
d	1.0		[m]	Width of the beam/plate
I	8.33E-02		[m4]	Moment of inertia of the beam/plate
Input formula 7.4				
Parameter	Value		Unit	Explanation
f	2		[Hz]	frequency of the system
m	1215991		[kg]	mass on top of the beam/plate
l	14.8		[m]	length of the beam/plate
A	1.0		[m2]	Cross-sectional area of beam/plate
E	2.599E+12		[N/m2]	Elasticity modulus of the beam/plate
Input plate elements PLAXIS				
Parameter	Value beam	Value mass	Unit	Explanation
EA	2.599E9	2.599E12	[kN/m]	Axial stiffness
EI	216.6E6	216.6E9	[kN m2/m]	Bending stiffness
w	0	121.6E3	[kN/m/m]	weight
v(nu)	0	0	[-]	Poisson's ratio

Table 7-10 Input parameters for frequency equation and PLAXIS model

Elastic concrete layer and base plate element

The elastic concrete layer and base plate element are added because of two reasons: ensure a good handling of the system and the possibility of easy model verification. The concrete is modelled with elastic volumetric soil elements with a relative high stiffness. Settlements will be low and therefore it won't affect the behaviour of the system on top of it. The properties of the soil layer are depicted in Table 7-11.

The base plate element is especially used for output purposes, this because forces and moments can be read out directly from plate elements. Properties of the plate are equal to the base plate used in the Angola project. Al properties are summarized in Table 7-11.

Model input concrete layer (linear elastic, non-porous)			
Parameter	Value	Unit	Explanation
$\gamma_{unsat}/\gamma_{sat}$	25	[kN/m3]	Volumetric weight
E	30.0E+6	[kN/m2]	Young's modulus
v(nu)	0.2	[-]	Poisson's ratio

Model input concrete base slab (plate element)			
Parameter	Value	Unit	Explanation
EA	24.00E6	[kN/m]	Stiffness in later direction
EI	1.28E6	[kNm2/m]	Bending stiffness
w	20	[kN/m/m]	weight
v(nu)	0.2	[-]	Poisson's ratio

Table 7-11 Input properties for concrete soil layer and concrete plate element

Plate elements of the support structure

The properties of the support structure are determined based on the principles presented in paragraph 7.5.1 and the properties of the vibrating beam. The horizontal support is supposed to be "infinitely" stiff compared to the surrounding element to ensure an equal distribution of the forces over all vertical supports. The support is massless and stiffness properties are based on the assumption: $EI_{horizontal\ support} >> EI_{vibrating\ beam}$, the same is applied for EA.

The vertical supports are intended to behave as vertical springs. Therefore their value of EA is most important. It seemed that small changes in values for EA and EI have big influence on the behaviour of the vertical supports and therefore the behaviour of the complete system. If the following condition is met: $EI_{vertical\ support} >> EA_{vertical\ support}$ and $EA_{vertical\ support} >> EI_{vibrating\ beam}$ without applying very strange dimension for the vertical supports, their behaviour is within expectations. Since the two relations above may not be entirely clear due to the comparison between EI (bending stiffness) and EA (axial stiffness), the problem is presented in Figure 7-15.

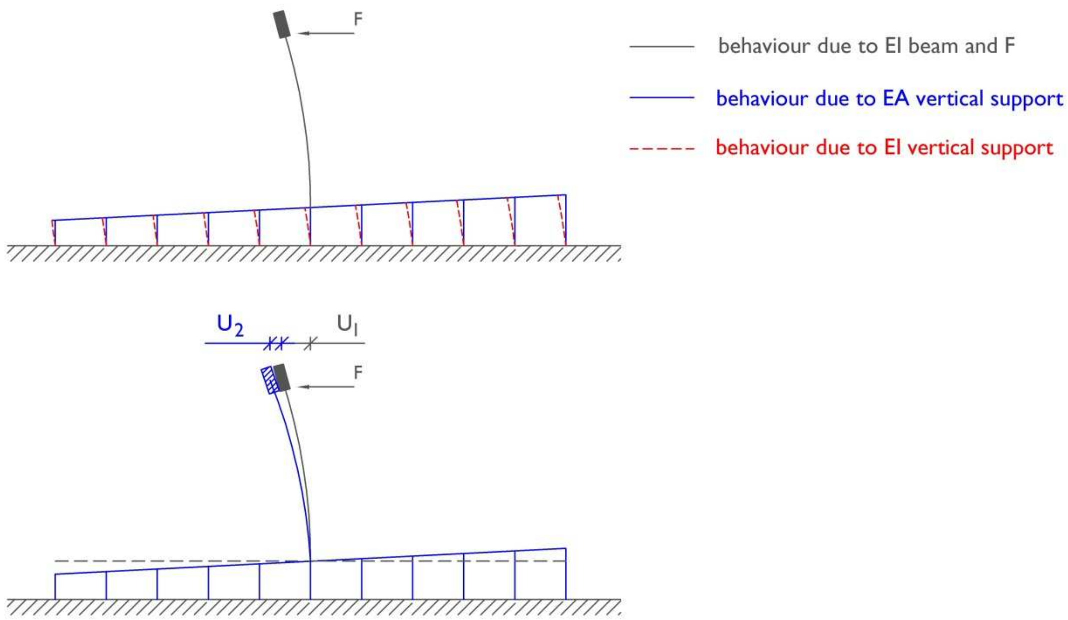

Figure 7-15 behaviour and stiffness auxiliary structure

The first relation indicates that the deformation behaviour induced by the EA of the vertical supports should be dominant over the deformation behaviour induced by the EI of the vertical supports (upper part of Figure 7-15). The second relation is meant to show the dominant displacement behaviour due to EI of the vibrating beam over the secondary displacement caused by the EA of the vertical supports. The secondary top displacement (u2) may be only a small proportion of the total displacement, in this way the frequency is not affected.
All input properties for the horizontal and vertical supports are depicted in Table 7-12.

Model input for auxiliary structure (plate elements)				
Parameter	Horizontal supports	Vertical supports	Unit	Explanation
EA	2.500E18	250.0E9	[kN/m]	Axial stiffness
EI	250.0E16	250.0E12	[kN m2/m]	Bending stiffness
w	0	0	[kN/m/m]	weight
v(nu)	0	0	[-]	Poisson's ratio

Table 7-12 Input properties for plate elements of auxiliary structure

The vertical supports have to ensure a proper introduction of forces into the base slab. It is important that, up to a certain level, the force distribution corresponds to the force distribution caused by a uniform distributed liquid. As a first assumption, the location of vertical supports is determined based on the pile geometry. Vertical supports are placed on top of every foundation pile and exactly in between two piles.
The length of the vertical supports is chosen as 0.5 m. This is only 3% of the length of the vibrating beam. Deflections and displacements are therefore supposed to be small compared to the vibrating beam-plate, especially in combination with the chosen EI and EA, and won´t affect the behaviour of the vibrating beam.

Calculations
The calculation phases are the same as used for the situation of a single beam. In total four phases are used:

0. Initial;
1. Building;
2. Loading;
3. Free vibration

In Phase 2 (loading) the top of the beam is loaded with a horizontal force in x-direction of -2500 kN. This force is randomly chosen and its goal is to bring the beam out of balance so it can vibrate in the next phase. In phase 3 (Free vibration) the applied force from phase 2 is released and then the system is allowed to vibrate for 3.0 seconds. These 3.0 seconds are sufficient as the modelled frequency of the LNG mass is 2 Hz. This means two cycles per second, so 6 cycles in total. This is sufficient to determine the frequency of the system on a proper and reliable way without introducing unnecessary long calculation times.

Results

The results are checked by the frequency of the vibrating beam and the force that is transferred by the auxiliary structure to the base plate. In this latter aspect, it is important that the correct forces are brought into the base plate whereby the behaviour in time is correct. The preceding sections have shown that the deflections and frequencies of a single beam/plate in PLAXIS are consistent with the results to be expected according to the analytical formulas.

Frequency

The first aspect that is judged is the frequency of the vibrating beam in combination with the auxiliary structure. The results of the lateral deflection (Ux) in time are depicted in Figure 7-16 for the top, blue line, and the auxiliary structure, red line, of the vibrating beam. The auxiliary structure shows only very small lateral deflections in the range of 0 - 0.1% of the top deflection. These deflections are negligible (as shown in Figure 7-16) and are not affecting the frequency of the system. The frequency of the system in 2 Hz as expected according to the input parameters, see Figure 7-17.

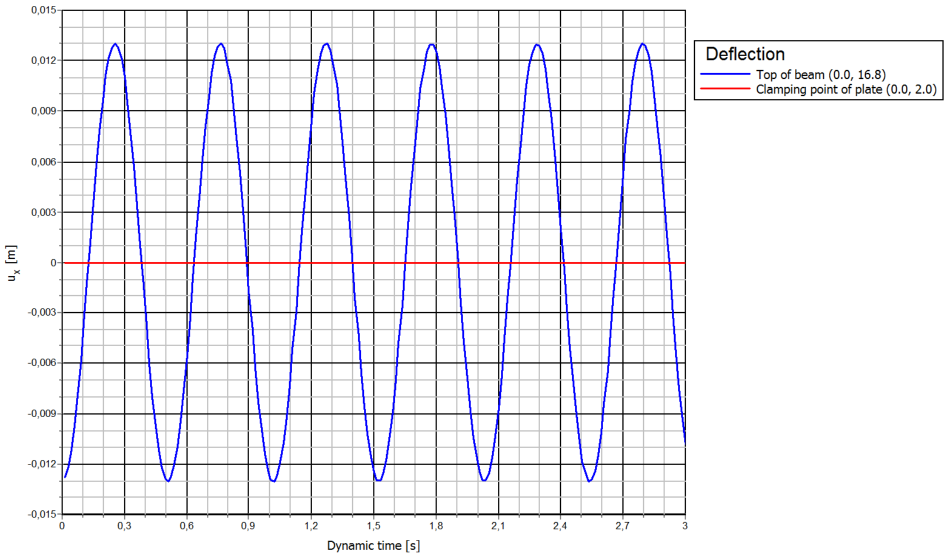

Figure 7-16 Deflection Ux of vibrating plate

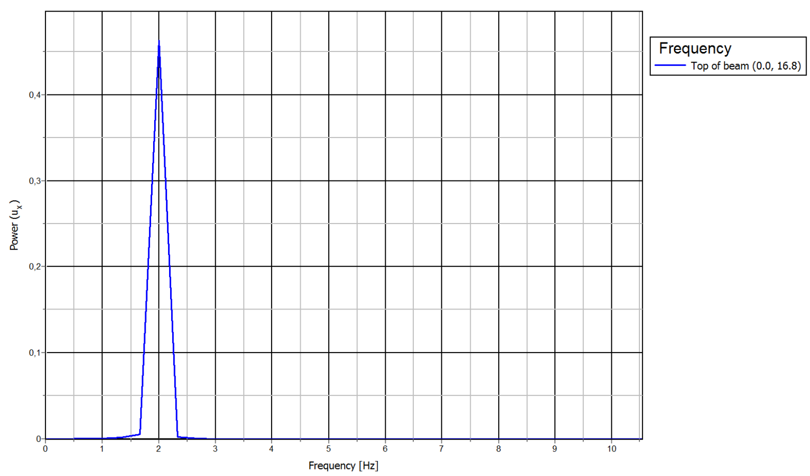

Figure 7-17 Frequency result

Forces

The forces in the system are introduced by the mass on top of the vibrating plate element. The mass is transferred as a force to the auxiliary structure and spread over the base plate. Forces that are introduced in the base plate are judged in building-, loading- and free vibration phase.

Due to the "infinitely" stiff[3] horizontal support all mass should be equally divided over all vertical supports. This is almost the case; axial forces in the vertical supports are ranging from 164 to 226 kN/m, with an average value of 176 kN/m per vertical support (see Figure 7-18). The sum of axial forces in all vertical supports is equal to the input value of 12,160 kN.

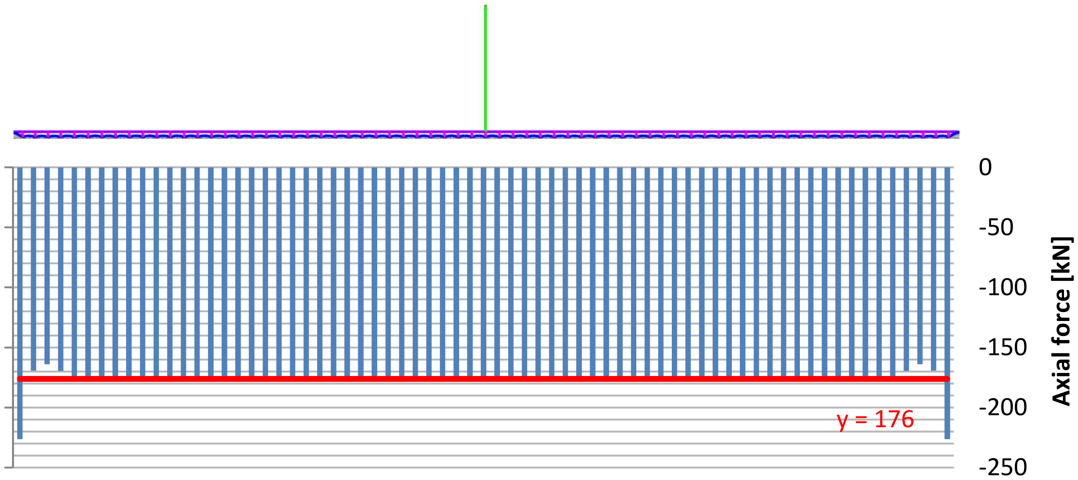

Figure 7-18 Axial forces in vertical supports of auxiliary structure after building phase

There are small variation, located at the edges, which are a result of small differences in the distance between successive vertical supports and therefore the area that remits on a specific vertical support. In Figure 7-19 the geometry of the edge fields of the auxiliary structure is displayed in combination with the area which remits, according to theory with EI=∞, on each vertical support. In Table 7-13 the axial force expected per beam is compared with the actual force found in PLAXIS. Especially the first two edge elements on both sides exhibit a larger deviation which cannot be fully explained, and is probably the result of numerical "problems/imperfections".

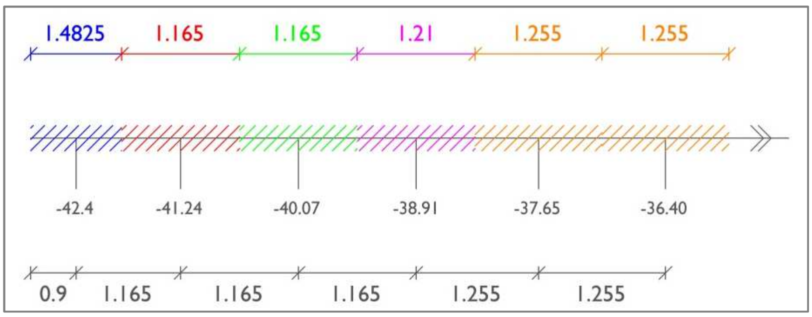

Figure 7-19 Geometry of edge fields auxiliary structure

[3] Infinite stiffness in PLAXIS is created by applying a high stiffness ratio compared to the construction elements in the surrounding (factor 1000-10000). Applying excessive stiffness (differences) can lead to numerical instability and inaccurate results.

X-coördinate [m from center]	Remittance area [m2]	Expected force [kN/m]	Force in PLAXIS 2D [kN/m]	Error [%]
-36,4	1,255	-175	-175	0%
-37,65	1,255	-175	-175	0%
-38,91	1,210	-169	-170	1%
-40,07	1,165	-163	-164	1%
-41,24	1,165	-163	-169	4%
-42,4	1,483	-207	-226	9%

Table 7-13 Axial force in vertical supports of edge fields

In phase 2: loading, a horizontal force of -2500 kN is applied at the top of the vibrating beam. This force A (see Figure 7-20) introduces a moment which allows for redistribution of axial forces, introduced by the weight on top of the vibrating plate, in the vertical supports.
As a result of the different geometry of the edge field the forces in the vertical supports are again higher. This can be found in as well the plot for axial and the plot of lateral forces. Besides this aspect there is still a deviation of the first two edge elements on either side. The deviation is in the range of 5-10%, shown in Table 7-13. A clear explanation for the deviation of the edge fields could not be found. This is no problem, since the deviations are very limited and do not affect the general behaviour. A linear trend line is added to show the gradient in axial forces ranging from 198 kN/m on the left, to 163 kN/m at the right-hand side. This trend line shows how well the axial force is distributed over the width of the base plate. The average deviation per vertical support towards this trend line is smaller than 2%.

In addition to the axial forces, also the lateral forces in the vertical supports are examined. The shear forces are almost uniformly distributed over the width of the base plate. Again the edge fields are showing some deviating values due to the different geometry. The most notable aspect is the peak on the left side. A clear explanation for this peak could not be found. However, the peak is not unrealistic compared to the actual situation, where the majority of the shear force is introduced under the connection between the inner tank wall and inner tank floor. The shear force is than distributed over the base slab through the insulation layer between the inner and base slab.

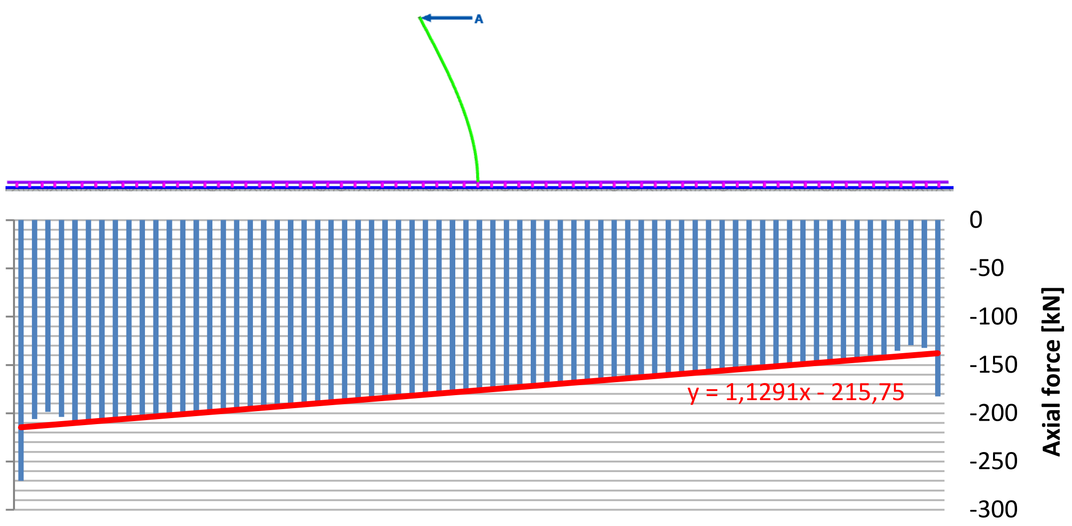

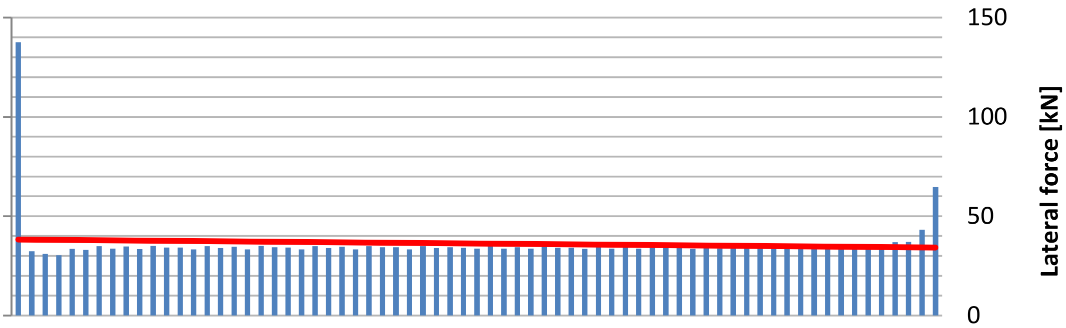

Figure 7-20 Axial and lateral forces in vertical supports of auxiliary structure after loading

In phase 3: free vibration, force A is released and the system is allowed to vibrate for 3 seconds. The plate element is vibrating with a frequency of 2 Hz, as already shown in Figure 7-16 and Figure 7-17. If the model works properly, the redistribution of axial forces in the vertical supports of the auxiliary structure goes with the same frequency. At this moment all models are completely elastic without damping; this means that after a half oscillation, the plate has reached its maximum deflection to the right (= equal to deflection after phase 2) and the force distribution is exactly mirrored with respect to the force distribution shown in Figure 7-20. Based on the frequency of 2 Hz (T = 0.5 s.) the maximum deflection to the right is found after 0.25 seconds. The force distribution after 0.268 seconds is shown below in Figure 7-21:

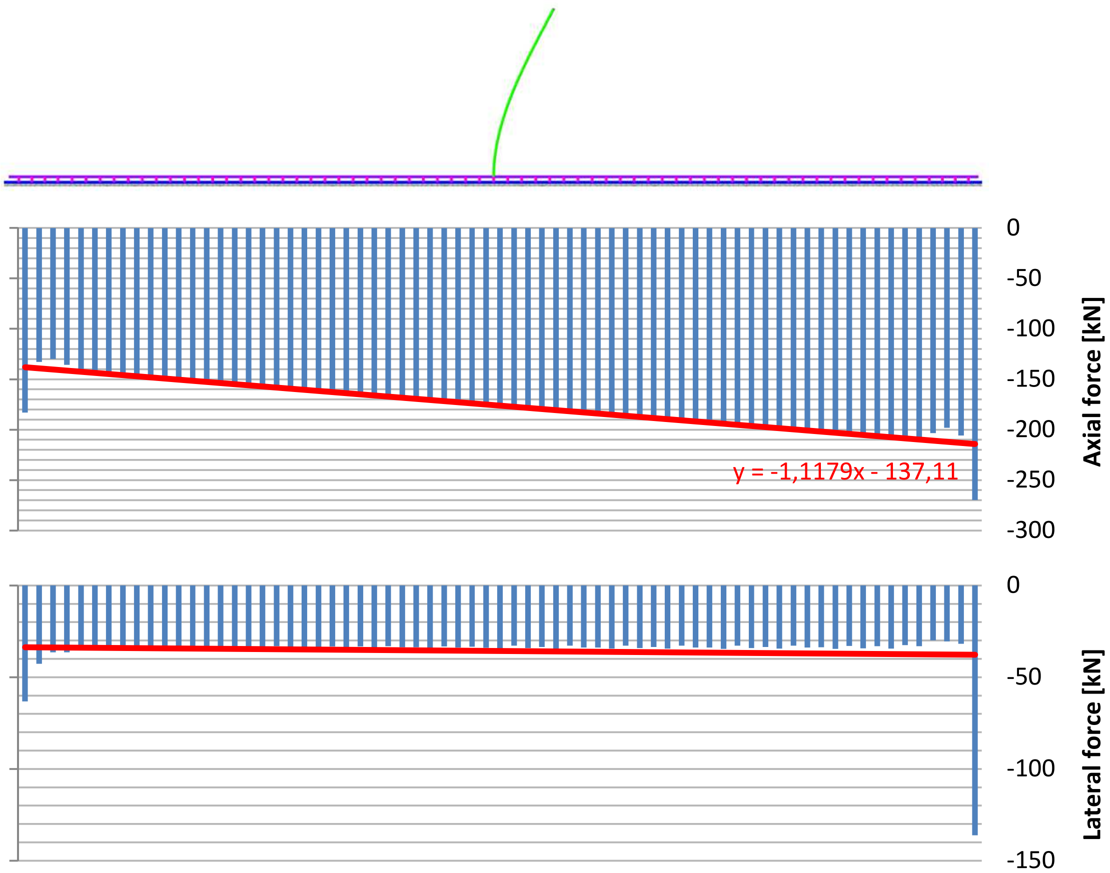

Figure 7-21 Axial forces in vertical supports of auxiliary structure after 0.25 s in Free Vibration

The distribution of as well the axial- and lateral forces is almost exactly mirrored to the force distribution at the end of phase 2: loading. There are only small differences with Figure 7-20. The differences are related to the time step from which the results are collected. This is after 0.268 seconds, which is 0.018 seconds after full deflection to the right. The sum of all lateral forces confirms this. In total the lateral forces is equal to 2466 kN which is lower than the initial applied lateral force at the top. Therefore top deflection in the situation presented in Figure 7-21 will be smaller than after the loading phase.

To get a better view of the behaviour of the vertical beams during the free vibration phase, a plot of the axial forces against the dynamic time is made. In Figure 7-23 the axial forces in 7 vertical supports at different distances from the centre of the base plate are plotted. The different supports which have been considered are shown in the cross-section of Figure 7-22. Colours used in the Figure 7-23 are corresponding to the colours in the cross-section.

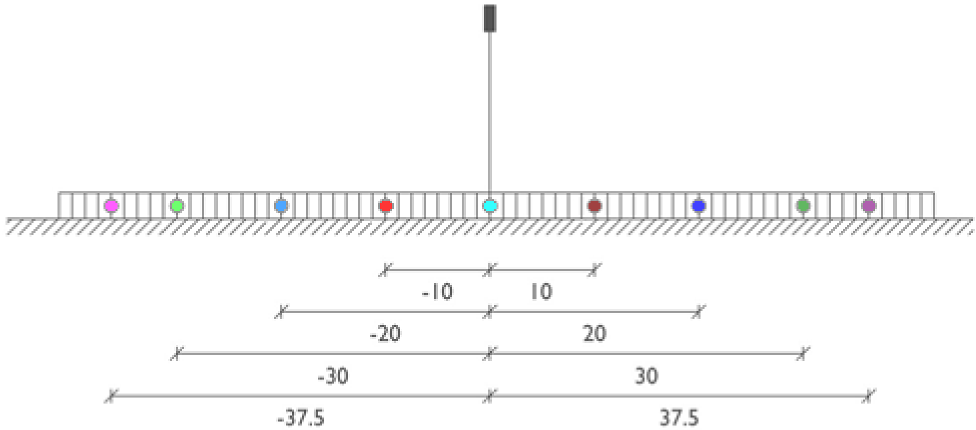

Figure 7-22 Location of the considered vertical supports

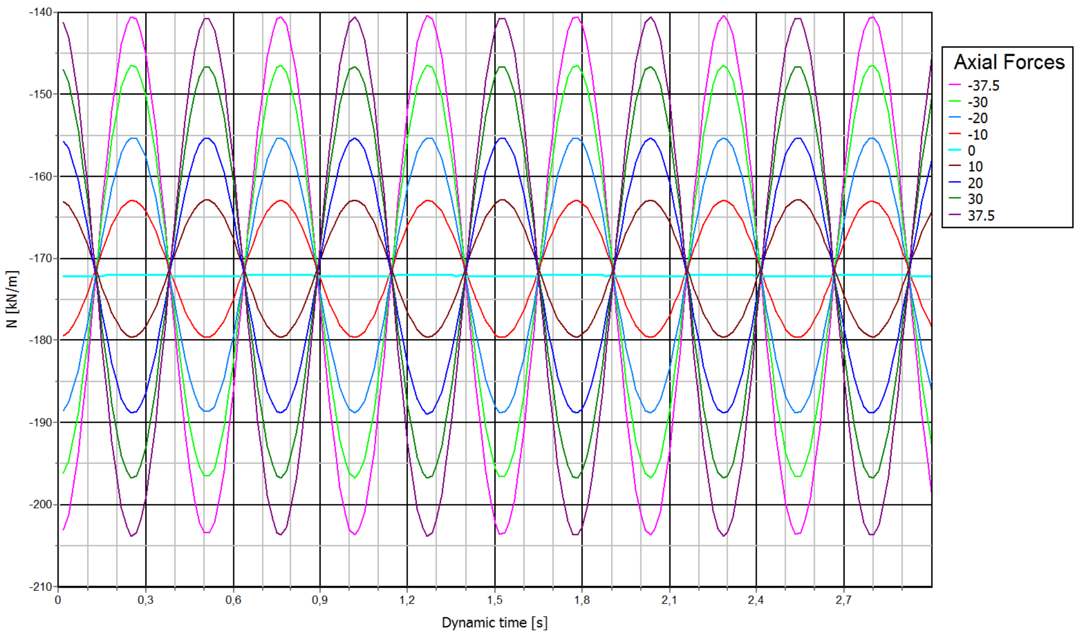

Figure 7-23 Axial forces vertical supports in time during free vibration

The behaviour is as expected. Force increments at the same distance left and right from the centre are equal but in opposite direction. In the time, forces are changing with the same frequency as the vibrating beam on top of the structure.
The model shows that mass is transferred over the width of the tank. The mass is transferred as vertical forces on the base plate; all these forces together introduce an overturning moment on the plate.

The behaviour of the shear forces in the vertical beams of the support structure in time is equal to the behaviour of the normal forces. Forces vary between a minimum and maximum with the same frequency of the vibrating beam on top of the auxiliary structure, see Figure 7-24. In the model shear forces are equally distributed over the width of the base plate, with exception of some edge effects and deviations due to numerical imperfections (see Figure 7-20).

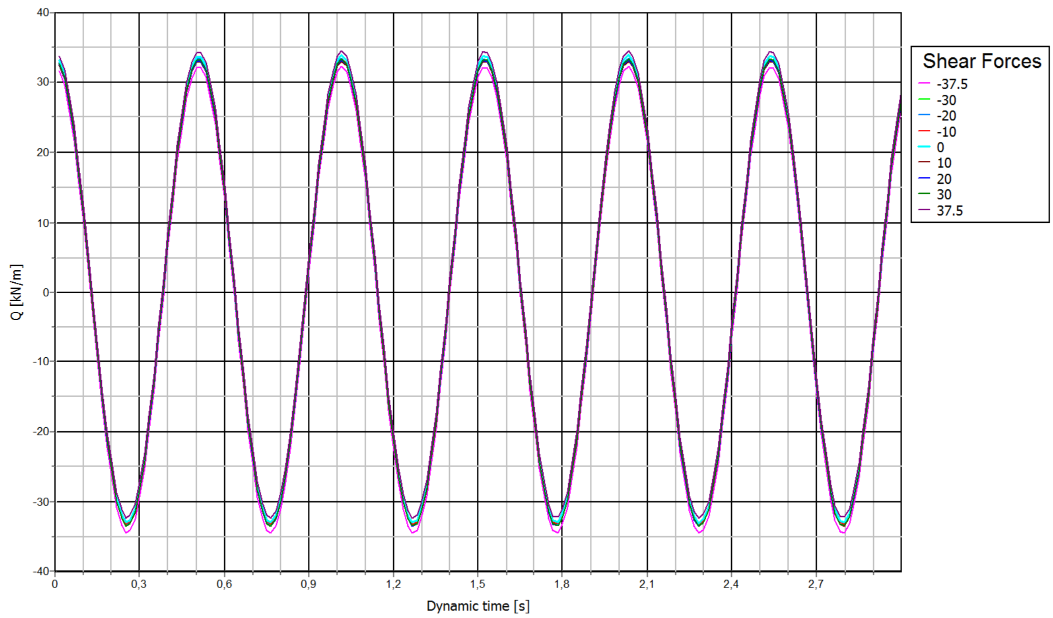

Figure 7-24 Shear forces vertical supports in time during free vibration

Damping
In reality damping is caused by friction or by irreversible deformations (plasticity or viscosity). With more viscosity or more plasticity, more vibration can be dissipated. Plasticity models already include these phenomena's and therefore show damping. In case this damping is not sufficient or if elasticity is assumed, matrix C (the damping matrix) can be used to take (extra) damping into account.

The model that is described in the previous paragraphs is purely elastic and therefore it does not account for damping. However, damping can be introduces by the so called Rayleigh damping formulation, already explained in paragraph 3.3.4. Rayleigh damping in PLAXIS is defined by:

$$C = \alpha_R M + \beta_R K \tag{7-11}$$

In this formulation, α_R and β_R are scalars, which determine the extent to which the damping is proportional to the mass and the stiffness. Considering Rayleigh damping, a relation can be established between the damping ratio ξ and the scalars α_R and β_R.

$$\alpha_R + \beta_R \omega^2 = 2\omega\xi \qquad and \qquad \omega = 2\pi f \tag{7-12}$$

In this formulation, ω is the angular frequency in rad/s and f is the frequency in Hz. PLAXIS solves this equation for two different target frequencies and corresponding target damping ratios given the required damping coefficients.

For LNG a damping ratio of about $\xi = 4.0\,\%$ has to be applied according to (Galanti en Courage, Seismic analysis of storage tanks with soil structure interaction 2006). This damping will be applied around the target frequency of 2 Hz. This leads to values of 0.5026 and 3.183E-3 for respectively α_R and β_R. If the damping is plotted against the frequency, this leads to the graphs depicted in Figure 7-25.

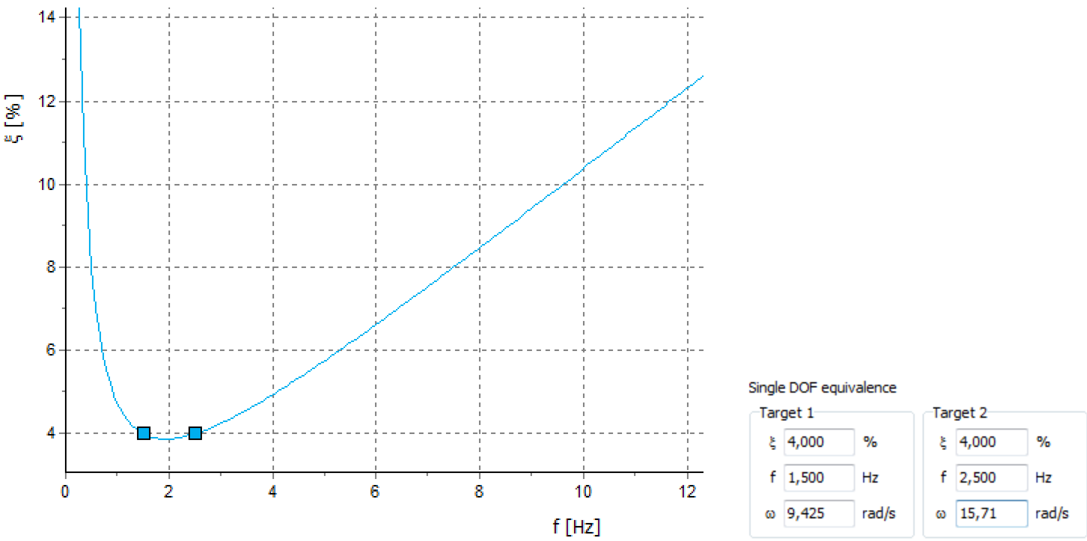

Figure 7-25 Damping ratio against frequency

In Figure 7-26 a new graph of the deflection Ux (top of shaking beam) against dynamic time is plotted for different damping ratios varying between 0% and 100%. The damping is modelled properly, peaks are located in the same moment of time and only amplitude is changing. For critical damping, $\xi = 1.0 = 100\,\%$, the beam is almost completely damped after one vibration (this is 1 second / 2 Hz = 0.5 Seconds). If a damping ratio of 4% is used, the system is completely damped afters approximately 8.5 seconds. Off course this is different for varying deflections.

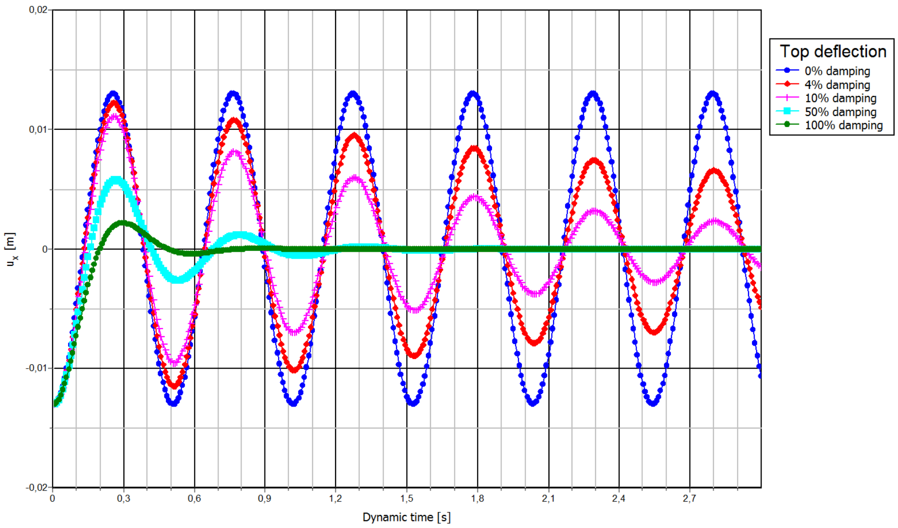

Figure 7-26 Top deflection against dynamic time for different damping ratios

7.6 Conclusions

Based on the results presented in the previous paragraphs some conclusions can be drawn about the modelling of the liquid inside the LNG storage tank.

- Only the impulsive (lower) part of the liquid mass will be modelled in the remainder of this thesis. This simplification can be justified on previous calculations performed by Protective storage engineers (PSE). The impulsive component ensures approximately 90% of the total base shear and 87% of the total overturning moment caused by the total liquid during a seismic event.

- The liquid is modelled as a linear mass-spring-system represented by a mass on top of a beam (PLAXIS 3D)/plate (PLAXIS 2D). Only difference between the situation in the 3D- and 2D-model is the shape of the cross-section of the "vibrating" beam/plate and therefore the determination of the moment of inertia. The 3D model is based on a square section, where the 2D is based on a rectangular cross section with one side equal to 1 meter.

- Frequency of a vibrating beam, clamped at the surface can be calculated equation (7-4). For convenience and to avoid errors, it is better to model a slender beam/plate. If a slender structure (d/l < 0,1) is used the deflection due to shear can be neglected. This means that the frequency (and frequency dependent elasticity modulus) can be described by equations (7-9) and (7-10)

- The results for both, the 3D and 2D model, are proper based on static deflection and frequency. Static deflection of the "vibrating" beam show only very small errors in the range of 0 – 0,3 % for as well the 2D as 3D model. The results for frequency also show negligible small errors. In most cases the error is determined by the number of the time steps that are used. In general a minimum of eight steps are needed to describe one cycle, with this rule of thumb the error on frequency can be limited to 1% for all frequencies. In the final model the LNG liquid is modelled with a frequency of 2 Hz, this means that time steps need to be smaller than 0.0625 sec for a proper modelling of the frequency.

- The auxiliary structure which is introduced in paragraph 7.5 ensures proper distribution of the liquid mass across the width of the base plate. The vertical force distribution is realistic in both, static- and dynamic situation. There are only minor deviations on the edge fields. This is most likely due to edge effects, large differences in stiffness and numerical impurities.
  The shear forces during the dynamic situation are equally distributed over the width of the base plate, with the exception of the edge fields. The peak shear forces found on the edge fields cannot be declared based on the model geometry/mechanical rules. However, the peak is not unrealistic compared to the actual situation, where the majority of the shear force is introduced under the connection between the inner tank wall and inner tank floor.

- Material damping of the LNG liquid in the tank can be introduced by Rayleigh damping. The damping ratio of LNG is estimated as 4.0 % by a frequency of 1.5 and 2.5 Hz., this results in Rayleigh damping coefficients of 0.4712 and 3.183E-3 for respectively α_R and β_R .

Based on the performed analyses and conclusions the following recommendations can be made:

- Time steps used in the dynamic analyses need to be checked with respect to frequency of the fluid (and other frequencies in the model). It is recommended to use at least 8 time steps per cycle which means: 1 / frequency [Hz] / 8 = time step [s]

- The spreading of the liquid load is only modelled in PLAXIS 2D. The auxiliary structure can probably also be used in PLAXIS 3D. A 3D model will have the advantage that there are spaces left between the horizontal and vertical supports, making it possible to model both the impulsive and convective mass. Further research is therefore recommended.

- At the moment only the distribution of the vertical- and horizontal forces over the width of the base slap are assessed. It is recommend that also the force distribution in the base slab is taken into account and compare to a real distributed liquid load. In this way the geometry of the auxiliary structure can be optimized for a realistic force distribution in the base slab.

8 FREE FIELD SITE RESPONSE ANALYSIS

A 1D PLAXIS analysis is performed to calculate the free field site response as a result of excitations at bedrock level. The 1D analysis is used as basis for the calibration of the final 2D dynamic model. Focus of the analysis will be on the influence of boundary disturbances, the effect of model width, mesh size, time stepping and performance of PLAXIS HS small model on site response.

A continuous layered soil profile is assumed to be representative in this study (see chapter 4). This assumption of a perfectly horizontally layered soil profile makes it possible to reduce the free field analysis to a 1D problem. Performing a 1D site response analysis in PLAXIS has been made possible by the relatively new “tied-degrees-of-freedom boundary”, which conceptually perfectly describes a 1D case. In the 2D situation the well-known absorbent- and newer free-field boundaries are used. It is known that reflections at these boundaries can disturb the free field site response within a region around the boundary. These effects can be excluded by modelling the boundaries far enough away. This prevents that reflection waves will significantly influence the site response in the middle of model.

8.1 Input signals

As already mentioned in chapter 1, the dynamic analysis in this thesis is limited to horizontal shear waves that propagate vertically. This simplification is justified on the fact that the most important motions and forces are expected in lateral direction over the length of the tank diameter.

In appendix B the seismic input signals are selected from the PEER ground motion database according to the site classification, code requirements and design response spectra presented in paragraph 4.3. In this thesis the site response analysis and dynamic calculations are, due to time limitations, performed for only two signals: one SSE and one for OBE. Both bedrock signals are presented in Figure 8-1 below.

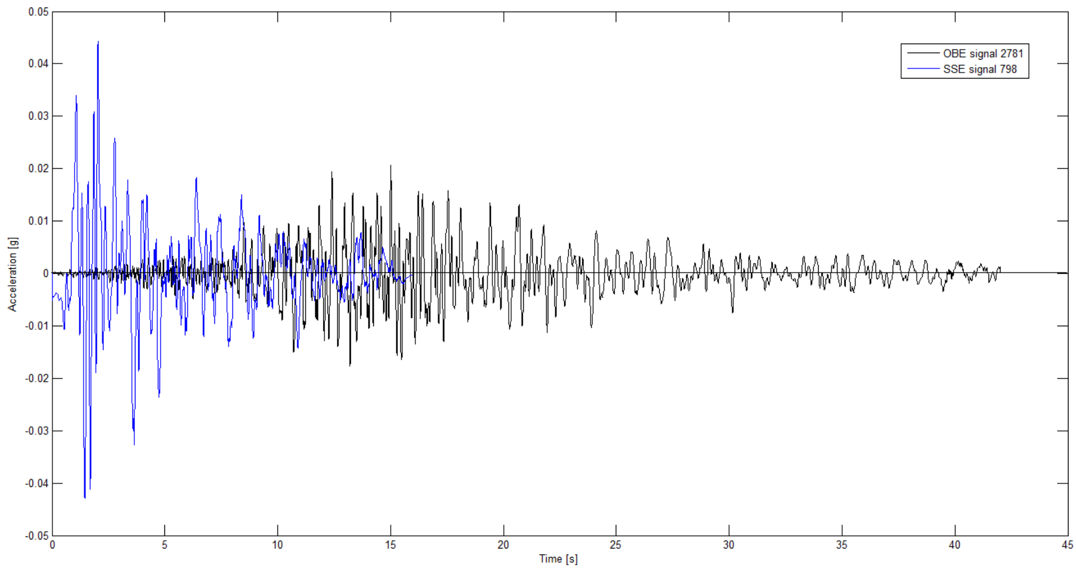

Figure 8-1 Bedrock signals 2781 and 798 for respectively OBE and SSE

8.2 Mesh element size and critical time step

To allow for proper modelling of the wave propagation inside the finite element model, the maximum element size and maximum time step need to be determined. The maximum element size can be calculated according to Lysmer and Kuhlmeyer (Lysmer en Kuhlmeyer 1969). In this theory the maximum element size in a layer is restricted by the maximum frequency and shear wave velocity of a layer according to equation (8-1) below:

$$element\ size_{layer} \leq \frac{\lambda_{layer}}{5} = \frac{v_{s;layer}}{5 \cdot f_{\max}} \tag{8-1}$$

The shear wave velocity is related to stiffness of the soil (see equation (3-3) in paragraph 3.2.2). Due to the stress dependency of stiffness in the HS small model the stiffness in the top of the clay layer and below the surface are relatively low. As a results small element are required in these zones, which computationally inconvenient. For a first approximation element sizes were calculated based on stress levels corresponding to the middle of different layers. Based on the results depicted in Table 8-1 this seems reasonable compared to stress levels corresponding to the top of the layers, even for the “softer” clay layer.

The maximum frequency in the model is determined by the natural frequency of the soil deposits, the natural frequency of structural elements and the frequencies inside the input signals. The dominant frequencies inside the two signals can be found by a Fast Fourier transformation of the signals from the time domain to the frequency domain. With the aid of a Matlab code (see appendix C) the dominant frequencies within input signals 2781 and 798 are determined and depicted in Figure 8-2.

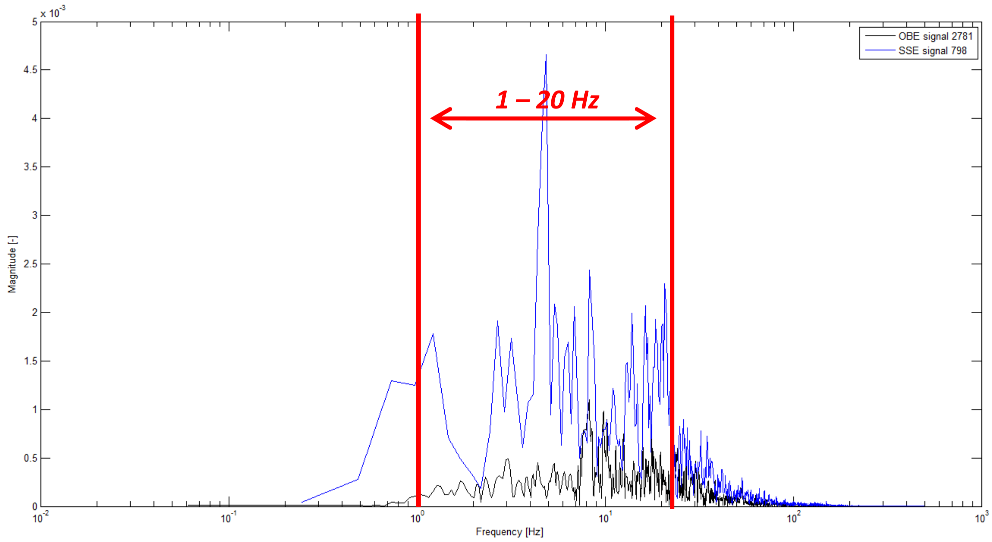

Figure 8-2 Dominant frequency range in signals 2781 (OBE) and 798 (SSE)

According to Figure 8-2 it can be conclude that signals 2781 and 798 have similar frequency characteristics. The dominant frequencies in the signals are spread in a range of 1 to 20 Hz, which is an important aspect for the mesh size and time stepping. Based on equation (8-1) the higher frequencies in combination with the lower shear wave velocity in the clay layer will be the most critical situation for element size and time stepping. This is shown in Table 8-1 on the next page.

The maximum allowable time step is based on Courant's condition (Forsythe en Wasow 2004), which restricts a time step by allowing a wave not to travel over more than one element length within a single dynamic time step. The maximum allowable time step ($\Delta t_{\max}$) can therefore be defined as:

$$\frac{v_{c;layer}\,\Delta t}{element\ size_{layer}} \leq 1 \qquad \Rightarrow \qquad \Delta t_{\max} \leq \frac{element\ size_{layer}}{\sqrt{\dfrac{E(1-\upsilon)}{\rho(1+\upsilon)(1-2\upsilon)}}} = \frac{element\ size_{layer}}{v_{s;layer}\sqrt{\dfrac{2(1-\upsilon)}{(1-2\upsilon)}}} \tag{8-2}$$

The maximum allowable time step is defined based on the compression wave velocity because wave reflections may cause compression wave disturbances although only shear waves are used as input at the model boundary. The compression wave velocity is higher and will therefore require smaller time steps. In Table 8-1 below the results for element size and maximum allowable time step are depicted.

Parameter	Sand Fill	Clay	Sand	Unit
	Loose - Medium dense	*Medium stiff*	*Medium Dense-Dense*	
$f_{soil\ deposit}$	5,5	0,6	3,0	[Hz]
$f_{signal;max}$	20	20	20	[Hz]
$f_{impulsive;max}$	2	2	2	[Hz]
$f_{important;max}$	12	12	12	[Hz]
σ'_{mid}	36	129	346	[kN/m2]
$E_{ur;mid}$	36000	18798	558032	[kN/m2]
$V_{s;mid}$	88	72	345	[-]
e $size_{soil\ deposit}$	3,20	23,20	23,20	[m]
e $size_{signal\ max}$	0,88	0,72	3,45	[m]
e $size_{impulsive\ max}$	8,76	7,16	34,50	[m]
e $size_{important\ max}$	1,46	1,19	5,75	[m]
Δt_{max}	0,0064	0,0061	0,0064	[s]
$\sigma' t_{top}$	9	56	201	[kN/m2]
$E_{ur;top}$	18000	8901	425323	[kN/m2]
$V_{s;top}$	62	49	301	[-]
e $size_{soil\ deposit}$	2,26	15,96	20,25	[m]
e $size_{signal\ max}$	0,62	0,49	3,01	[m]
e $size_{impulsive\ max}$	6,20	4,93	30,12	[m]
e $size_{important\ max}$	1,03	0,82	5,02	[m]
Δt_{max}	0,0064	0,0061	0,0064	[s]

Table 8-1 Maximum element size and critical time step

From Table 8-1 it can be noted that that the time step is limited to 0.0061 Sec. On the other hand, Figure 8-1 shows that the signals are respectively 17 and 42 seconds long and contain 3200-11000 data points with constant time step. For accurate modelling of the input signal all data point need to be transformed to separate time steps. Time steps are therefore already limited to 16/3200 = 0.005 for OBE and 42/11000 = 0.005 for SSE. Time steps are therefore limited by the input signal instead of the wave propagation. It is noted that the default number of required steps (additional steps x substeps) provided by PLAXIS is much higher than the required number of steps calculated based on a time step of 0.005 s. This is explained by the fact that PLAXIS calculates the number of steps based on a compression wave velocity that tend to infinity when the Poisson's ratio approaches 0.5 for undrained conditions.
The influence of mesh element size on the accuracy is investigated in more detail in the following chapter with the goal to reduce computational effort without affecting the results.

8.3 Boundaries and model width

In the free field site response analysis in PLAXIS 2D three types of boundaries are compared: 1D tied degrees of freedom, 2D viscous (or absorbent) boundaries and 2D free field boundaries. In this small study the 1D tied degrees of freedom boundaries are supposed to be correct. Previous research already showed good matches between these boundaries and different response analysis in as well the time- as frequency domain. The 1D analysis can therefore be seen as a reference for the different 2D analyses. More information about the different boundaries that are available in PLAXIS 2D can be found in (Brinkgreve, Engin en Swolfs, Manual Plaxis 2D 2012).

In total 9 analyses are performed for both earthquake signals, OBE and SSE. A 1D reference analysis with tied degrees of freedom, a 2D analysis with viscous boundaries at 50, 100, 150 and 200 meter from the centre of the model and a 2D analysis with free field boundaries at 50, 75, 100 and 125 meter from the centre. Note that boundary distances are defined from the centre of the model, complete model width is therefore varying between 100, 200, 300 and 400 for the viscous boundaries and between 100, 150, 200 and 250 for the free field boundaries.
During the investigation of the boundaries an average element size of 1.7 meters is use. This is supposed to be sufficient small for a first assessment of the boundary distance and performance. In the end the influence of finite element size is tested separately.

The required model width (boundary distant) in the 2D analysis will be determined on the free field side response in the middle of the model. Analyses are performed for both selected earthquake signals shown in Figure 8-1. The criteria for the determination of required model width are:

- Good match between the bedrock accelerations found in the model and the input signal;
- Convergence of horizontal accelerations at the centre of the 2D models (viscous boundaries and free field boundaries) with the 1D model (tied degrees of freedom);
- Convergence of horizontal displacements at different depths at the centre of the 2D models (viscous boundaries and free field boundaries) with the 1D model (tied degrees of freedom);
- In the centre of the 2D models only small amplitude of vertical oscillations may be found. Only horizontal shear waves (propagating vertically) are applied to the model. Vertical oscillations at ground level are therefore related to wave reflections at the boundaries resulting in Rayleigh (surface) waves.

8.4 Results site response analysis

8.4.1 Input signal

Especially the 1D model and the 2D free field boundaries show a good match between input signal and the actual signal present in the model at bedrock level (-60 m). This is shown in Figure 8-3 for the first 5 seconds of the SSE bedrock signal 798. Only small differences can be found compared to the input signal. These differences are mainly caused by the fact that the results from PLAXIS are plotted on the basis of additional steps, which are twice as large as the time steps used in the input signal. This difference is not present in the calculation model. By the use of sub steps, the number of steps in the input signal and calculation model is equal.
The 2D viscous boundaries show a bigger deviation from the input signal. Waves at the boundaries are partly reflected and start to disturb the signal. Based on the shear wave velocity and the boundary distance of 100 meter, a wave only needs 0.5 seconds to reflect and return to the centre of the model. In Figure 8-3 the disturbance is only evident after the higher amplitude part. At smaller boundary distances the disturbances are introduced even faster and they are bigger. The OBE signals (peak acceleration of 0.02 g) have smaller acceleration amplitudes and therefore disturbance is less than in the SSE signals. These aspects are made visible in appendix E.1, in which all results are presented.

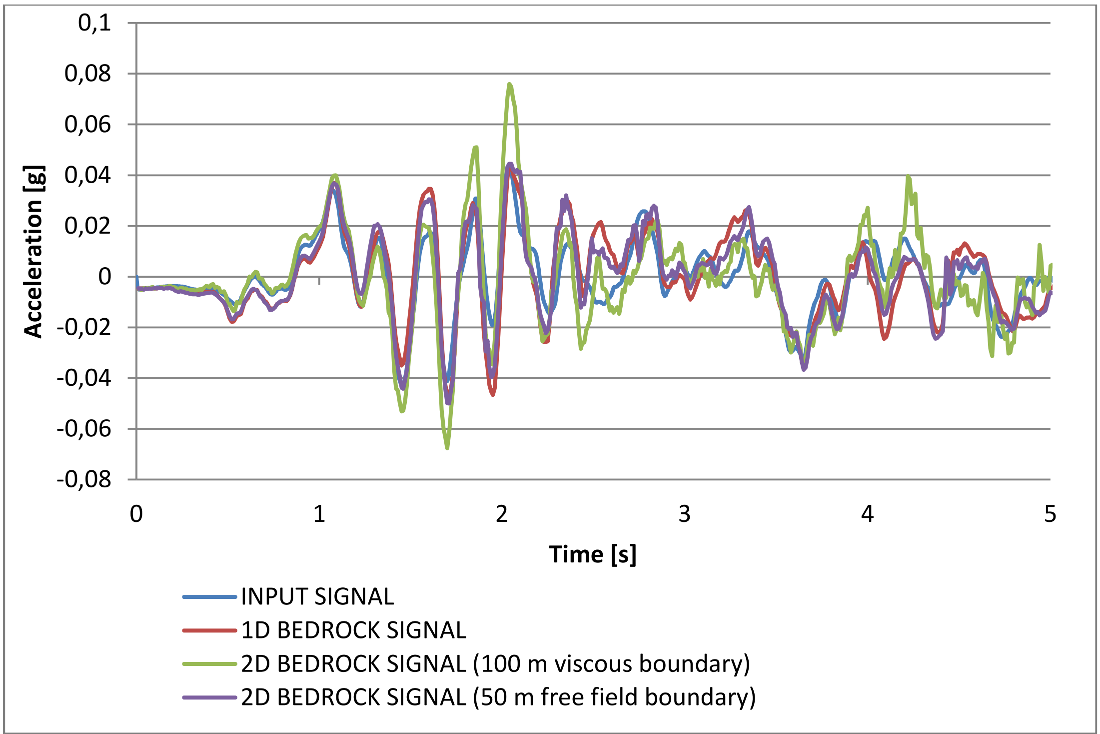

Figure 8-3 Check of SSE bedrock signal for different model boundaries

8.4.2 Horizontal acceleration

The horizontal accelerations in the middle of the model are examined in Figure 8-4. The response for all models with free field boundaries is fairly consistent. The general picture of the horizontal accelerations at ground level corresponds to the accelerations found in the 1D model. From the complete results, presented in appendix E.2, the free field boundaries show their independences of lateral boundary distance. This is also shown in the next paragraph were the horizontal displacement response is discussed. Peak amplitudes are sometimes a little bit lower and/or shifted in time but the general picture of the horizontal acceleration response seems to be acceptable.
Results for models with viscous boundaries show a less promising result. Acceleration response is influenced by the boundary distance and shows a lot of “noise” in especially the smaller models. Even in the model with a boundary distance of 200 meters (model width = 400 m.) the horizontal accelerations are affected by the boundary and show a lot of “noise” in especially the later, lower amplitude, part of the SSE signal.
The OBE situation (peak acceleration of 0.02 g) shows a better behaviour of the viscous boundaries. There is less “noise” and the horizontal acceleration response is converging with 1D model. Models with free field boundaries show a response that is almost identical to the 1D situation. It can be stated that boundary behaviour is earthquake depended, at lower amplitudes boundaries, especially viscous boundaries, perform better. This is also shown in appendix E.2, where al results of the site response analysis are presented.

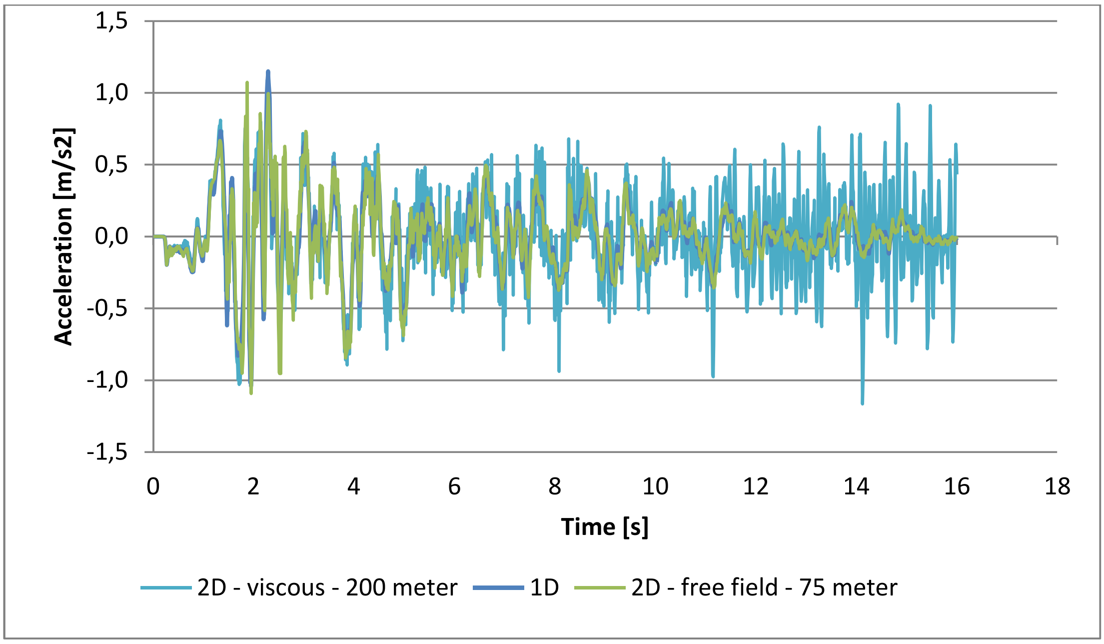

Figure 8-4 Check of horizontal accelerations at the surface - centre of the models - SSE signal

8.4.3 Horizontal displacement

The actual displacement response in the centre of the 2D models needs to converge with the response in the 1D tied degrees of freedom model. In Figure 8-5 the SSE displacement response at ground level in the middle of the model is plotted for different boundary types and distances.

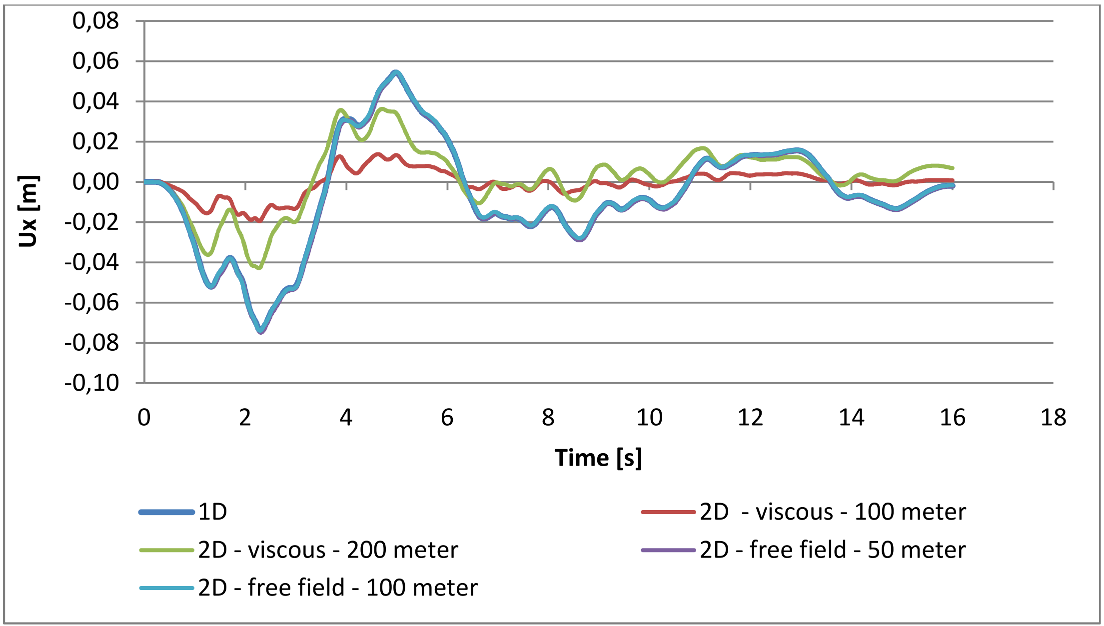

Figure 8-5 Horizontal surface displacement - SSE - different model boundaries and distances

The displacement response for the models with free field boundaries is converging with the 1D model. The displacement response for these models is, in contrast to the response in models with viscous boundaries, independent of boundary distance. All free field boundary models have a horizontal displacement response that is converging with the response found in the 1D model with tied degrees of freedom.

On the other hand the viscous boundaries show a response that is very depending on boundary distance. There is an improvement in the response seen with increasing boundary distance, but even for a distance of 200 meters (400 m model width) the response is not converging with the response found is the 1D analysis.

In Figure 8-5 the result for the SSE signal are plotted. Results for the OBE situation (peak acceleration of 0.02 g) show a similar response of the distance dependency of viscous boundaries. Although the displacement response with viscous boundaries is converging more than in the SSE situation, free field boundaries seem to perform better. This is shown in appendix E.3, together with the complete results of the SSE situation.

8.4.4 Vertical acceleration

Vertical accelerations at ground level are the last aspect that has been considered. Because all models are subjected to horizontal shear waves that are propagating vertically, only small vertical oscillations at ground level are expected. Vertical acceleration amplitudes are the results of reflection from boundaries, or other objects, resulting in compression and surface waves (Rayleigh waves).

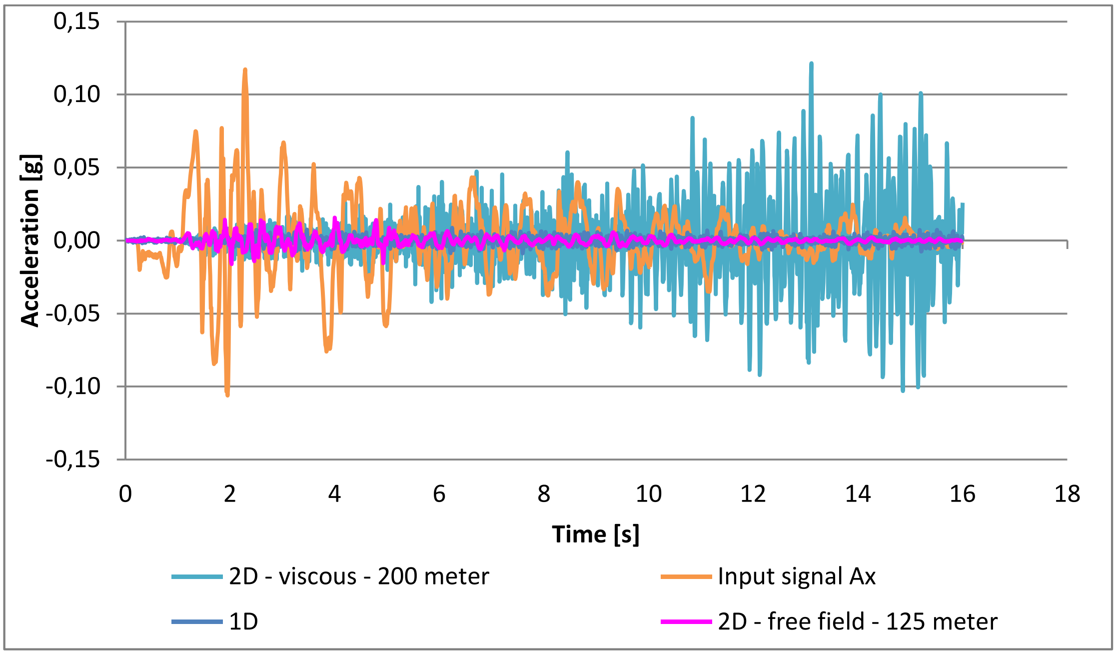

Figure 8-6 Vertical surface acceleration - SSE - different boundary types and distances

In Figure 8-6 the vertical acceleration at ground level are plotted for different boundary types and distances. As a reference also the horizontal accelerations implemented inserted in the model are plotted. Both 2D boundaries, as well the 1D tied degrees of freedom, show oscillations of vertical accelerations at ground level. When viscous boundaries are applied, oscillations grow rapidly during time and closer to the boundaries. This aspect is more severe for SSE than OBE, vertical acceleration even surpass the accelerations imposed horizontally at the bottom of the model.

The 1D tied degrees -of freedom – and 2D free field boundaries also show vertical accelerations at ground level but clearly much lower than in case of viscous boundaries. When subjected to the SSE signal, peak accelerations in the centre region are about 0.01 g, which is less than 10% of the horizontal peak accelerations applied to the model. Even better results are expected when mesh optimizations are made. All results, including for the OBE situation, can be found in appendix.

8.5 Conclusions

Based on the free field site response analysis the following conclusions can be made:

- Viscous boundaries appear to respond both, distance and signal dependent. Higher peak accelerations cause more noise at greater distances from the boundary. When viscous boundaries are applied, the influence of these boundaries on ass well the horizontal and vertical acceleration at the centre of the model should be examined.

- Free field boundaries appear to respond signal dependent but not distance dependent. The response for higher peak accelerations differ a little bit more with the 1D solution (tied degrees of freedom) than for lower peak accelerations.

- For this thesis viscous boundaries prove to be inapplicable. Wave reflections at the boundaries cause too much "noise" when applied at 200 meter from the model centre. The use of larger boundary distances will lead to computational inconveniences.

- Free field boundaries are the best solution for the following of this thesis. Based on a comparison with a 1D tied degrees of freedom model a boundary distance of at least 100 meter should be applied. Horizontal accelerations and displacements at ground level are converging while vertical peak accelerations are limited to less than 8 % of the applied horizontal peak acceleration at bottom of the model.

- In all analyses the soils are modelled by use of the hardening soil small strain model without additional Rayleigh damping. According to (Brinkgreve, Bonnier en Kappert, Hysteretic damping in a small-strain stiffness model 2007) 1-2% Rayleigh damping should be added to account for realistic damping behaviour. This damping has a positive effect on the operation of the boundaries (mainly viscous).

Based on the free field site response analysis the following recommendations can be made:

- Boundaries are tested for only two signals: OBE (peak acceleration of 0.02 g) and SSE (peak accelerations of 0.05 g). For a real good assessment of different boundary types more analyses with a wider range of signals should be performed.

- Performance of the 2D viscous- and free field boundaries are verified with a 1D model with tied degrees of freedom. For a real good assessment of the different 2D boundary types a comparison with other solutions in both the time- and frequency domain is recommended.

- Influence of reflecting waves from a structure inside the mesh is not investigated. Especially the performance of the viscous boundaries is different for other wave angles and should be investigated.

- Influence of element size should be investigated in more detail. Especially the impact on vertical accelerations at ground level is interesting.

9 2D FINAL MODEL

The remaining two research questions of this thesis, wave propagation effects and calculation method, are investigated by means of a 2D fully dynamic model in PLAXIS 2D. Starting point for this model is the information gathered in previous chapters. The model is set up according to the geometry and boundary conditions given in chapter 4, piles are modelled using embedded piles (chapter 6), the (impulsive) liquid is modelled according to the theory presented in chapter 7 and the model meets the dynamic boundary conditions arising out of chapter 8.

9.1 Geometry and model elements

The considered cross-section of the LNG tank is already presented in Figure 4-2 and a larger scale drawing can be found in appendix A. In the cross-section the piles are modelled as embedded piles, the base plate and impulsive liquid are modelled with the aid of plate elements and the concrete outer tank is schematized by two vertical loads modelled at the connection with the base plate. This modelling is chosen because of the high rigidity of the outer tank due to pré-stressing. The contribution of the outer tank to the total overturning moment, caused by impulsive liquid mass, will therefore be limited.
Figure 9-1 gives an overview of the cross-section as modelled in PLAXIS 2D.

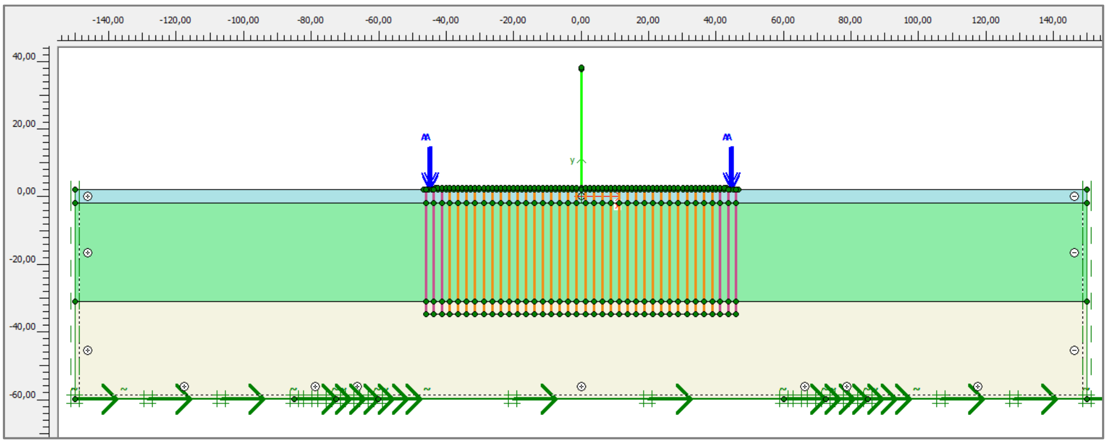

Figure 9-1 model geometry

9.1.1 Soil structure and soil parameters

The soil profile is a simplified representation of the actual soil structure in the Angola case. The eight soil layers that were actually present have been reduced to three layer system, assuming: a medium dense (man-made) top layer of sand, a thick medium-stiff clay layer in the middle and a deep medium-dense sand layer. The profile is shown in Figure 9-1
To account for the dynamic behaviour, all soil layers are modelled with the hardening soil small strain model (see 3.4.6 Hardening soil small model). Although this model has not been designed specifically for dynamic application, it does have capabilities to describe dynamic soil behaviour to some extent. The small-strain stiffness formulation involves degradation of the shear stiffness with increasing shear strain, and it takes into account that the high small-strain stiffness is regained upon load reversal. When subjected to cyclic shear loading the model shows hysteresis. This feature provides damping in dynamic calculations (Brinkgreve, Bonnier en Kappert, Hysteretic damping in a small-strain stiffness model 2007).

The soil properties for all three layers are presented in Table 9-1 and are determined according to correlations explained and presented in paragraph 4.4.

Parameter	Sand Fill *Loose - Medium dense*	Clay *Medium stiff*	Sand *Medium Dense-Dense*	Unit
Top level	2	-2	-31	[m]
Bottom level	-2	-31	-60	[m]
γ_{unsat}	18	15	18	[kN/m3]
γ_{sat}	20	15	20	[kN/m3]
$E_{50;ref}$	20000	3000	40000	[kN/m2]
$E_{oed;ref}$	20000	1500	40000	[kN/m2]
$E_{ur;ref}$	60000	15000	120000	[kN/m2]
power (m)	0.5	0.9	0.5	[-]
P_{ref}	100	100	100	[kN/m2]
e_{init}	0.5	0.5	0.5	[-]
c'_{ref}	0	$S_{u;inc}$ = 1.591 Y_{ref} = -2.00	0	[kN/m2]
ϕ'	32		34	[°]
ψ'	2		4	[°]
$Y_{0.7}$	1.66E-04	9.00E-04	1.33E-04	[-]
$G_{0;ref}$	78261	37500	156522	[kN/m2]
v_{ur}	0.15	0.2	0.15	[-]

Table 9-1 Soil parameters

According to the relation of (Hardin en Drnevich 1972) for G/G_0 as function of shear strain, the hysteretic damping in the HS small model will be negligibly small for very small motion amplitudes, which appears to be unrealistic compared to actual soil behaviour. Therefore it is recommended, according to (Brinkgreve, Bonnier en Kappert, Hysteretic damping in a small-strain stiffness model 2007), to introduce additional Raleigh damping in the model. For this Rayleigh damping, 1-2% of the critical damping is assumed to be reasonable. This Rayleigh damping is added to the frequency range of 1-12 Hz for all soil layers, in such a way that all important frequencies are covered. The default input method of PLAXIS is used for the modelling of damping. With a damping ratio of 2% for frequencies 1 and 12 Hz, values for α_R and β_R are respectively 0.2320 and 0.4897E-3. In this way all target frequencies are ensured of at least 1% Rayleigh damping.

9.1.2 Piles

The piles in the cross-section can be separated in two types: edge piles and middle-field piles. The geometry of the piles is exactly the same but the relative out-of-plane distance varies. Edge piles are arranged at a distance of 1.5 meter from each other in accordance with a circular geometry, while the field piles are spaced with a distance of 2.51 meter from each other according to a square geometry. The actual geometry is shown on the drawings in Appendix A. Further pile properties are the same for all piles and presented in Table 9-2.

Parameter	Explanation	Value	Unit
E	*Elasticity modulus*	2,1 E8	[kN/m2]
γ	*Gamma, specific weight of steel*	78	[kN/m3]
Pile type	*Predefined Circular tube*		
D	*Outer diameter*	0,61	[m]
t	*Wall thickness*	0,017	[m]
$T_{top;max}$	*Maximum skin resistance at the top of the pile*	0	[kN/m]
$T_{bottom;max}$	*Maximum skin resistance at the bottom of the pile*	145	[kN/m]
F_{max}	*Maximum base resistance of the pile*	2650	[kN]

Table 9-2 Pile parameters

Bearing capacity of the embedded piles is supposed to be equal to the Angola case. This means that the T_{top}/T_{bottom} and F_{max} are determined under the assumption of a plugging pile, although this may not be completely realistic in the ground structure describe above. It is expected that this assumption of a plugging pile has no significant effect on the results.

9.1.3 Earthquake loads

Final calculations are performed for two scenarios: OBE (peak ground acceleration of 0.02 g) and SSE (peak ground acceleration of 0.05 g). Both scenarios are calculated with only one earthquake signal, in contrast to the minimum of 3 as required by the Euro code. This is done due to time limitations. The signals that are used for OBE (signal 2781) and SSE (signal 798), depicted in Figure 8-1, are selected from the PEER NGA ground motion database based on the response spectra presented in paragraph 4.3. The selection procedure of the signals can be found in appendix B.

From the signals only the horizontal accelerations in one direction are assessed in the calculations. This simplification is justified on the fact that the most important motions and forces, during an earthquake event, are expected in lateral direction over the length of the tank diameter. The signals from the PEER NGA ground motion database are selected as bedrock signals. Although bedrock level will be even deeper in reality, signals are applied as bedrock signals at a depth of -62 m. below ground level (bottom of the model). The signals are implemented as acceleration multipliers over a prescribed displacement which has been imposed on the bottom of the model.

9.1.4 Impulsive liquid

In this thesis only the impulsive, sliding, liquid mass inside the LNG tank is modelled. As already explained in paragraph 7.1, this part of the fluid is normative for the resulting forces on the foundation. The steel inner tank moves in accordance with the impulsive liquid and therefore both masses are added. The entire mass is modelled as a vibration beam (linear mass-spring-damper system) with properties based on its natural frequency of 1.85 Hz.
The mass that is related to the impulsive motion is calculated according to the cross-section presented in Figure 4-2 (or appendix A) and the regulations of API 620, appendix L and NEN-EN 1998 Annex A. For the considered cross-section the weight of the impulsive liquid is 314 MN, which has to be modelled on a height of 34.26 m above the base plate. This height is significantly higher than the actual fluid height due to the predominant contribution of bottom pressures to the acting moment on the base slab. The complete calculations of all input parameters for the impulsive liquid mass are presented in appendix F.
The mass is modelled on a beam with a stiffness that is related to the natural frequency of the impulsive LNG liquid (1,85 Hz.). The calculation of the stiffness is performed according to the theory presented and verified in chapter 7.1. For the beam, used in the final model, calculations of the frequency depended stiffness can also be found in appendix F.

For a realistic distribution of all forces on the base plate an auxiliary construction (Figure 7-13) has been used. The theory of this auxiliary structure is already presented and verified in section 7.5. The behaviour of the beam with auxiliary structure that will be used in the final model is verified in static and dynamic situation with the aid of three models (see Figure 9-2):

A : The auxiliary structure is modelled on a rigid foundation, modelled as an elastic layer with high stiffness.

B1 : The auxiliary structure is modelled on the actual foundation and the base plate has a realistic stiffness.

B2 : The auxiliary structure is modelled on the actual foundation and the base plate is “infinitely” stiff.

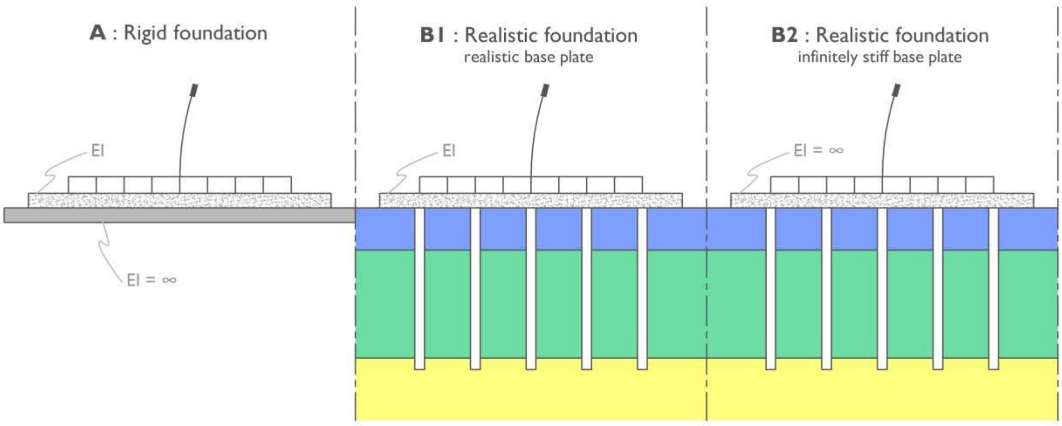

Figure 9-2 different calculations model

The complete results of this verification analysis can be found in appendix F. Most important results are treated now.

Results model A

The structure, beam and auxiliary structure, has a natural frequency of 1.83 Hz. All forces are properly distributed over the width of the base plate, only the edge fields show small deviations; probably the deviations are a result of edge effects in combination with numerical impurities.

Results model B1

In contrast to the system on a rigid foundation two dominant frequencies are found based on the horizontal excitations (Figure 9-3). The first frequency of 1 Hz is related to the soil, piles and base plate while the second frequency of 1.83 Hz is related to the impulsive fluid mass. This shows that there is interaction between the inner tank/fluid and underlying foundation.

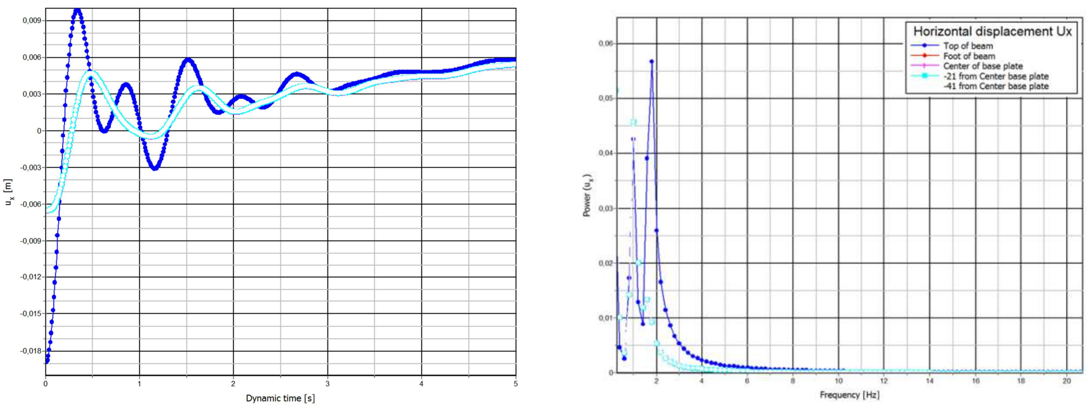

Figure 9-3 Horizontal displacements and their frequency

The axial force is distributed over the base plate by the auxiliary structure. In as well the static, loading as free vibration phase this distribution is realistic. The force in a vertical support of the auxiliary structure is determined by its remittance area and their stiffness. Half of the vertical supports of the auxiliary structure are placed on top of an embedded pile; their response is therefore stiffer than the vertical supports in between them. As a result the vertical supports in the middle fields play a minor role in the description of total forces, this is shown in Figure 9-4.

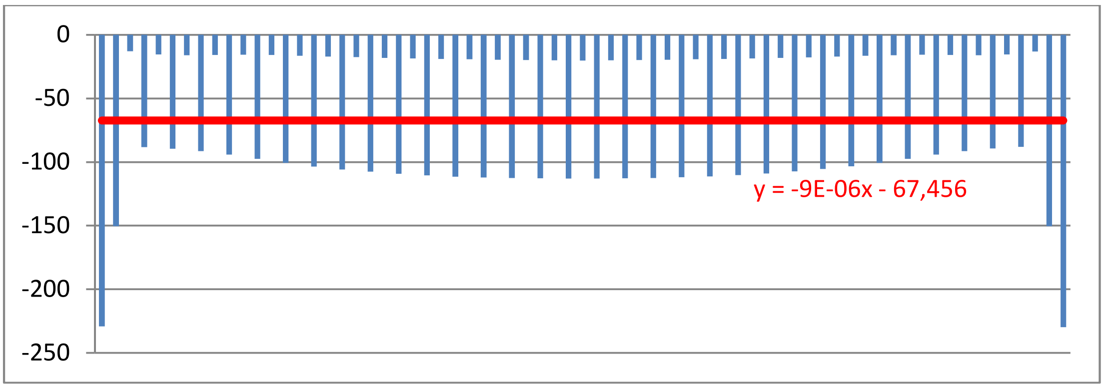

Figure 9-4 Axial forces [kN/m] in vertical supports after building phase – model B1

All the vertical supports together reflect the effect of the inclination of the LNG liquid on the base plate. The inclination of the liquid in time can be assessed by plotting the axial forces in the vertical supports, depicted in Figure 9-5. Two dominant frequencies are found. The frequency related to the impulsive liquid (1.83 Hz) is far more dominant. Therefore the fluid is modelled properly.

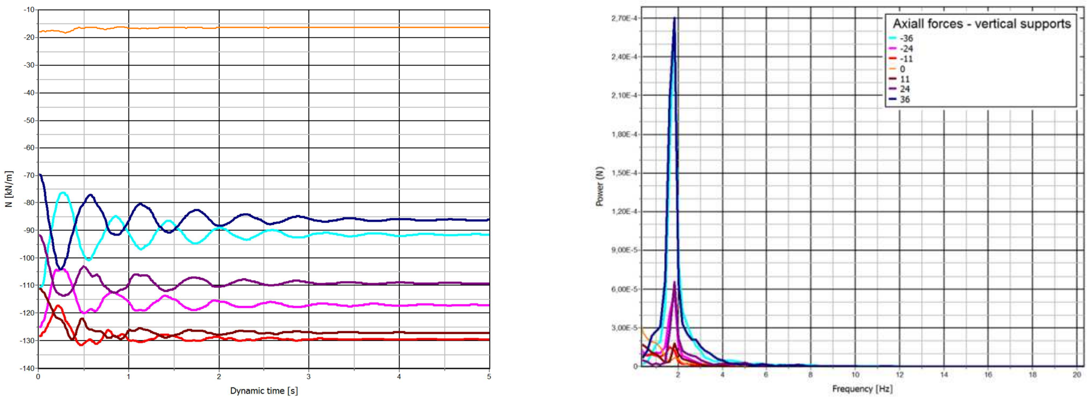

Figure 9-5 Frequency of axial forces in vertical supports at different distances from centre

A big difference between the PLAXIS model and the reality is the existence of a true connection between the auxiliary structure (inner tank) and base plate. In reality the inner tank is not anchored to the baseplate. It is more or less loosely placed on the base plate with in between an insulation layer of foamglass. Therefore the distribution of the especially the shear forces over the base plate is not completely realistic. In the model shear forces during loading are distributed over the complete diameter of the tank with peaks at both sides, while in reality the shear forces are mainly transmitted through the walls of the inner tank. This means that peak values of shear force, located under the inner tank wall, are probably underestimated.

<u>Results model B2</u>

Results for model B2 are identical to model B1 based on horizontal displacement and frequencies. Differences are found in the distribution of forces over the vertical supports of the auxiliary structure. The infinitely stiff base plate provides a uniform stiffness for all vertical supports of the auxiliary structure. The force in these vertical supports is mainly determined by its remittance area and therefore all vertical supports contribute to the description of total forces, this is shown in the Figure 9-6.

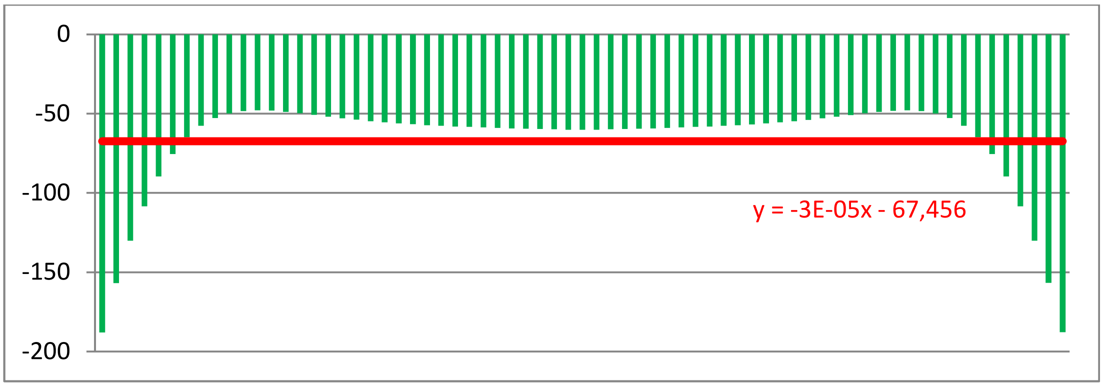

Figure 9-6 Axial forces [kN/m] in vertical supports – model B2

Complete overview of the operation of the auxiliary structure in model A, B1 and B2 can be found in appendix G. When the parameters, described in Table 9-3, are applied for the fluid and auxiliary structure their behaviour is modelled in a realistic way in all models.

Parameter	Vibrating beam	Mass on vibrating beam	Horizontal support	Vertical supports	Units
l	*34.26*	0.5	-	0.5	[m]
EA	1.233 E9	1.233 E12	2.5 E17	2.5 E12	[kN/m]
EI	9.250 E8	9.250 E11	2.5 E18	2.5 E13	[kNm2/m]
v (nu)	*0*	0	0	0	[-]
w	*0*	0	0	0	[kN/m/m/]
Rayleigh α	*0.4619*	-	-	-	[-]
Rayleigh β	*-3.441 E-3*	-	-	-	[-]

Table 9-3 input parameters auxiliary structure

9.1.5 Boundaries of the model

The centre of the base plate is modelled at (x , y) = (0 , 2), this means that the lateral model boundaries are situated at X, -150 and +150. The bottom boundary is situated at Y -60. Ground level is equal to Y +2 and the top of the model, which is also the top of the "shaking" beam, is situated at Y +37.26. Total model dimension are therefore 300m x 98.5 m. Lateral boundaries distance is investigated based on stresses and displacements.

For a proper modelling of an earthquake, dynamic boundaries are applied to exclude wave reflection at the model boundaries. In the final model a distinction can be made between base and lateral boundaries. The bottom of the mesh is modelled by aid of a compliant base (absorbing) boundary. Since the earthquake signals that are used as input at the bottom of the model are bedrock signals, it would be more obvious to apply a non-absorbing boundary. A comparison was made between the two and it showed that there was no effect of boundary type on the response in the upper 55 meters. Therefore the choice was made to retain the compliant base boundaries in the final model.

Based on the investigations in chapter 8 the lateral boundaries are modelled as free field boundaries (FF boundaries). These boundaries showed a far better response during the free field site response analysis than the older viscous boundaries. This applies to both, the OBE- as SSE earthquake signals. Another advantage of the free field boundaries is the smaller distance that is required compared to the viscous boundaries. Based on the results from chapter 8 a boundary distance of 75 m is sufficient for FF boundaries compared to a distance of more than 200 m for viscous boundaries.

9.1.6 Finite element mesh

Important aspect of the PLAXIS 2D model is the finite element mesh. The configuration of the mesh is a complex interaction between accuracy, computational requirements and time. The element size in the model is limited by two aspects; embedded pile geometry and high frequencies. The zone between two consecutive embedded piles must consist of at least two finite elements (see chapter 6), while on the other hand the element size is limited by the maximum frequency in the model and the local prevailing stiffness (see paragraph 8.2).
Generally the size limitation by the maximum frequency is normative, and therefore a range of important frequencies should be defined. Both earthquake signals, OBE and SSE, have similar frequency characteristics. The dominant frequencies in the signals are spread in a range of 1 to 20 Hz. However, since the natural frequency of the impulsive liquid is 1.85 Hz, the high frequencies are expected to be of minor importance for resulting forces. Therefore, as a starting point, the element size is determined based on a maximum frequency of 12 Hz. Reference is made to appendix D and paragraph 8.2, in which an element size of 1.08, 0.82 and 5.02 is calculated for respectively the sand fill, clay and deep sand layer. With these element sizes all frequencies up to 12 Hz are modelled in a proper way.
In an optimal mesh, all elements meet the requirements for element size. This however leads to a total of 11,800 elements inside the finite element mesh, which is too much in combination with the FF boundaries that are applied. A major drawback of the free field boundaries is the introduction of a non-symmetric stiffness matrix. In combination with the damping- and mass matrix, this leads to a large increase in the number of data points. For meshes with more than 10,000 elements (15 node), the kernel of PLAXIS 2D is unable to solve the matrix. Besides this, the required internal computer memory is exceeding the 32Gb that is available. PLAXIS 2D is therefore unable to perform the dynamic calculations. Only solution is a reduction of the number of elements without significantly affecting the accuracy of the results.
With the aid of a number of trial calculations the chart, presented in Figure 9-7, was made. In this chart, the memory use is linked to the number of elements according to a 3rd power polynomial. By means of Figure 9-7, it is clear that a mesh can contain a maximum of 8800 elements on the basis of the currently available hardware.

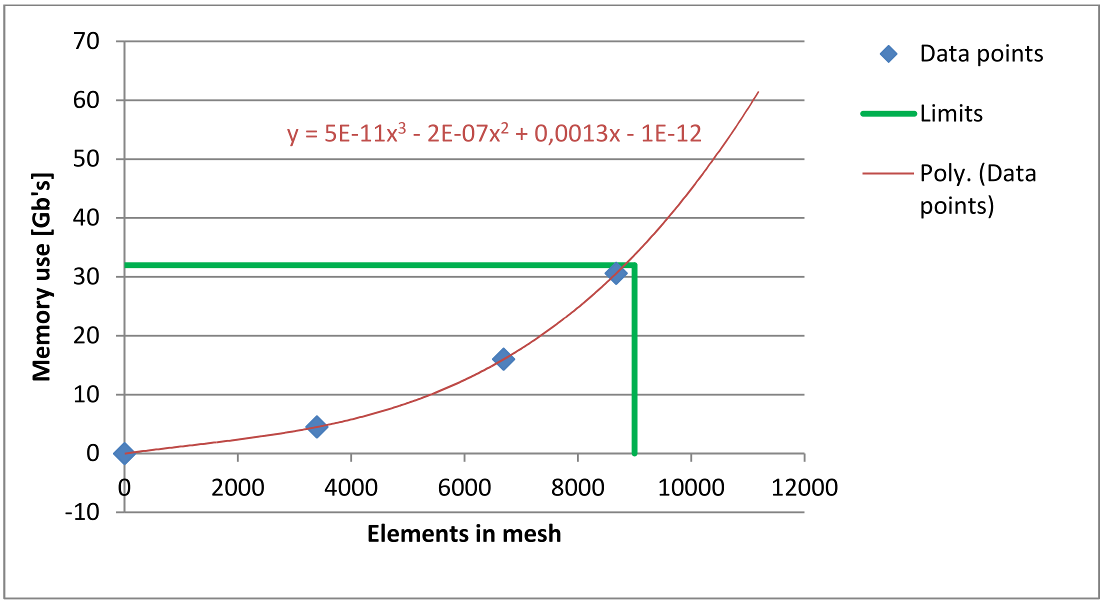

Figure 9-7 Limits of the finite element mesh

Due to this limitation the decision has been made to enlarge the element size gradually towards the model boundaries. This means that the elements in the mesh have to meet the dimension requirements within a distance of 20 meters to the left and to the right of the structure. Outside this zone, the size may increase slowly towards the model boundaries. The final mesh that is used in all calculations consists of 8677 elements with an average element size of 1,85 m. and depicted in the Figure 9-8 below.

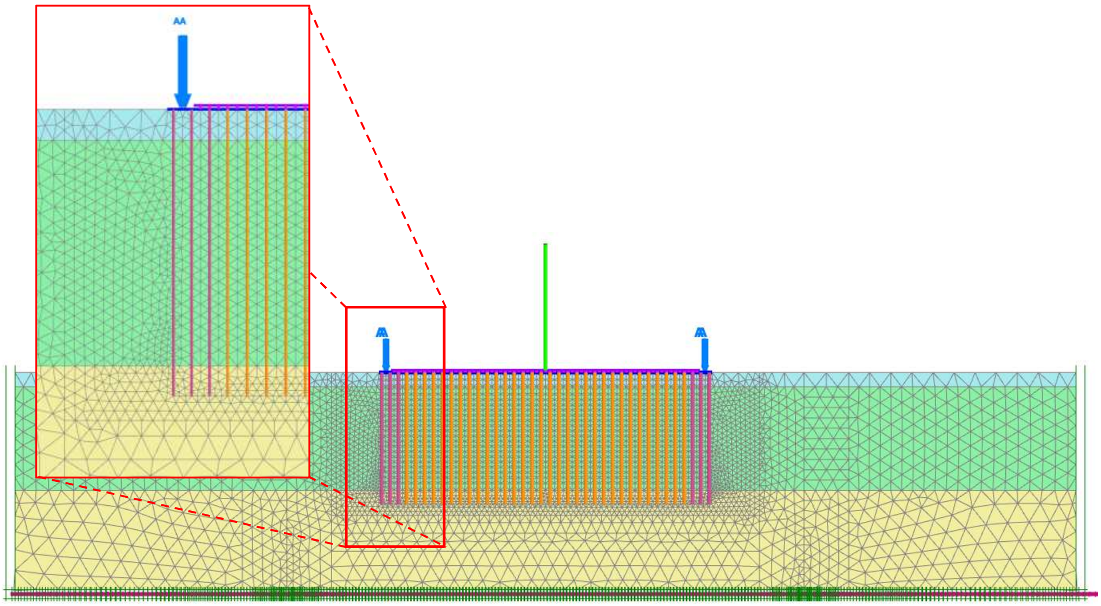

Figure 9-8 Final mesh configuration

9.1.7 Time stepping

Like explained in paragraph 8.2, the maximum allowable time step is based on Courant's condition (equation (8-2)). This condition restricts a time step by allowing a wave not to travel over more than one element length within a single dynamic time step. Based on this demand the time step is limited by the element size and compression wave velocity in the top of the clay layer. The small elements in combination with the higher compression wave velocity require a time step of 0.0061 seconds or smaller.
Both signals, OBE signal 2781 and SSE signal 798, consist of a large number of constant time steps of 0.005 seconds. For accurate modelling of the input signal all data point need to be transformed to a separate time step in PLAXIS 2D. Time steps are therefore already limited to 0.005 seconds, which meets the requirements according to courant's condition.

9.2 Calculations

FEM calculations are performed to:
- Investigate the influence of wave propagation on the behaviour of the base plate and piles;
- Verify the calculation method used in the MDOF model, based on a comparison between dynamic and pseudo static calculations.

In the MDOF model the assumption is made that the base plate behaves infinitely stiff. Therefore, the final model in PLAXIS 2D will be calculated using both a realistic - as an infinitely stiff base plate (model B1 and B2 from paragraph 9.1.4). In this way, the influence of model choices can be assessed and conclusion about the MDOF model can be drawn. In total, six different dynamic calculations are performed:
- Free vibration – base plate with normal stiffness;
- Free vibration – infinitely stiff base plate;
- Earthquake SSE signal 798 – base plate with normal stiffness;
- Earthquake SSE signal 798 – infinitely stiff base plate;
- Earthquake OBE signal 2781 – base plate with normal stiffness;
- Earthquake OBE signal 2781 – infinitely stiff base plate;

Due to the higher accelerations in the SSE earthquake signal, resulting forces on the base plate will be higher. The SSE situation is therefore more interesting for the comparison of dynamic- and pseudo static calculations of the pile reaction forces. In addition, there were more results from the MDOF model for the SSE situation and calculation times for SSE in PLAXIS 2D is much shorter. The analysis of the results will therefore focus on the SSE earthquake phase with signal 798 and neglect the results from the OBE situation.
The results of the free vibration phases are already discussed in paragraph 9.1.4 and appendix G together with the free vibration of the auxiliary structure on a completely rigid foundation (model A). Results are therefore not further discussed.

All 6 dynamic calculations consist of the 12 or 13 phases, presented in Table 9-4 on the next page. Only the last two phases vary depending on the existence of a free vibration or earthquake calculation. All static phases are calculated using the option: “ignore undrained behaviour” while the dynamic earthquake phases are calculated completely undrained.

Phase	Previous phase	Description
0	-	Initial phase, water pressure and initial stresses are generated. Because of the horizontal surface and soil layers parallel to the surface the K_0 procedure is used.
1	0	Installation piles
2	1	Installation of base plate
3	2	Construction outer tank 20%
4	3	Construction outer tank 40%
5	4	Construction outer tank 60%
6	5	Construction outer tank 80%
7	6	Construction outer tank 100%
8	7	Plastic nil-step[4]

[4] A plastic nil-step is used to solve existing out-of-balance forces. No changes in geometry, load level, load configuration and water pressure distribution should be made.

9	8	Installation auxiliary structure
10	9	Impulsive liquid
11	10	Plastic nil-step[1]
$12A_{free;vibration}$	11	Loading
$12B_{earthquake}$	11	Earthquake (OBE signal 2781 or SSE signal 798)
13	12A	Free vibration of 5 seconds with 500 additional steps[5] and 2 sub steps

Table 9-4 Phases in final models PLAXIS 2D

The additional steps that are used during the earthquake calculation vary for OBE and SSE. In the SSE situation 1600 additional steps and 2 sub steps are used to model/calculate a signal of 3200 data points. The option “save max time step” is set at 800, this requires a lot of space and the output program will be slower. However, the behaviour of different points in the mesh can be viewed afterwards with sufficient accuracy. This is way faster than recalculating the project with a different selection of pré-calculation points. Calculating the SSE earthquake phase lasts for 16 hours and the OBE phase will last even longer, probably about 48 hour.

[5] Additional steps are used as input for graphs in the output program. 500 additional steps for 5 seconds mean that all frequencies below 13 Hz are covered.

9.3 Results

9.3.1 Static behaviour after building phases

The static behaviour is examined to assess the general performance of the model. Focus is on the difference between models B1 and B2 in which respectively a realistic base plate stiffness and infinitely stiff base plate is used.

Vertical displacements
The vertical displacements in model B1 and B2 are plotted in Figure 9-9. The displacement of the baseplate is represented by the blue and red line for respectively the normal and stiff base plate. The green lines represent the displacement of the surface.

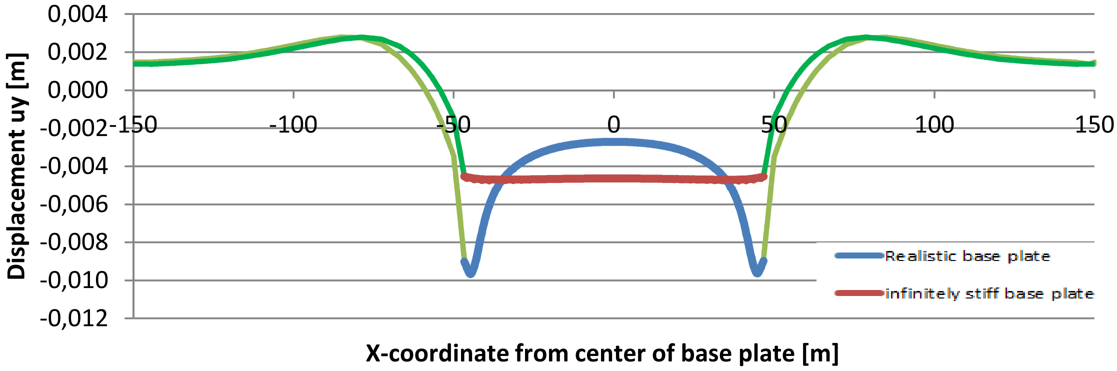

Figure 9-9 vertical displacements after static loading (end of phase 10)

The vertical displacements are according to expectation. In model B1 maximum displacement is found at both edges while the settlement in the middle is very limited. Model B2 shows a uniform vertical displacement over the complete width of the base plate. The displacements are in the same order of magnitude as measured values. One should consider that only the impulse part of the liquid mass is modelled. This is only 45% of the total LNG mass in the tank.

Axial forces in piles
The infinitely stiff plate shows a uniform distribution of settlements, the localised wall forces at both sides of the tank are redistributed by the stiff base plate (model B2) over all piles. Vertical pile forces in the middle fields are therefore much higher compared to the situation with realistic base plate stiffness (model B1). On the other hand the vertical pile forces in the side fields are significant lower (see Figure 9-10 for model B1 & Figure 9-11 for model B2).

Figure 9-10 Axial forces in pile heads – model B1 : realistic base plate stiffness

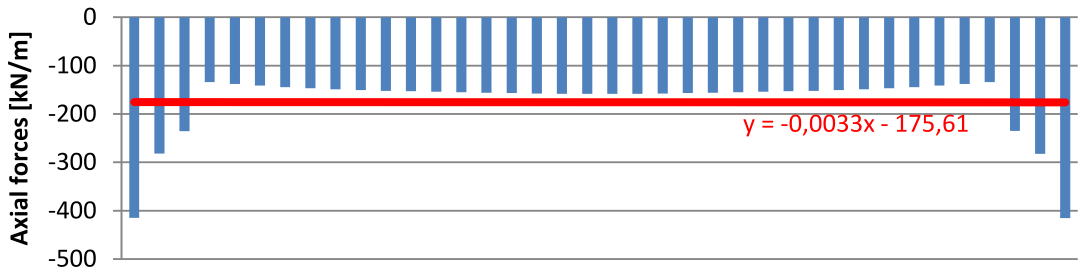

Figure 9-11 Axial forces in pile heads – model B2 : infinitely stiff base plate

9.3.2 Dynamic behaviour

The dynamic behaviour is assessed in more detail. Wave propagation effects, similarity with MDOF model and dynamic- versus pseudo static pile forces are investigated based on the results from de SSE earthquake calculations.

Wave propagation effects

Horizontal displacements are the result of the horizontal acceleration implemented at the bottom of the model. In Figure 9-12 the horizontal displacement of different construction elements and soil nodes is plotted. The focus is on differential displacements between the top soil layer, the pile heads and the base plate over the complete width of the tank.

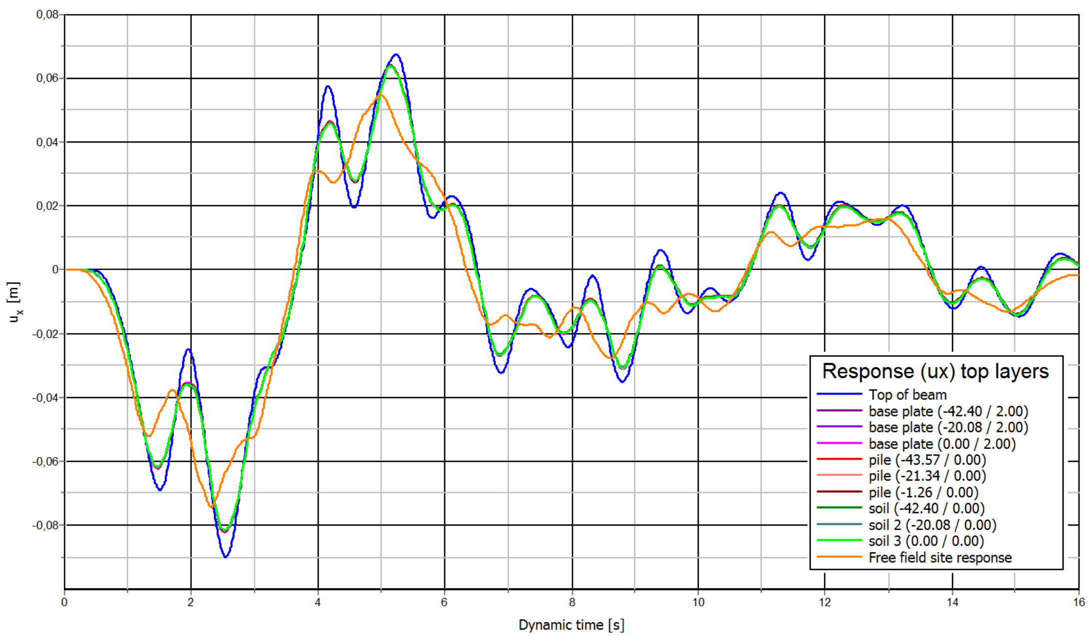

Figure 9-12 Response (ux) of base plate, pile heads and soil between pile heads

Based on Figure 9-12, the conclusion can be drawn that the base plate, pile heads and soil in between the piles are moving as a whole. There is no clear effect of wave propagation over the width of the tank. Other depths show a similar image; piles and soil in between these piles exhibit the same, especially horizontal, movement.

On the other hand, wave propagation effects are found over the length of the piles. The displacements depicted in Figure 9-13 show that larger displacements are found closer to the surface. This is the result of wave amplification of the earthquake load in combination with wave amplification effects by the liquid on the base plate. If displacements in model B1 and B2 are compared to the free field site response, the influence of the impulsive liquid mass is clear.

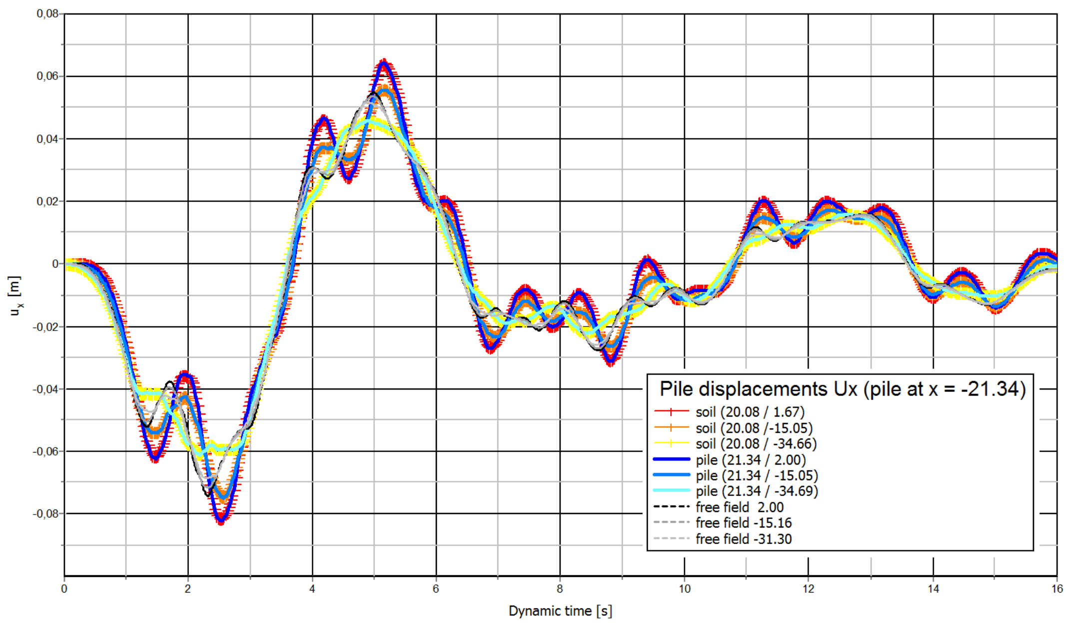

Figure 9-13 Response (Ux) of pile at x = -21.34

Based on Figure 9-12 and Figure 9-13 there is load coupling effect. The liquid inside the inner tank is put in motion by the earthquake (soil movement) but after that the liquid itself affects the movement of the soil, piles and base plate. It amplifies the signal with its own frequency, this results in higher peak displacements U_x in especially the top layers. The influence of the structure above ground level on the earthquake signal can be visualized by the plot of vertical accelerations in Figure 9-14. The plot clearly shows that accelerations are different in the zone below the tank, a result of the interaction with the liquid in the tank.

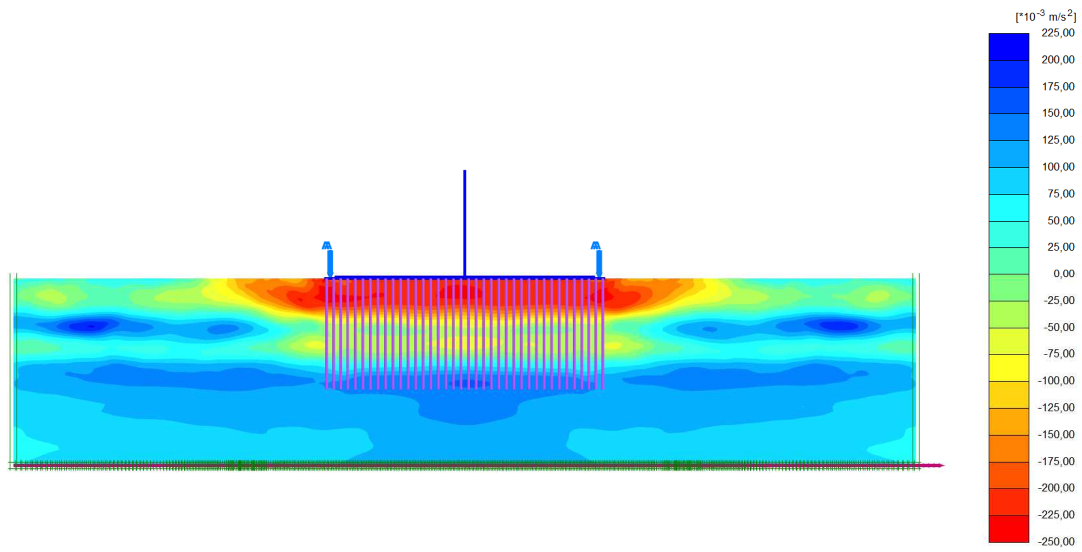

Figure 9-14 horizontal accelerations ax, sse earthquake signal 798 after 8.5 seconds

Figure 9-14 also shows minor differences between the accelerations that are found for different piles rows at equal depths. This means that the base plate is moving as a whole (already shown in Figure 9-12), and there is no influence of wave propagation effects over the width of the tank floor. However, there are three aspects that this 2D model does not take into account:

- Piles are modelled by using PLAXIS 2D embedded pile rows. Although these plate elements show group behaviour, they are still plate elements. This means that waves cannot pass them from left to right and vice versa. If the problem was modelled in 3D; waves, on certain spots, were able to travel through the pile field and therefore accelerations between different pile rows can differ. However, piles are installed close to each other and therefore show a lot of interaction. For a proper assessment a 3D model should be applied.
- Under the assumption that the base of the model can be seen as bedrock; the earthquake load is applied over the complete width of the model base. As a result the base encounters an equal direction of movement at the same moment in time. The earthquake load could also be applied at one side of the structure, therefore wave propagation effects becomes more important. Displacements at both sides of the tank can be different based on the tanks diameter and wave velocity and length.
- Only horizontal waves are considered in this model, while there is also vertical movement during an earthquake event. Adding a vertical signal could introduce wave propagation effects over the width of the tank. However, this will not contribute to the normative situation for reaction forces in the piles and base plate since the horizontal component is much larger.

Comparison with MDOF model

In the MDOF model, developed by TNO, the seismic response was calculated by a system of seven different masses, springs and dampers that represent the foundation, inner tank, outer tank and liquid inside the tank (impulsive and convective). During a seismic event all masses are set in motion due to excitations applied at base slap level and this result in a vertical reaction force, base shear and overturning moment. The overturning moment and base shear caused by the impulsive fluid mass can be compared to the overturning moment and base shear found in the PLAXIS 2D model (only considers impulsive liquid mass). This way, it is possible to judge the order of magnitude of the results.

The overturning moment in PLAXIS can be determined by multiplying the axial forces in the vertical supports with their lever arm, in this case the distance to the centre of the base plate. The maximum overturning moment occurs when the difference in the axial force between two vertical supports of the auxiliary structure, at an equal distance from the centre of the base plate, reaches its maximum. This moment is determined with the aid of Figure 9-15, in which the axial forces in the vertical supports of the auxiliary structure are shown during the first 8 seconds of the earthquake. From Figure 9-15 it can be stated that the maximum overturning moment occurs after 1.93 or 4.19 seconds from the start of the earthquake. This is the same for model B1 (realistic base plate stiffness) and model B2 (infinitely stiff base plate).

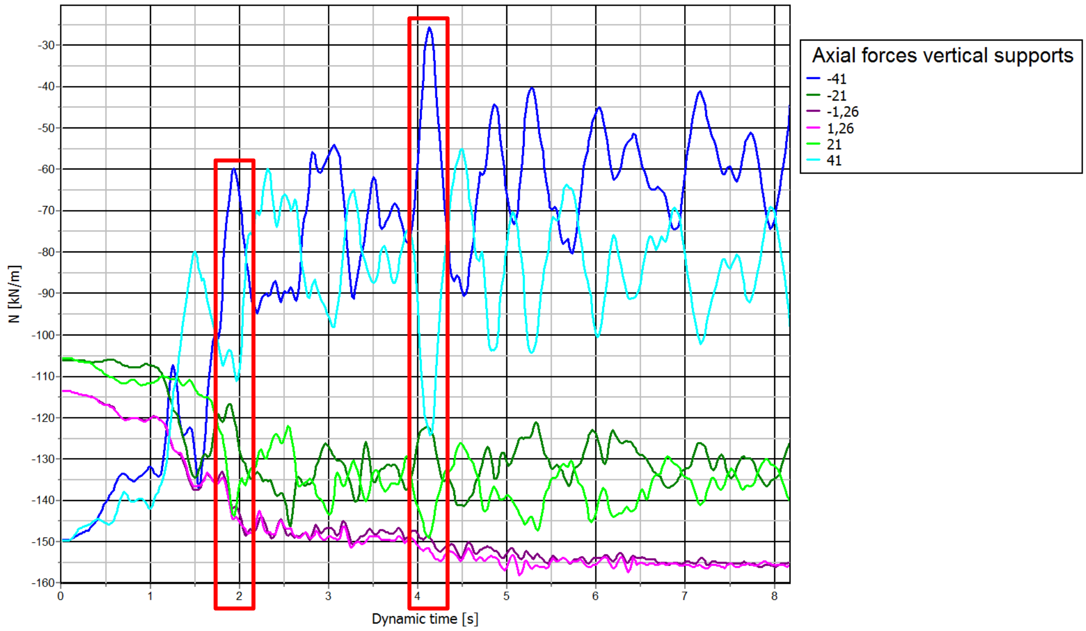

Figure 9-15 Axial forces in vertical supports - realistic base plate stiffness

The axial forces in Figure 9-15 are relevant for a 2D cross-section. For a proper comparison with the MDOF model they need to be transformed to the 3D tank area. This transformation is done according to the scheme presented in Figure 9-16 for half the tank. Every force from PLAXIS 2D (green dots) is related to an area (green area) and can be transferred to the 3D situation (red area) by multiplying with the distance in y-direction. After this, the same procedure for the calculation of the overturning moment can be performed.
Shear forces in the 3D situation can be determined in the same way. The forces associated with red shaded areas in Figure 9-16 are added to calculate the total shear force.

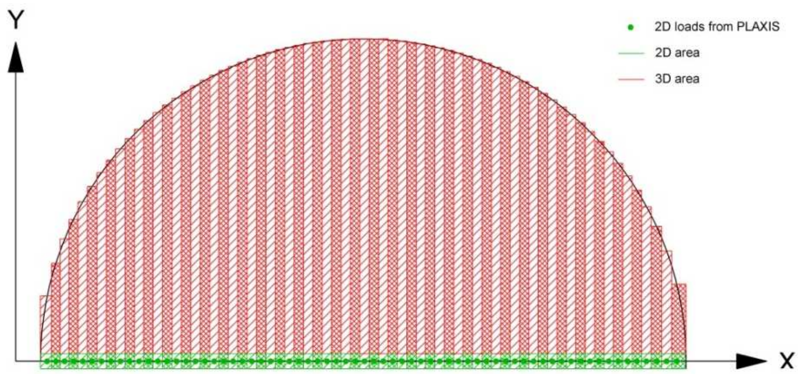

Figure 9-16 Relation 2D > 3D forces in vertical supports

With the described procedure, overturning moment and shear forces are calculated for all situations: 1.93 and after 4.13 seconds in model B1 (realistic base plate stiffness) and model B2 (infinitely stiff base plate). All results are summarized in Table 9-5 together with the results from the MDOF model delivered by (Meijers 2013).

	MDOF model				Units
Overturning moment	976				[MNm]
Base shear	87				[MN]
	PLAXIS 2D model				Units
	B1: normal base plate stiffness		B2: Infinitely stiff base plate		
	1.93 sec	4.19 sec	1.93 sec	4.19 sec	
Overturning moment	867	884	937	963	[MNm]
Percentage of MDOF	90	92	96	99	[%]
Base shear	35.5	37.5	42.4	45.1	[MN]
Percentage of MDOF	41	44	49	52	[%]

Table 9-5 comparison between MDOF model and PLAXIS 2D

The overturning moment shows values identical to the MDOF model. The fluid in PLAXIS 2D is represented by a linear mass-spring-damper system identical to the MDOF model. Input parameters of both systems are determined according to the same standards and geometry. When a comparable signal at base plate level is applied, response of the mass-spring-damper should be equivalent. In contrast to the MDOF model, signals in PLAXIS 2D are implemented as bedrock level rather than as base plate excitations. However, both have been selected on the same design response spectra and therefore response at base slab level (ground level) should be substantially identical.

The shear forces however, show deviations up to 50%. However, a possible cause for this big deviation was not yet found.

Pile forces in dynamic model and pseudo static model

The MDOF model is only applied to assess the above ground behaviour of the LNG tank during an earthquake event. In this model the complete stiffness of the foundation and piles is included but individual pile forces cannot be determined directly. Therefore an uncoupled method is used to assess the individual pile forces. Reaction forces from the superstructure on the base plate are determined for the most normative situations during an earthquake and applied as input for a static model that include all piles.

In order to assess this method a comparison is made using the results from the dynamic calculations in PLAXIS 2D. Normative forces on the base plate are determined during the occurrence of the maximum overturning moment. This is, as indicated in the previous paragraphs, after 1.93 and 4.19 seconds. The forces are then applied in a static PLAXIS 2D calculation. A distinction is made between model B1 (realistic base plate stiffness) and model B2 (infinitely stiff bas plate). In model B2 the forces are applied in two ways: as summarized forces (vertical-, horizontal force and overturning moment) at the centre of the base plate and as small forces (vertical and horizontal) located at the connection between the auxiliary structure and the base plate. In Figure 9-17 a schematic view of the three different methods used for the calculation of the pile reaction is presented.

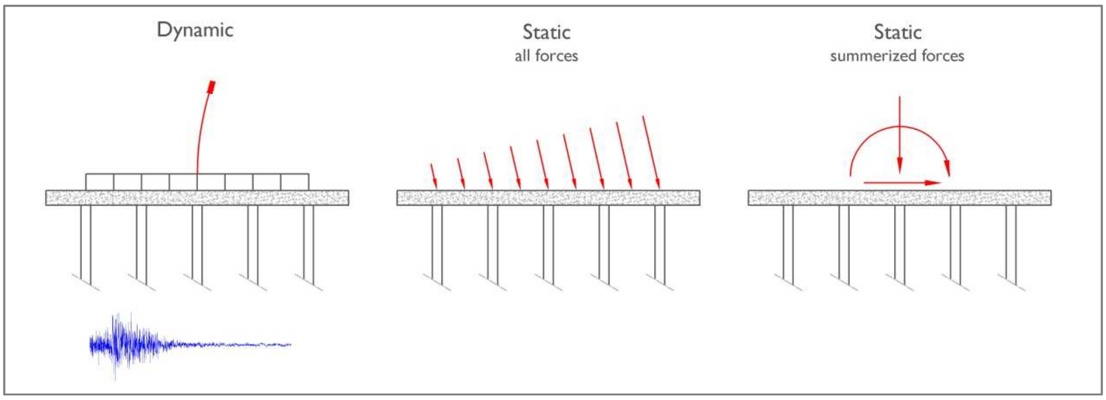

Figure 9-17 Calculations method in comparison dynamic vs. static

The first comparison is made between the dynamic calculations; model B1 and model B2. The normative edge- and field pile are compared based on pile moments and forces. In both models the exact same piles are normative: the second and fourth pile from the left (in cross-section), this can be seen in appendix H. Notice that forces and moments presented in this appendix are per meter, this means that the out-of-plane-spacing must be taken into account. This is already done in the graph presented in Figure 9-18.

Pile forces found in model B2 are significantly lower, even though the overturning moment is larger. This especially applies for the edge piles. Due to the high stiffness the base plate is capable of redistributing all the forces (especially the localized wall forces) over all the piles; therefore the peak moments are smoothed. Peak moments are 40% and 25% lower for respectively the edge- and field piles.

In a full dynamic FEM calculation in PLAXIS it is better to model the base plate with a realistic stiffness. The behaviour of the liquid is not influenced by the stiffness of the base plate. However, the displacements of the base plate are much more realistic which leads to a better estimation of the pile forces during an earthquake event.

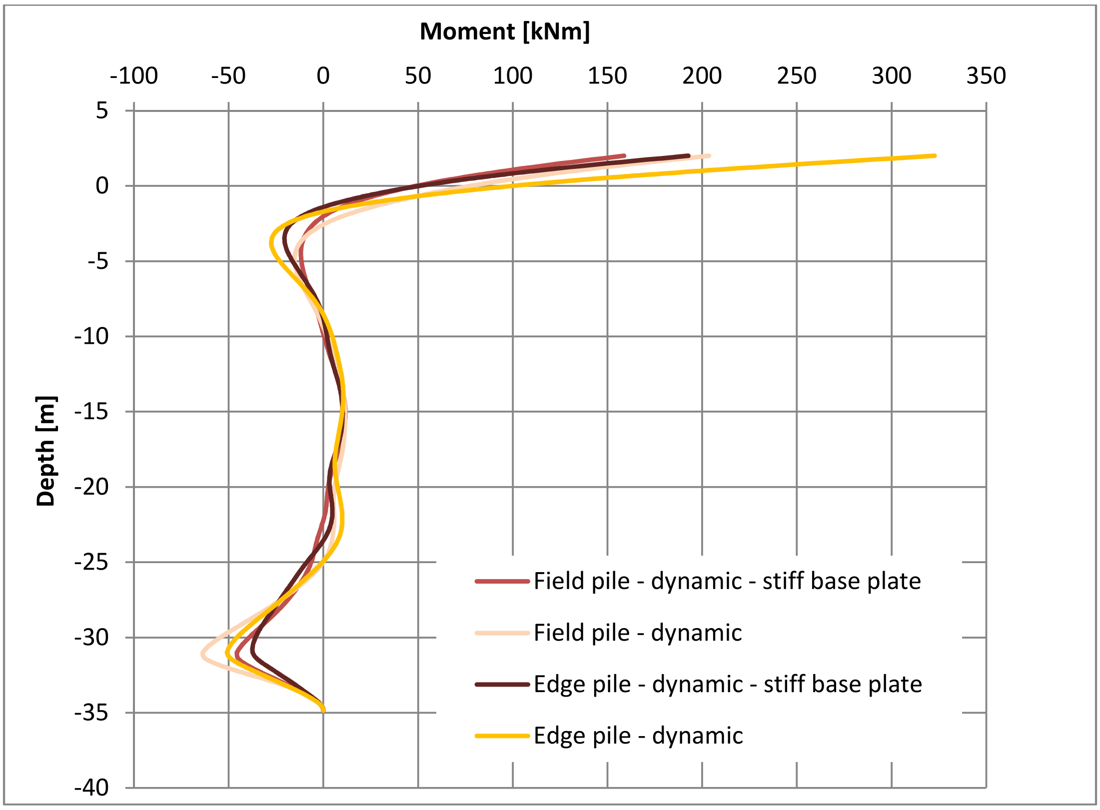

Figure 9-18 normative pile forces in dynamic calculations: realistic- vs infinitely stiff base plate

The second comparison is made between the dynamic model B1 (realistic base plate stiffness) and a static variant. All axial and lateral forces at the connections between the auxiliary structure and the base plate are read out from the dynamic model. In the static model these forces are used as input. Only the normative situations (1,93 and 4,19 seconds dynamic time) are considered. All soil and construction properties are exactly the same in both models.

Both normative situations show the same results: the edge piles are normative based on forces and moment. Although the smaller out of plane spacing, forces are significantly higher. The static model only shows pile head moments, other moments over the length of the pile are negligible small. The piles in the dynamic situation on the other hand show reasonably moments over the length of the pile. Mainly the “clamping moment” in the deeper sand layer shows a large difference compared to the dynamic model, this is depicted in Figure 9-19. Complete results are presented in appendix H.
The differences in peak moments and forces are summarized in Table 9-6. The biggest differences are found in positive shear force (Q_{max}) and negative moment (M_{min}). The force and moment are related to each other and occur in the deeper sand layer, the already mentioned “clamping moment” in Figure 9-19. Differences are in the range of 60 to 80 percent.
On the other hand the peak forces and moment, found in the static model, are similar to the forces and moments found in the full dynamic model. Pile head forces found in the pseudo static model show deviation in the range of 10 to 15%.

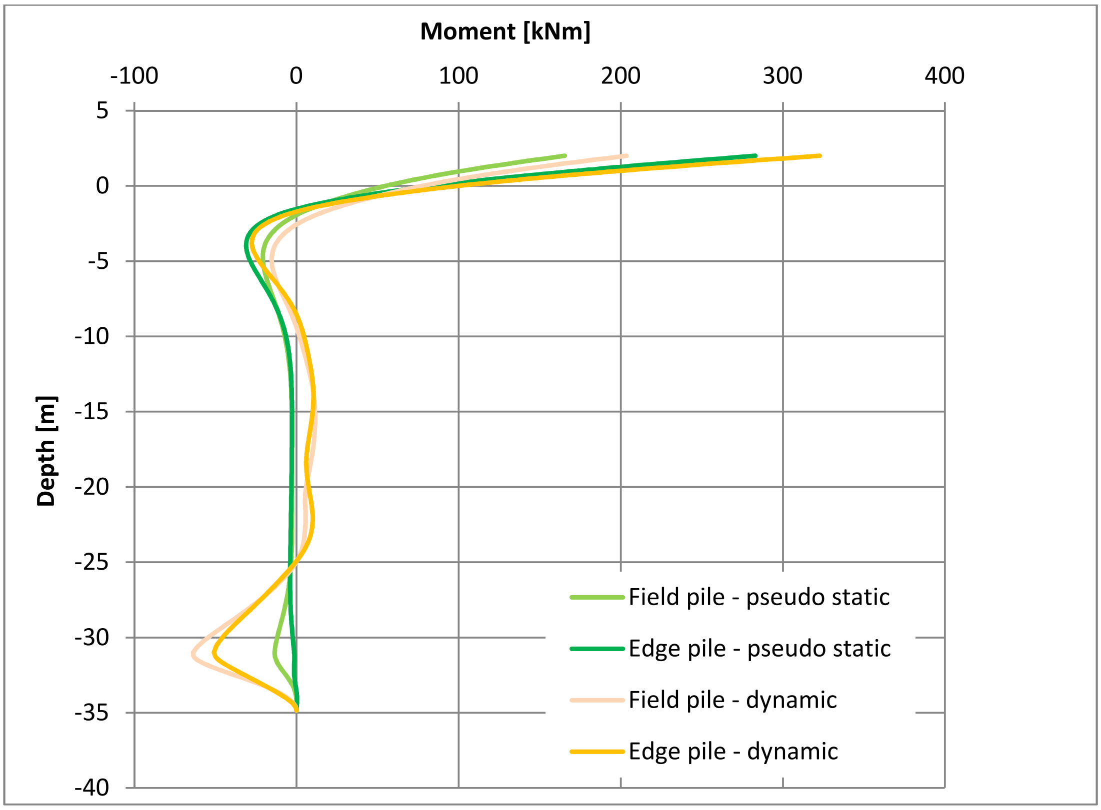

Figure 9-19 normative pile forces for model B1: dynamic versus pseudo static

	Units	Dynamic	Static	Error
Edge pile				
Nmax	[kN]	708	689	3%
Qmax	[kN]	18	6	68%
Qmin	[kN]	-130	-116	11%
Mmax	[kNm]	323	283	12%
Mmin (-32)	[kNm]	-51	0	100%
Field pile				
Nmax	[kN]	341	323	5%
Qmax	[kN]	27	3	88%
Qmin	[kN]	-76	-68	10%
Mmax	[kNm]	204	166	19%
Mmin (-32)	[kNm]	-64	-13	80%

Table 9-6 Comparison between forces found in dynamic and static situation – model B1

The last comparison is made between the dynamic- and static situation in model B2, with an infinitely stiff base plate. In Figure 9-20 the pile moments are plotted for the normative edge- and field pile in the dynamic and two static models. Due to the high stiffness of the base plate, forces are divided more equally and pile reactions for edge- and field piles are more in line.
The two static models show, as expected, substantially identical results. Compared to the dynamic model, the peak forces/moments in the pile heads are approached properly. However, the rest of forces and moments in the pile are underestimated. Mainly the “clamping moment” in the deeper sand layer shows a large difference compared to the dynamic model.

In Table 9-7 the differences between the peak forces and moments are summarized. Peak forces and moments in the pile head show only small differences up to an error of 10%. However, the pile reactions at the level of the deeper sand layer show large deviations. Both forces and moments are underestimated by 65-85%.

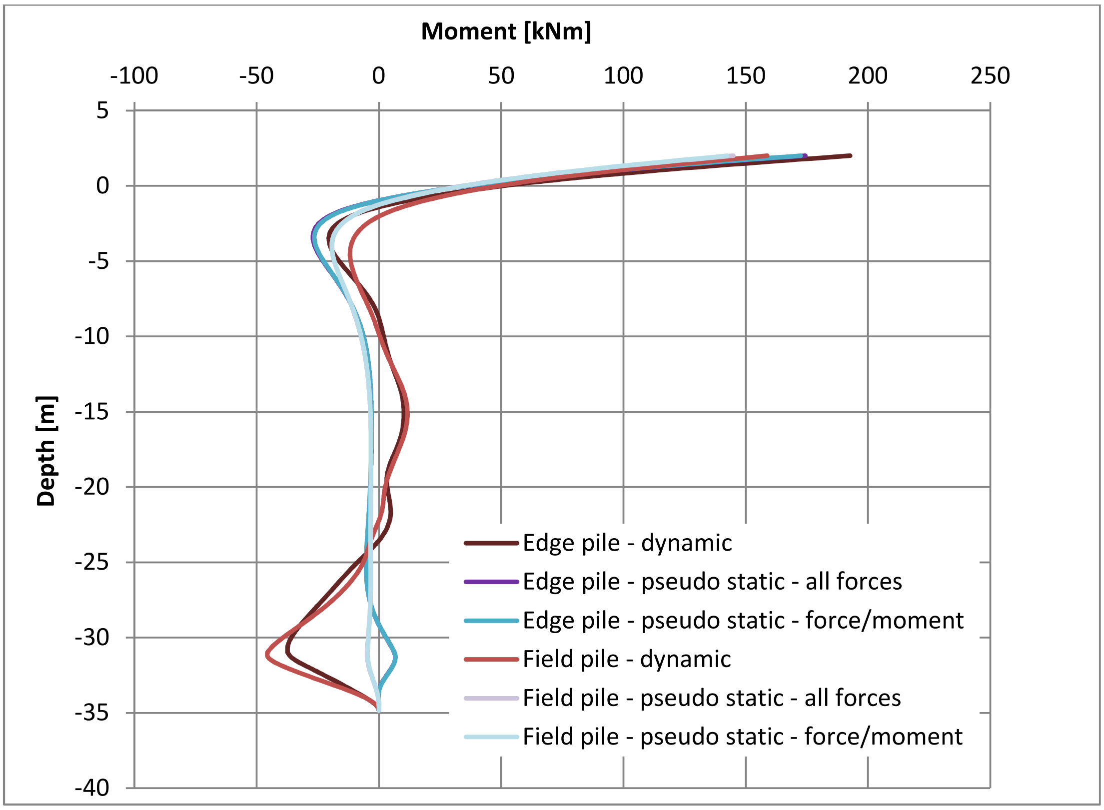

Figure 9-20 normative pile force for model B2: dynamic versus pseudo static

	Units	dynamic	Static all forces	Error	Static force/moment	Error
Edge pile						
Nmax	[kN]	387	402	-4%	400	-3%
Qmax	[kN]	12	4	64%	4	65%
Qmin	[kN]	-87	-87	0%	-86	2%
Mmax	[kNm]	193	174	9%	172	11%
Mmin (-32)	[kNm]	-37	7	100%	7	100%
Field pile						
Nmax	[kN]	384	367	4%	365	5%
Qmax	[kN]	17	3	85%	3	85%
Qmin	[kN]	-67	-70	-4%	-69	-2%
Mmax	[kNm]	159	145	9%	142	10%
Mmin (-32)	[kNm]	-46	-4	91%	-4	91%

Table 9-7 Comparison between dynamic and pseudo static situation – model B2

10 CONCLUSIONS & RECOMMENDATIONS

10.1 Conclusions

In this chapter the conclusions and recommendations of this research are presented by answering the main and sub research objectives formulated in chapter 1.2.

Main objectives:

1. *Assess the feasibility of a 3D full dynamic model for the analysis of a LNG tank (foundation) under seismic loading;*
2. *Assess the influence of wave propagation effects in the soil on the base plate*
3. *Compare the uncoupled calculation method with a full dynamic method.*

Sub objectives:

4. *Assess (embedded) pile group effects in PLAXIS and compare them with available literature.*
5. *Schematize the liquid inside the tank to make the calculation process easier and faster*
6. *Assess the influence of boundaries, mesh properties and time stepping for dynamic calculation (Free field site response analysis)*

Firstly the conclusions related to the sub objectives are discussed, followed by the elaboration of the three main objectives is presented.

Assess (embedded) pile group effects in PLAXIS and compare them with available literature.
Pile group effects of embedded piles were investigated by static calculations in PLAXIS 3D. Different pile line- and pile group geometries were modelled in medium dense sand. Pile heads were loaded by a lateral displacement varying from 1/50 to 1/12 D. All geometries were judged on pile group, pile row and side-by-side efficiency compared to efficiency factors presented by (Reese en Impe 2001) and (Mokwa 1999). It is concluded that:

1. Factors for (embedded) pile group efficiency found in PLAXIS are realistic compared to factors from (Mokwa 1999). PLAXIS 3D shows differences between efficiency of pile lines and pile groups. This means that distinction is made between pile row- and side-by-side efficiency.

2. Based on a comparison with (Reese en Impe 2001) and (Mokwa 1999) PLAXIS embedded piles show lower efficiency values for trailing rows in particular. PLAXIS 3D shows differences between efficiency of front and trailing rows until the fourth trailing row. Efficiency compared to (Reese en Impe 2001) is underestimated. However, PLAXIS distinguishes between different trailing rows while (Reese en Impe 2001) does not. Compared to values summarized in (Mokwa 1999) especially the efficiency of trailing rows is underestimated. Pile row efficiency appears to be displacement dependent.

3. Proper results are found for side-by-side efficiency of embedded piles in PLAXIS 3D compared to values from (Reese en Impe 2001). In contrast to (Reese en Impe 2001) embedded piles in PLAXIS make a distinction between efficiency of side and middle piles.

4. PLAXIS embedded piles are found to be mesh dependent during lateral loading. Different piles must be divided by at least 2 volumetric soil elements in the zone with significant pile displacements.

Schematize the liquid inside the tank to make the calculation process easier and faster
The LNG liquid inside the tank can be split into two components characterised by their natural frequency: an impulsive (1,85 Hz) and a convective component (0,1 Hz). In this thesis only the impulsive component, lower part of the fluid mass, is considered because this component is normative for the resulting forces on the foundation.
The impulsive liquid can be modelled as a linear mass-spring-damper system represented by a mass on top of a clamped beam (PLAXIS 3D) or clamped plate (PLAXIS 2D). The stiffness properties of the beam/plate are based on the mass and natural frequency of the liquid. It can be concluded that:

5. The frequency of a vibrating beam, clamped at the surface can be calculated by equation (7-4). For convenience and to avoid errors, it is preferable to model a slender beam/plate. If a slender structure ($d/l < 0,1$) is used the deflection due to shear may be neglected. This means that the frequency (and frequency dependent elasticity modulus) can be described by equations (7-9) and (7-10). The moment of inertia (I) is based on a square cross-section in case of a beam in PLAXIS 3D and a rectangular cross-section in case of a plate element in PLAXIS 2D.

6. Beam (PLAXIS 3D) and plate elements (PLAXIS 2D) modelled according to conclusion 5 show proper results based on static deflection and frequency during a free vibration analysis. Error in the output frequency found in PLAXIS is especially determined by the number of time steps used. In general, eight steps are needed to describe one cycle.

7. For a proper distribution of all forces over the base plate an auxiliary structure as shown in Figure 10-1 can be used:

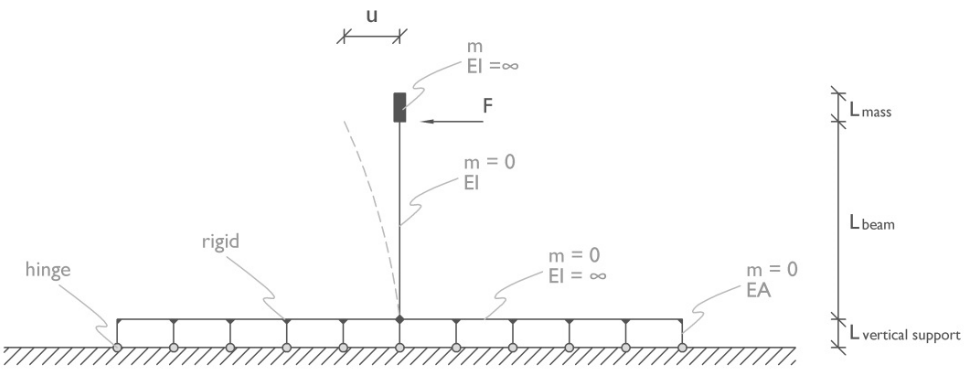

Figure 10-1 Vibrating beam/plate on auxiliary structure

Horizontal support is “infinitely” stiff compared to the vibrating beam and base plate for a proper distribution of the forces introduced by the vibrating beam/plate. Vertical supports act as vertical springs. Deformation in the auxiliary structure is limited (<5%) compared to the deformation in the vibrating beam/plate, in this way the modelled frequency is not affected.

8. A vibrating beam/plate and auxiliary structure modelled on a rigid foundation has one single natural frequency. This frequency is directly related to the vibrating beam on top of the structure.

9. A beam/plate on an auxiliary structure modelled on a realistic foundation (soil & piles) has two natural frequencies. One frequency is related to the vibrating beam and the other to the soil-pile foundation. The natural frequency of the vibrating beam is dominant.

10. Displacement behaviour and frequencies of the vibrating beam and auxiliary structure modelled on a realistic foundation is not influenced by the stiffness of the base plate. Only force distribution towards the piles is influenced.

11. Overturning moment is modelled realistic on both, clamping point level of vibrating beam and at base slab level. The overturning moment at base slab level is introduced by differences in axial forces in the vertical support of the auxiliary structure.

12. Shear force distribution over the base plate is unrealistic compared to actual situation. In reality the shear force is largely localized beneath the wall of the inner tank while in PLAXIS the shear forces are more uniform distributed over the base slab with only small peak values on both sides.

Assess the influence of boundaries, mesh properties and time stepping for dynamic calculation

A free field site response analysis is performed to investigate mesh element size, time stepping and lateral boundary effects during dynamic calculations. A 1D PLAXIS with tied-degrees-of-freedom is used as reference for all analyses performed in the 2D domain. Two different earthquake signals (OBE and SSE) consisting of vertically propagating horizontal shear waves are considered. It can be concluded that:

13. According to (Lysmer & Kuhlmeyer R.L., 1969) element size is limited to 1.08, 0.82 and 5.02 for respectively the sand fill, clay and deep sand layer. Between the piles the demands according to conclusion 4. are leading.
    Using these conditions all frequencies between 1-12 Hz can be properly described by the mesh. This range of frequencies is expected to be important for resulting forces based on dominant frequencies in the signals, soils and structural elements.

14. Time steps during dynamic calculations are limited based on Courant's condition and by the number of data points inside the input signal. For this thesis the number of data points inside the input signal was normative. Maximum allowable time step is considered to be 0.005 seconds.

15. Viscous boundaries appear to respond both distance and signal dependent.
    When applied in combination with the SSE signal; wave reflections at the boundaries cause a lot of "noise" even if the boundaries are applied at 200 meters from the model centre. For this thesis viscous boundaries prove to be inapplicable.

16. If the soil during dynamic analyses is modelled by use of the hardening soil small strain model, additional Rayleigh damping of 1-2% should be applied to account for realistic damping behaviour (Brinkgreve, Bonnier en Kappert, Hysteretic damping in a small-strain stiffness model 2007). This damping has a positive effect on the operation of especially viscous boundaries.

17. Free field boundaries appear to respond distance independent but signal dependent. When applied in combination with higher peak accelerations more disturbances are found. Based on a comparison with a 1D tied degrees of freedom model a boundary distance of at least 100 meters should be applied. Horizontal accelerations and displacements at ground level are converging while vertical peak accelerations are limited to less than 8 % of the horizontal peak acceleration.

18. In models consisting of more than 10,000 elements in combination with free field boundaries; the kernel of PLAXIS 2D is unable to handle the size stiffness matrix and therefore the model cannot be calculated. This problem is caused by the non-symmetrical stiffness matrix introduced due to the application of free field boundaries.

19. In models consisting of more than 9,000 elements in combinations with free field boundaries and dynamics; the kernel of PLAXIS 2D uses more than 32 Gb of internal memory and therefore calculations are difficult to perform on common hardware.

Assess the feasibility of a 3D full dynamic model for the analysis of a LNG tank (foundation) under seismic loading

Feasibility of a 3D full dynamic model in PLAXIS is assessed on the basis of computational time and usability. PLAXIS 3D calculations performed in chapter 6 in combination with a global model of the complete geometry are used to estimate calculation time based on number of elements. It can be concluded that:

20. For a good description of both soil behaviour and soil-structure interaction, a model will require about 500,000 elements. According to (Brinkgreve 2013, personal communication), models with 500,000 elements or more in combination with a dynamic calculation are currently not feasible. Calculation times will be up to several days or even a week and handling of output will be time-consuming.

Assess the influence of wave propagation effects in soil on the base plate

Wave propagation effects of the LNG tank base slab are investigated in a full dynamic 2D model in PLAXIS based on displacement and acceleration behaviour. The model was only subjected to horizontal shear waves propagating vertically. It can be concluded that:

21. No influences of wave propagation effects over the width of the base slab were found in the results of the dynamic calculations in PLAXIS 2D. The base slab is moving in its entirety together with the pile heads and the top soil layer.

22. Wave propagation effects were found over the length of the piles. The response (displacements and accelerations) is amplified towards the surface by the thick soft clay layer and the interaction with the fluid on top.

23. Load coupling effects were found between the construction, impulsive liquid mass and the earthquake signal. The original input signal is affected by the mass and frequency of the impulsive liquid.

Compare the uncoupled calculation method with a full dynamic method
The uncoupled calculation method is compared to a full dynamic method using PLAXIS 2D. The normative situations during an SSE earthquake event are considered. Reaction forces from the superstructure (auxiliary structure) are read out from the dynamic model and used as input for a (pseudo) static model with exact the same geometry and properties. Three situations are considered to compare the full dynamic and pseudo static approach, summarized below and schematized in:

- *Model B1 versus B1.1*: Full dynamic model with realistic base plate stiffness compared to (pseudo) static model with realistic base plate stiffness. All forces from the dynamic calculation are applied as static forces in a separate static calculation;
- *Model B2 versus B2.1*: Full dynamic model with infinitely stiff base plate compared to (pseudo) static model with infinitely stiff base plate. All forces from the dynamic calculation are applied as static forces in a separate static calculation;
- *Model B versus B2.1:* Full dynamic model with infinitely stiff base plate compared to (pseudo) static model with infinitely stiff base plate. All forces from the auxiliary structure are summarized and applied as vertical force, shear force and overturning moment at the base slab centre.

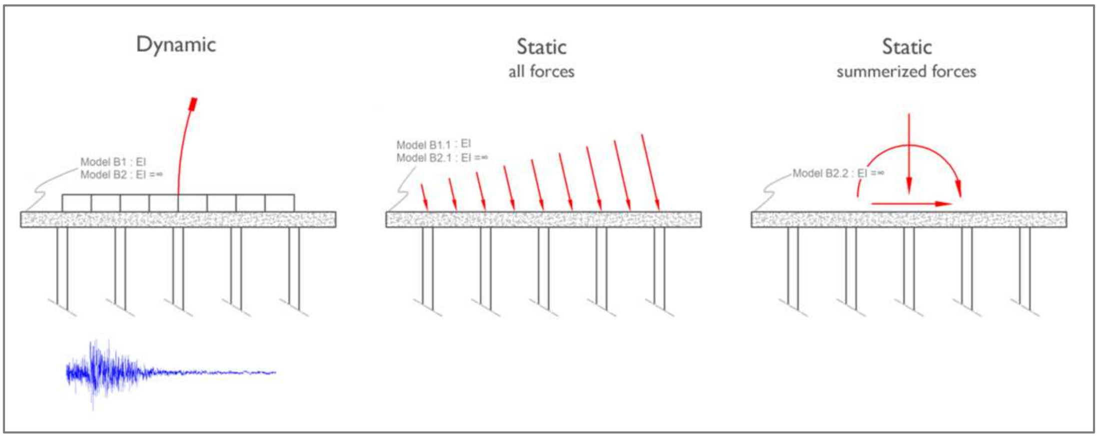

Figure 10-2 Considered models for comparison of uncoupled- and full dynamic method

It can be concluded that:

24. Normative overturning moments on the base plate found in the PLAXIS 2D full dynamic earthquake calculation are comparable to the overturning moments found in the MDOF model. For SSE deviations are 5-10% for model B1, compared to 1-5% for model B2.

25. Normative shear forces on the base plate found in PLAXIS 2D full dynamic earthquake calculations are significant lower than the shear forces expected in the MDOF model. For SSE deviations are 55-60% for model B1, compared to 45-50% for model B2.

26. Clamping forces/moments in the pile heads found in the dynamic models (B1, B2) and pseudo static models (B1.1, B2.1, B2.2) are identical, deviations are in the range of 0 - 10%. However, the pseudo static models do not show clamping forces/moments in the pile foot at the transition between the clay- and deeper sand layer. Pile forces/moments at this point are underestimated by 80-100%. These clamping forces are the result of differential soil displacements due to dynamic excitations; this aspect is neglected in the static models.

In general it can be concluded that pile forces, other than pile head forces, are underestimated by the static models. Differential soil displacements due to dynamic excitations are neglected. Mainly layer transitions, involving large stiffness differences, are sensitive to this aspect. For the reference case in this thesis (Angola case) this underestimation has no effect if piles are dimensioned on pile head forces.

For the behaviour of the vibrating beam on the auxiliary structure (impulsive LNG mass) it has no effect whether or not it is modelled on an infinitely stiff base plate (model B2) or on a base plate with realistic stiffness (model B1). Deformation of the base plate and resulting forces in the piles however are expected to be more realistic in model B1. Therefore it is recommended to use a realistic base plate stiffness to calculate pile forces in a dynamic PLAXIS model.

10.2 Recommendations

Most recommendation are directly related to the conclusions and don't need further elaboration. Recommendations are divided into five subgroups: pile group effects, modelling of fluid, free field site response, wave propagation effects, MDOF calculation methods and a general recommendation:

Recommendations for optimizing the insight in embedded pile group effects:

- Further investigation on the influence of mesh configuration on the behaviour of embedded piles and embedded pile groups;
- Further investigation on the influence of soil models (elasticity, plasticity) and different soil parameters, especially:
  - Friction angle;
  - Dilatancy angle;

Recommendations for optimizing of the fluid modelling:

- Perform an extensive analyse on the influence of stiffness differences between the vibrating beam, vertical and horizontal support(s) of the auxiliary structure;
- Investigate the possibilities of modelling roller supports in PLAXIS to ensure a better distribution of the shear forces on the base plate;
- Investigate the possibilities of modelling the convective liquid part as well.

Recommendations related to site response, dynamic boundaries and mesh configuration

- Extensive investigation on the influence of mesh configuration on the site response. Especially the accuracy of response with increasing element size towards the boundaries.

Recommendations related to wave propagation effects over the width of the base plate

- It is realized that the assumption of applying only vertical propagating horizontal shear waves may be an oversimplification, because Rayleigh waves and vertical motions may also affect the structure (especially base plate) seismic response. It is therefore suggested to investigate the influence of applying a combination of motions: horizontal and vertical accelerations at bedrock level.
- Piles are modelled by using PLAXIS 2D embedded pile rows. Although these plate elements show group behaviour it are still plate elements, so wave can't pass them from left to right and vice versa. It is therefore recommend to investigate the influence of wave propagation in PLAXIS 3D. A cross-section consisting of only one or two pile diameter in out of plane direction can be sufficient in this case.
- Under the assumption that the base of the model can be seen as bedrock; the earthquake load is applied over the complete width of the model base. As a result the base encounters an equal direction of movement at the same moment in time, based on their wave velocity. In areas of low seismicity, the epicentre of the earthquakes can be very far from the site. Different waves will reach the site at different moments in time. It is therefore recommended to investigate the influence of applying the earthquake load at one side of the structure. In this situation wave propagation effects will become more important and response at both sides of the tank can be different based on: the tanks diameter, wave velocity and wave length.

Recommendations related to calculation method used in MDOF

- It is realized that pile forces based on the pseudo static approach of the MDOF model seem to underestimate the pile forces, especially at greater depths at the transition of layers with large stiffness differences. The underestimation can be solved by applying a multiplication factor. The factor should be based on a comprehensive study for various geometries and soil profiles.

This report is closed with a general recommendation based on the observations made during this thesis:
Finite Element Modelling has been an important part of this master thesis and most important conclusions are related to results from FEM calculations. FEM software creates opportunities to model complex problems, such as seismic analysis, in a relatively easy way. It is important to realize that a user is responsible for the design and results of a model. FEM software makes it possible to achieve results quickly but it is still the pre and post-processing that makes sure that the output is reasonable. It is therefore recommended to use extensive verification of all steps by other software and/or colleagues.
In addition, FEM software creates the expectation that the most difficult and complex problems are easy to solve. However, this thesis also shows the opposite. Current FEM software provides the possibility to analyse dynamic behaviour but computational demand required for a full 3D dynamic analysis of a LNG tank (foundation) exceeds the reasonable limits for design purposes.

REFERENCES

Ahn, N. van. *The effect of non-linear soil behavior.* Graduation Thesis, Delft: Delft University of Technology, 2008.

American Petroleum Institute. *API 620: Design and Construction of Large Welded Low-Pressure Storage Tanks.* standard, Washington D.C.: American Petroleum Institute, 2002.

Association, National Fire Protection. *NFPA 59A Standard for the Protection, Storage, and Handling of Liquefied Natural Gas (LNG).* Standard, Quincy: National Fire Protection Association, 2006.

Avitabile, Peter. *Natural frequencies for common systems.* Modal analysis and controls laboratory, Lowell: University of Massachusetts, 2012, 2-6.

Benz, T. *Small-Strain Stiffness of Soils and its Numerical Consequences .* PhD thesis, Stuttgart: Universitat Stuttgart, 2006.

Brinkgreve, R.B.J., E Engin, and H.K. Engin. "Validation of emperical formulas to derive model parameters for sands." In *Numerical methods in Geotechnical Engineering*, by Nordal and Benz, 137-142. London: Taylor & Francis Group, 2010.

Brinkgreve, R.B.J., E. Engin, and W.M. Swolfs. *Manual Plaxis 3D.* Software manual, Delft: Plaxis bv, 2012.

Brinkgreve, R.B.J., E. Engin, and W.M. Swolfs. *Manual Plaxis 2D.* Delft: Plaxis bv, 2012.

Brinkgreve, R.B.J., P.G. Bonnier, and M.H. Kappert. "Hysteretic damping in a small-strain stiffness model." In *Numerical models in Geomechanics*, by Pande & Pietruszczak. London, 2007.

Engineers, American Society of Civil. *ASCE 98-4 Seismic Analysis of Safety-Related Nuclear Structures and Commentary.* Reston: American Society of Civil Engineers, 2000.

Forsythe, G.E., and W.R. Wasow. *Finite difference methods for partial differential equations.* New York, 2004.

Galanti, F.M.B., and W.M.G. Courage. *Seismic analysis of storage tanks with soil structure interaction.* Delft: TNO Built Environment and Geoscience, 2006.

Galanti, F.M.B., and W.M.G. Courage. *Seismic analysis of three storage tanks in Angola.* Final design report, Delft: TNO Built Environment and Geoscience, 2009.

Hanks, T.C., and H Kanamori. "Moment magnitude scale." *Journal of Geophysical research*, 1979: 2348-2350.

Hardin, B.O., and V.P. Drnevich. *Shear modulus and damping in soils.* Reston: American Society for Civil Engineers, 1972.

Hicks, M.A. "Computational modelling of engineering materials (lecture notes)." Delft: Delft University of Technology, 2012.

Housner, G.W. "The dynamic behaviour of water tanks." *Bulletin of the seismological society of America* 53 (1963): 381-387.

Johnston, A.C. "Assesment of large earthquake potential." In *The earthquakes of stable continental regions*, by Electric power research institute, 187-191. Palo Alto: Memphis State University, 1994.

Kanamori, H. "Magnitude Scale and Quantification of Earthquakes." *Tectonophysics*, no. 93 (1983): 185-199.

Kappert, M. *Hysteretic damping in the Hardening Soil Small strain model.* Graduation Thesis, Enschede: University of Twente, 2006.

Kramer, S.L. *Geotechnical earthquake engineering.* New York: Prentice Hall, 1996.

Lysmer, J., and R.L. Kuhlmeyer. "Finite Dynamic Model for Infinite Media." *Journal of Engineering and mechanical division* (ASCE), 1969: 859-877.

Meijers, S. J. H. *Lateral force method.* email conversation, Amersfoort: Royal HaskoningDHV, 2013.

Mokwa, R. L. “Mechanics of pile cap and pile group behavior.” Blacksburg, 1999.

NEN. *NEN-EN 1998-4 Eurocode 8 - Ontwerp en berekening van aardbevingsbestendige constructies - Deel 4: Silo's, opslagtanks en pijpleidingen.* Delft: Nederlandse Norm (NEN), 2006.

Paulissen, J.H. *Seismic analysis LNG tank - Phase 1.* Delft: TNO, 4 january 2013.

Poulos, H. G., and E.H. Davis. *Pile Foundation analysis and design.* Berkshire: Transport Research Laboratory, 1980.

Reese, Lymon C., and William F. van Impe. *Single piles and pile groups under lateral loading.* London: A.A. Balkema Publishers, 2001.

Rijswijk, A., and S. Negi. *Angola lng project bechtel, dynamic analysis procedure.* Vol. rev2. Delft: TKK, 2007.

Rijswijk, A., P. Wolters, and R. Vonk. *Dynamic analysis for seismic coefficient estimation.* Tokyo: TKK, Tokyo Kanetsu K.K., 2008.

Robert W. Day. *Geotechnical earthquake engineering handbook.* New York: McGraw-Hill, 2002.

Santos, J. A., and A.G. Correia. “Reference treshold shear strain of soil, its aplication to obtain unique strain-dependent shear modulus curve for soil.” *15th International Conference on Soil Mechanics and Geotechnical Engineering.* Istanbul, Turkey, 2001. 267-270.

Schrier, J. van der. *Palm Deira Marine Waterfront Structures.* Geotechnical Design Report, Infrastructure, Nijmegen: Royal Haskoning, 2009, 6-12.

Sluys, L.J. *Wave propagation, Localisation and dispersion in softening solids.* Dissertation, Delft: Delft University of Technology, 1992.

Thornton, Charles. *NEHRP Recommended Provisions for seismic regulations for new buildings and other structures.* NEHRP 2003 (FEMA 450), Washington D.C.: Building Seismic Safety Council, 2003.

Vardanega, P., and M.D. Bolton. “Practical methods to estimate the non-linear shear stiffness of fine grained soils.” Seoul, Korea: International Symposium on deformation characteristics of geomaterials, 2011.

Visone, C., E. Bilotta, and F. Santucci de Magistris. *Remarks on site response analysis by using Plaxis dynamic module.* Geotechnical Engineering, University of Naples, Naples: Plaxis, 2008, 14-18.

Wolf, J.P. *Foundation vibration analysis using simple physical models.* Chicago: Prentice Hall Int., 1994.

Yang, Young-myung. “Development of the world's largest above-ground full containment LNG storage tank.” *23rd World Gas Conference.* Amsterdam: Korea Gas Corporation, 2006. 5.

Zienkiewicz, O.C., and R.L. Taylor. *The Finite Element Method.* London, UK: McGraw-Hill, 1967.

—. *The finite element method; solid and fluid mechanics.* Vol. fifth edition. London, UK: McGrawHill, 1991.

Zoback, M. L., and M.D. Zoback. “Tectonic stress field of the continental U.S.” In *Geophysical framework of the continental United States*, by L.C. Pakiser and Walter D. Mooney, 523-540. Boulder, Colorado: Geological Society of America, Inc, 1989.